


Summer November 2014

## Guanidinium-Rich ROMP Polymers Drive Phase, Charge, and Curvature-Specific Interactions with Phospholipid Membranes

Michael T W Lis  
*University of Massachusetts - Amherst*

Follow this and additional works at: [https://scholarworks.umass.edu/dissertations\\_2](https://scholarworks.umass.edu/dissertations_2)

 Part of the [Biophysics Commons](#), and the [Polymer Chemistry Commons](#)

---

### Recommended Citation

Lis, Michael T W, "Guanidinium-Rich ROMP Polymers Drive Phase, Charge, and Curvature-Specific Interactions with Phospholipid Membranes" (2014). *Doctoral Dissertations*. 231.  
<https://doi.org/10.7275/v9r6-cp77> [https://scholarworks.umass.edu/dissertations\\_2/231](https://scholarworks.umass.edu/dissertations_2/231)

This Open Access Dissertation is brought to you for free and open access by the Dissertations and Theses at ScholarWorks@UMass Amherst. It has been accepted for inclusion in Doctoral Dissertations by an authorized administrator of ScholarWorks@UMass Amherst. For more information, please contact [scholarworks@library.umass.edu](mailto:scholarworks@library.umass.edu).

**GUANIDINIUM-RICH ROMP POLYMERS DRIVE PHASE, CHARGE, AND CURVATURE-SPECIFIC  
INTERACTIONS WITH PHOSPHOLIPID MEMBRANES**

A Dissertation Presented

By

MICHAEL THOMAS WOODS LIS

Submitted to the Graduate School of the  
University of Massachusetts Amherst in partial fulfillment  
of the requirements for the degree of

DOCTOR OF PHILOSOPHY

September 2014

Department of Polymer Science and Engineering

© Copyright by Michael T. W. Lis 2014

All Rights Reserved

**GUANIDINIUM-RICH ROMP POLYMERS DRIVE PHASE, CHARGE, AND CURVATURE-SPECIFIC  
INTERACTIONS WITH PHOSPHOLIPID MEMBRANES**

A Dissertation Presented

by

MICHAEL THOMAS WOODS LIS

Approved as to style and content by:

---

Gregory N. Tew, Chair

---

Maria Santore, Member

---

Anthony Dinsmore, Member

---

David Hoagland, Head  
Department of Polymer Science and  
Engineering

## **DEDICATION**

Dedicated to my wonderful wife Vera, without whose care and tolerance none of this would have been possible, and to our newborn son Jonathan, who already means everything to me.

## **ACKNOWLEDGMENTS**

I would like to thank Professor Gregory N. Tew for his support, guidance, and direction in the work of this thesis. I would like to thank my committee members, Professors Anthony Dinsmore and Maria Santore for their always engaged and incisive commentary and helpful suggestions on my research. Meetings with them presented a real turning point in the progress of this research. I have been very fortunate to have exceptionally productive and helpful collaborators in Professor Gerard Wong, Dr. Karen Lienkamp, Dr. Frederica Sgolastra and Dr. Nathan Schmidt. Dr. Lienkamp, Professor William T. Verts, Dr. Semra Colak and Dr. Ahmad Madkour have also been exceptional mentors during my graduate career, keeping me firmly grounded in reality at all times. Professor Lara A. Estroff, Dr. Farhad Riahi, and Dr. Rebecca Jackman provided inspiration and a drive for research in my formative years. Much of how I approach science is a credit to them. Lastly, I would like to thank my wife, my parents and my sister for their endless love and support, and for creating an environment where any question can be asked at any time.

## ABSTRACT

### GUANIDINIUM-RICH ROMP POLYMERS DRIVE PHASE, CHARGE, AND CURVATURE-SPECIFIC INTERACTIONS WITH PHOSPHOLIPID MEMBRANES

SEPTEMBER 2014

MICHAEL T. W. LIS, B.S.E., CORNELL UNIVERSITY

M.S., UNIVERSITY OF MASSACHUSETTS AMHERST

Ph.D., UNIVERSITY OF MASSACHUSETTS AMHERST

Directed by: Professor Gregory N. Tew

Protein transduction domains (PTDs) and their synthetic mimics (PTDMs) are short sequences capable of unusually high uptake in cells. Several varieties of these molecules, including the arginine-rich Tat peptide from HIV, have been extensively used as vectors for protein, DNA, and siRNA delivery into cells. Despite the wide-ranging utility of PTDs and their mimics, their uptake mechanism is still under considerable debate. How the molecules are able to cross phospholipid membranes, and what structural components are necessary for optimal activity are poorly understood. This thesis explores how PTDMs interact with phospholipid membrane phase, anionic lipid content and negative Gaussian curvature generation along the structural variables of polymer length, charge density, hydrophobicity, aromaticity, and architecture.

Chapter 1 of the thesis provides a thorough introduction and history both of antimicrobial polymer-membrane interactions and PTDs and PTDMs. While much of the thesis is focused on the latter category, the rich history of cationic antimicrobial polymers provides an extensive framework with which to study PTDMs.

Chapter 2 examines the link between membrane phase and PTDMs activity. It is shown that cooling phospholipid membranes reduces PTDM activity, but that this barrier can be

overcome by increased polymer hydrophobicity. Cooling cells to 4°C is a common practice to distinguish between energy-dependent and energy-independent uptake. If cooling cells alters energy-independent activity, such an experiment may claim a higher fraction of the uptake is endocytotic than actually occurs at room temperature.

Chapter 3 shows that for ROMP-based PTDMs, anionic lipid content in the phospholipid membrane is also a barrier to activity. This is counter to the commonly-cited “adaptive translocation” model of PTDM activity, where anionic content is seen as a vital component. Furthermore, it is demonstrated through the use of zeta potential and surface plasmon resonance experiments that hydrophobicity, not cation-anion interactions. Anionic lipids, instead, serve to “pin” the PTDM onto the lipid surface, limiting membrane activity. As with the studies regarding membrane phase in chapter 2, this barrier is overcome by added polymer hydrophobicity. These results suggest that cationic content may not strictly speaking be necessary to PTDM activity, as is generally assumed, and that a sufficient balance of hydrophobicity and water solubility are more critical. It may then be possible to introduce charge-neutral PTDM variants.

Chapters 4 and 5 explore the relationship between PTDM functionality and architecture and negative Gaussian curvature formation in high-phosphatidylethanolamine (PE) lipid systems. These studies measure negative Gaussian curvature across polymer length, hydrophobicity, charge density, and copolymer arrangement. While all of these factors are found to alter curvature formation in high-PE bulk systems, it is still unclear how well these results correlate to PTDM activity in cellular systems.



## TABLE OF CONTENTS

	Page
DEDICATION .....	iv
ACKNOWLEDGMENTS .....	v
ABSTRACT .....	vi
LIST OF TABLES .....	x
LIST OF FIGURES .....	xi
Chapter	
1 INTRODUCTION .....	1
1.1 Phospholipid Membranes and Model Systems .....	2
1.2 Antimicrobial/Biocidal Polymer-Membrane Interactions .....	4
1.2.1 Cations in the Main Chain .....	4
1.2.2 Acrylic Polycations .....	7
1.2.3 Peptide-Based Polycations .....	10
1.2.4 Imide-Based ROMP Polycations .....	13
1.2.5 Ester- and Amide-Based ROMP Polycations .....	17
1.2.6 Conjugated Polycations .....	20
1.2.7 The State of Antimicrobial and Biocidal Cationic Polymer Research .....	23
1.3 Protein Transduction Domains and their Synthetic Mimics .....	24
1.3.1 Cell Studies of PTDs .....	24
1.3.2 Biophysical Studies of PTDs .....	28
1.3.3 Molecular Dynamics Simulations .....	32
1.3.4 Polymer-Based PTDMs .....	33
1.4 The Scope of this Thesis .....	40
1.5 References .....	42
2 THE LOW TEMPERATURE UPTAKE OF PROTEIN TRANSDUCTION DOMAIN MIMICS IS AFFECTED BY LIPID PHASE .....	48
2.1 Introduction .....	48
2.2 Materials and Methods .....	50
2.2.1 Materials .....	50
2.2.2 Instrumentation .....	50
2.2.3 Monomer Synthesis .....	51
2.2.4 Polymer Synthesis .....	51
2.2.5 Cell Culture and Uptake Studies .....	55
2.2.6 Dye Release Studies .....	56
2.3 Results and Discussion .....	59
2.3.1 Polymer Design .....	59
2.3.2 Cellular Uptake Studies .....	61
2.3.3 DPPC Dye Release .....	63
2.3.4 EYPC Dye Release .....	69
2.4 Conclusions .....	71
2.5 References .....	72
3 ANIONIC LIPID CONTENT PRESENTS A BARRIER TO ROMP-BASED PTDM ACTIVITY .....	76
3.1 Introduction .....	76
3.2 Materials and Methods .....	78
3.2.1 Polymer Synthesis .....	78

	3.2.2	Dye Release Studies.....	79
	3.2.3	Dynamic Light Scattering and Zeta Potential Measurements .....	81
	3.3	Results and Discussion.....	85
	3.3.1	Polymer Design.....	85
	3.3.2	Dye Release Studies.....	86
	3.3.3	Size and Zeta Potential .....	89
	3.3.4	Surface Plasmon Resonance.....	91
	3.4	Conclusions.....	97
	3.5	References .....	98
4		GUANIDINIUM-RICH POLYMERS DISPLAY LENGTH- AND HYDROPHOBICITY- DEPENDENT NEGATIVE GAUSSIAN CURVATURE GENERATION.....	101
	4.1	Introduction.....	101
	4.2	Materials and Methods.....	105
	4.2.1	Synthetic Procedures.....	105
	4.2.2	Dye Release Studies.....	108
	4.2.3	Antimicrobial and Hemolysis Testing .....	110
	4.2.4	SAXS Studies.....	110
	4.3	Results and Discussion.....	112
	4.3.1	SAXS Study of PGON Polymers with Lipid Membranes .....	114
	4.3.2	SAXS Study of Amphiphilic Butyl-GON and Phenyl-GON Polymers with Lipid Membranes.....	119
	4.3.3	Biological Activity of PGON, Butyl-GON, and Phenyl-GON Polymers .....	124
	4.4	Conclusion.....	126
	4.5	References .....	127
5		PTDM LENGTH, AROMATICITY AND ARCHITECTURE: SEARCHING FOR IDEAL PARAMETERS FOR NEGATIVE GAUSSIAN CURVATURE GENERATION.....	132
	5.1	Introduction.....	132
	5.2	Experimental Methods .....	134
	5.2.1	Monomer Synthesis.....	134
	5.2.2	Polymer Synthesis.....	134
	5.2.3	SAXS Studies.....	136
	5.2.4	Dye Release Studies.....	138
	5.3	Results and Discussion.....	139
	5.3.1	Polymer Design .....	139
	5.3.2	Random Copolymer Series.....	141
	5.3.3	Block Copolymer Series .....	145
	5.4	Conclusions.....	151
	5.5	References .....	151
6		Summary and Future Work.....	154
	6.1	Conclusions.....	154
	6.2	Future Work.....	155
	6.2.1	More complex membrane systems .....	155
	6.2.2	Membrane activity and osmotic pressure.....	156
	6.2.3	Biophysical studies of polymer-cargo complexes.....	156
	6.2.4	Zwitterionic PTDMs.....	157
	6.3	References .....	157
		BIBLIOGRAPHY .....	159

## LIST OF TABLES

	Page
<b>Table 2.1.</b> Compiled dye release data for all polymers. With increasing hydrophobic content, the EC <sub>50</sub> values above and below T <sub>g</sub> converge. The ratios are larger for the single-lipid DPPC system than the mixed-acyl EYPC.....	71
<b>Table 3.1.</b> EC <sub>50</sub> values for the dye release experiments. ....	88
<b>Table 3.2.</b> Peak and final change in reflectance for SPR experiments.....	93
<b>Table 3.3.</b> Fitting parameters for transport (kM), association (ka), and disassociation (kd) for all three polymers. Fitting was performed using a transport-limited rate model.....	94
<b>Table 3.4.</b> GPC molecular weights of the polymers.....	97
<b>Table 4.1.</b> Activity against Human Erythrocytes, <i>S. aureus</i> , and <i>E. coli</i> .....	125
<b>Table 5.1.</b> Polymers used in this study. ....	140
<b>Table 5.2.</b> Collected SAXS data. Cells designated “-“ were tested but displayed no Pn3m phase peaks.....	143

## LIST OF FIGURES

	Page
<b>Figure 1.1.</b> Polymers with cations in the main chain.....	5
<b>Figure 1.2.</b> Acrylic Polymers.....	8
<b>Figure 1.3.</b> Peptide-based antimicrobial polymers.....	11
<b>Figure 1.4.</b> Imide-based ROMP antimicrobials. ....	14
<b>Figure 1.5.</b> Ester-based ROMP antimicrobials. ....	18
<b>Figure 1.6.</b> Conjugated Polycations .....	21
<b>Figure 1.7.</b> Lipids and intrinsic curvature.....	32
<b>Figure 1.8.</b> Amide and Imide-based ROMP PTDMs. ....	35
<b>Figure 1.9.</b> Ester-based ROMP PTDMs.....	37
<b>Figure 1.10.</b> Carbonate-Based PTDMs.....	40
<b>Figure 2.1.</b> Monomers used in this study. ....	51
<b>Figure 2.2.</b> PTDMs used for this study. a) Polymer structures, with guanidinium moieties colored blue and aromatic/hydrophobic moieties colored green. m=4 or 8. b) Cartoon representations of <b>G<sub>16</sub>-r-Ph<sub>4</sub></b> (left) and <b>PhG<sub>10</sub></b> (right) with the same coloring scheme. Dye-labeled analogs of PhG <sub>10</sub> and dG <sub>10</sub> were also synthesized. ....	59
<b>Figure 2.3.</b> Internalization studies. Jurkat T cells (1x10 <sup>6</sup> cells/mL) were incubated for 30 min with the indicated compound either after cellular ATP depletion (with 10 mM NaN <sub>3</sub> , purple) or at 4°C (blue) and compared to uptake under normal conditions (37 °C, red dotted line). a) Representative flow cytometry analysis for the cellular uptake of 50 nM Transferrin-FITC (Tf-FITC), as a control, at the indicated conditions; b) Relative uptake values are normalized to the cellular uptake (in MFI) at 37°C in normal growth media. Each point represents the mean±SE (standard error) of three independent experiments. *** (p<0.001); n.s. (p>0.05), as calculated by unpaired two-tailed student t-test.....	62
<b>Figure 2.4.</b> Dye release from single-component DPPC⇌CF LUVs. Values represent fraction of dye released from vesicles at 600s after the addition of PTDM. Red triangles were taken at 50°C, which is above the liquid-to-gel transition. Blue squares were taken at 25°C, which is below the liquid-to-gel transition. Red lines and blue dashes are least-squares fits to the Hill Equation. ....	65

<b>Figure 2.5.</b> Dye release from DPPC $\supset$ CF LUVs. Values represent fraction of dye released from vesicles at 600s. Red triangles were taken at 50°C, above $T_g$ . Blue squares were taken at 25°C, below $T_g$ . Red lines and blue dashes are least-squares fits to the Hill Equation. a) and c) compare the same polymer with and without dye, showing little difference in their release profile.....	67
<b>Figure 2.6.</b> Dye release from mixed-acyl chain EYPC $\supset$ CF LUVs. Values represent fraction of dye released from vesicles at 600s after the addition of PTDM. Red triangles were taken at 25°C. Blue squares were taken at 4°C. Red lines and blue dashes are least-squares fits to the Hill Equation.....	69
<b>Figure 2.7.</b> Dye release from EYPC $\supset$ CF LUVs. Values represent fraction of dye released from vesicles at 600s. Red triangles were taken at 25°C, above $T_g$ . Blue squares were taken at 4°C, below $T_g$ . Red lines and blue dashes are least-squares fits to the Hill Equation. a) and c) compare the same polymer with and without dye, showing little difference in their release profile.....	70
<b>Figure 3.1.</b> The polymer design used for this study. (Top) Cartoon representation of random copolymer 2. (Middle) Generic polymer structure for the series. ....	86
<b>Figure 3.2.</b> Dye release for the polymers a) <b>1</b> b) <b>2</b> and c) <b>3</b> from carboxyfluorescein-loaded EYPC (green squares) and 80:20 EYPC:Brain PS (red triangles) vesicles. Green lines and red dashes are fits to the Hill Equation.....	88
<b>Figure 3.3.</b> Dye release of polymer 2 from DOPC (green squares) and 80:20 DOPC:DOPS (red triangles) vesicles. Green lines and red dashes are fits to the Hill Equation. ....	88
<b>Figure 3.4.</b> a) Number mean particle size by dynamic light scattering and b) zeta potential measurements for the interaction of varying concentrations of polymer <b>2</b> with phospholipid vesicles. Green squares represent data for zwitterionic DOPC vesicles, while red triangles represent data for anionic 80:20 DOPC:DOPS vesicles. Green and red dashes represent the dye release EC50 values for the DOPC and 80:20 DOPC:DOPS vesicle systems, respectively. ....	89
<b>Figure 3.5.</b> Dynamic light scattering of 10 $\mu$ M polymer in buffer solution. ....	91
<b>Figure 3.6.</b> Surface plasmon resonance binding and unbinding curves for 10 $\mu$ M of polymer (a) <b>1</b> , (b) <b>2</b> and (c) <b>3</b> . Green lines represent binding to the zwitterionic DOPC lipid system, while red lines represent binding to the anionic DOPC:DOPS system. The bilayer was exposed to a continuous flow of polymer solution starting at t=0 and then flushed with buffer starting at t=20 minutes. Black lines represent model fits.....	92
<b>Figure 3.7.</b> GPC traces of polymers 1, 2, and 3.....	96
<b>Figure 4.1.</b> Diels-alder synthesis of oxanorbornene imide.....	105

- Figure 4.2.** Synthesis of di-boc protected Guanidine monomer. .... 106
- Figure 4.3.** Generation of negative Gaussian curvature by guanidinium-rich polymers depends on average polymer length and average spacing between monomers. (A) Representative scattering spectra of PGONs with degree of polymerization 7, 18, and 50 (top to bottom) with DOPS/DOPE = 20/80 membranes at the polymer to lipid isoelectric point. Arrows indicate the first order reflection of the Pn3m cubic phase. A first order reflection at higher Q indicates the generation of greater negative Gaussian curvature. (B) Plots of polymer-induced average negative Gaussian curvature generation,  $|\langle K \rangle|$ , versus polymer length for both PGON and poly arginine. The maximum amount of  $|\langle K \rangle|$  occurs around Arg<sub>9</sub> for poly arginine, while for PGON it is around an average degree of polymerization of 14. The lines are to guide the eye (see Experimental Section for details). (C) Schematic showing structural features of PGON and poly arginine, and effective spacing between guanidine groups..... 113
- Figure 4.4.** Illustration showing the connection between toroidal pores and saddle surfaces. The interior of a torus (top) has the same curvature as a ‘toroidal’ membrane pore. Close examination of the surface (bottom left) reveals that it bends in opposite directions at every point. This surface has saddle-splay curvature, positive curvature and negative curvature in orthogonal directions, as shown by rotating the surface (bottom right). ..... 116
- Figure 4.5.** Hydrophobicity increases the amount of negative Gaussian curvature that guanidinium-rich polymers generate. (A) Butyl-GON polymer, N = 11, butyl/guanidine molar ratio = 6/5, generates Pn3m cubic phases in DOPS/DOPE = 20/80 membranes at peptide/lipid = 1/60 and 1/30 molar ratios. The arrow points to the first (110) reflection of the Pn3m, which shifts to higher Q for greater P/L ratios. (B) A similar trend is observed for the phenyl-GON polymer, N = 11, phenyl/guanidine molar ratio = 6/5. (C and D) Calculation of the Pn3m phase lattice parameters for butyl-GON (P/L = 1/30, red, P/L = 1/60, dark red) and phenyl-GON (P/L = 1/30, blue, P/L = 1/60, dark blue). Smaller lattices are seen for greater P/L ratios. (E) Average negative Gaussian curvature,  $|\langle K \rangle|$ , versus polymer/lipid charge ratios for polymers of similar charges and sizes. The hydrophobic butyl-GON and phenyl-GON induce greater  $|\langle K \rangle|$  than the hydrophilic PGONs..... 119
- Figure 4.6.** Hydrophobicity broadens the range of lipid compositions where guanidinium-rich polymers induce negative Gaussian curvature. (A) At P/L = 1/30, amphiphilic butyl-GON and phenyl-GON polymers both generate Pn3m cubic phases in membranes with reduced amounts of negative spontaneous curvature lipids, DOPS/DOPE/DOPC = 20/70/10. Inset shows indexation of the Pn3m cubic for both polymers. (B–E). Phase diagrams for guanidinium-rich polymers over a range of lipid compositions, DOPS/DOPE/DOPC = 20/x/(80 – x) where x = %DOPE, and peptide/lipid ratios. The amphiphilic butyl-GON and phenyl-GON polymers generate cubic

phases over a larger region of the phase diagram compared with the hydrophilic PGON polymers. ....	121
<b>Figure 4.7.</b> Phase diagrams of the PGON polymers used in this study.....	123
<b>Figure 4.8.</b> Fractional calcein release from EYPC 400 nm vesicles as a function of polymer concentration. The polymer with added hydrophobes induces more release than any of the PGON samples.....	124
<b>Figure 5.1.</b> Polymers used for this study. Polymers were synthesized with n values of 2, 4, and 8.....	140
<b>Figure 5.2.</b> Small-angle X-ray scattering plots for 20:80 DOPS:DOPE lipid systems combined with a) the random phenyl copolymer series and b)the random cyclohexyl copolymer series. Arrows indicate the (110) peak of the Pn3m phase. The series show similar ability to generate negative Gaussian curvature, and no length dependence.....	142
<b>Figure 5.3.</b> Dye release of all four polymers of length 20 with EYPC large unilamellar vesicles. Very little variation is shown between samples. ....	145
<b>Figure 5.4.</b> Small-angle X-ray scattering plots for the block phenyl series with a) 20:80 DOPS:DOPE and b) 20:70:10 DOPS:DOPE:DOPC lipid systems. Arrows in a) indicate the (110) peak of the Pn3m phase. Arrows and b) indicate the (110), (111), (200), and (211) phases. The polymer series shows a strong length dependence on curvature generation in a) and only <b>G<sub>32</sub>-b-Ph<sub>8</sub></b> shows and Pn3m phase generation in b). ....	147
<b>Figure 5.5.</b> Compiled curvature generation as a function of polymer length for all three series. The two random series show little separation and little length dependence, while the block copolymer series shows a strong length dependence.....	148
<b>Figure 5.6.</b> Dye release for the block copolymer series with large unilamellar vesicles. x-axis is given in units of $\mu\text{g/mL}$ instead of $\mu\text{M}$ to maintain a fixed polymer cation to lipid anion ratio, as was done with the SAXS experiments.....	150

## CHAPTER 1

### INTRODUCTION

Note: Portions of this work appear in:

Lis M. and G. Tew (2012) *Polymer–Membrane Interactions*. In: Matyjaszewski K and Möller M (eds.) *Polymer Science: A Comprehensive Reference*, Vol 9, pp. 289–315. Amsterdam: Elsevier BV.

Protein transduction domains (PTDs) and their synthetic mimics (PTDMs) are short sequences capable of unusually high uptake in cells.[1-3] Several varieties of these molecules, including the arginine-rich Tat peptide from HIV, have been extensively used as vectors for protein, DNA, and siRNA delivery into cells.[4] For Tat-based systems, it has been shown that guanidine functionality, but not specific secondary structure, is critical for uptake,[5] providing a set of basic parameters for a variety of synthetic mimics. Despite the wide-ranging utility of PTDs and their mimics, their uptake mechanism is still under considerable debate.[6-12] How much of their activity is due to endocytosis, how the molecules are able to cross phospholipid membranes, and what structural components are necessary for optimal activity are just some of the questions that remain largely unanswered.

While the understanding of PTD(M)-membrane interactions is still in its adolescence, we have a more mature understanding of a close cousin in antimicrobial molecules. These peptides, small molecules and polymers possess a similar requirement for a balance between their cationic nature, water solubility, and hydrophobicity. The techniques used to study these polymer/peptide-membrane interactions is quite robust, and much of the polymer design and characterization techniques can be (but largely still hasn't been) applied to the PTDM literature.

This opening chapter will give an introduction to the current understanding of cationic polymer-membrane interactions, looking at both antimicrobial polymers and PTD(M)s. While



the rest of this document does not spend much time explicitly discussing the antimicrobial literature, much of the work herein is inspired by techniques and polymer designs created for that field. A proper grounding in the PTDM literature, then requires the context of the antimicrobial literature. The entirety of the antimicrobial literature is vast. There are already excellent resources dedicated to the understanding of the entire field.[13-15] Instead, the first half of this introduction will focus on the narrower field of polymer antimicrobials and biocides and the studies of their interaction with lipid membranes. There is a particular focus on highlighting both the diversity of polymer structures created and the techniques used to study them.

The second half of this chapter will recount a general history of the study of guanidinium-rich PTDs and PTDMs. The focus here will be on the evolution of our understanding of the interaction of PTD(M)s with the cell membrane, with a focus on areas that still need more attention.

## **1.1 Phospholipid Membranes and Model Systems**

Since this section revolves around interactions with biological or biomimetic membranes, a brief discussion of the membrane is worthwhile. A more detailed primer focused on biological structure can be found in most introductory biochemistry textbooks,[16] while a physical view of lipid membranes can be found in books by Israelachvili[17] and Cevc and Marsh.[18] The biological membrane is composed of a self-assembled bilayer of phospholipids (20–50%), proteins (20–70%), and sterols (0–20%) and is usually 5–8 nm thick. These self-assembled lipids provide the structural basis for the membrane. Membrane lipids are amphiphilic, containing a hydrophilic headgroup and a hydrophobic tail. In mammals, most of these lipids are glycerophospholipids, which link the headgroup to the tails by glycerol, and

contain a phosphate ion as part of the headgroup. Mammalian membranes are dominated by lipids containing the zwitterionic headgroups phosphatidylcholine (PC) and phosphatidylethanolamine (PE). Anionic lipids such as phosphatidylserine are also present, but in smaller quantities. These lipids contain fatty acid chains of different lengths and degrees of saturation. Natural systems contain a mixture of many lipid tails. The two other significant components of mammalian membranes are cholesterol, which control the stability and fluidity of the membranes, and proteins, which add ion channels, receptors, connections between the membrane and cytoskeleton, and other functionalities to the membranes. Bacterial membranes contain no cholesterol and their lipid headgroup composition is dominated by the anionic phosphatidylglycerol (PG), diphosphatidylglycerol (DPG), [19] also known as cardiolipin, and zwitterionic PE.

Apart from the biological activity of the membrane components, the structural and physical properties of the membrane are uniquely complex. First, these lipids can be solid-like or liquid-like, depending on their chemical composition and temperature. For example, PC lipids containing saturated chains of 16, 18, and 20 carbons melt from a gel (or solid-like) to a fluid (liquid-like) state at 41, 55, and 66 °C, respectively. The temperature of this transition is usually denoted as  $T_m$ . PC containing 18 carbon saturated acyl chains (DSPC) melts at 55 °C, while PC containing 18 carbon acyl chains with one cis-double bond (DOPC) melts at -22 °C. Mixtures of lipids have a marked effect on their melting behavior. Egg PG (with mixed lengths and mixed degrees of unsaturation in the acyl tails) has a broad, heterogeneous melting transition around 10-20 °C, pure DPPC (saturated tails) gives a much sharper transition at 40-50 °C, and a 50:50 mixture of the two melts over the range of 20-30 °C. [20]

Above  $T_m$ , the membrane is fluid, allowing the individual lipid molecules to diffuse within the self-assembled structure. Lateral diffusion of lipids within the plane (or one leaflet) is

rapid, while flip-flop (one leaflet to another) has a much higher energy barrier and, thus, requires longer timescales. The fluid nature of the membrane also means that interactions with outside forces can influence this phase-mixed or phase-separated state. The fluid nature also allows fluctuations to occur, which lead to both transient and irreversible responses. When two lipid components are present, lipids can be phase-mixed or phase-separated, depending on both intermolecular affinity as well as the thermodynamic states of the lipids. 'Lipid rafts' are formed when lipids are phase-separated, and one of the lipids is below its melting point. These rafts are most often gel-like, but are able to move freely through the fluid phase of the membrane. These heterogeneities are proposed to be an essential function of biology. Thus, the membrane, even in its simplest form, is dynamic and complex.

Much of the literature uses simpler synthetic mimics of cell membranes, consisting of vesicles (also known as liposomes) and occasionally flat bilayers supported on a substrate. Most contain no protein in order to focus on polymer–lipid interactions. Membranes meant to mimic mammalian membranes generally consist of PC and may include some cholesterol. Red blood cells (RBCs) also serve as a model system, as they do not divide. Gram-positive bacteria mimics generally consist of PG and cardiolipin, while gram-negative bacteria mimics have PE and PG.

## **1.2 Antimicrobial/Biocidal Polymer-Membrane Interactions**

### **1.2.1 Cations in the Main Chain**

Polymers containing cations in the main chain were extensively examined by Ikeda et al. through the 1980s and 1990s. The biguanide polymers were based on well-known commercial biocides, while the quaternary phosphonium and ammonium salts provided more easily adjustable structures to study structure–function relationships. Small-molecule biguanides were

initially developed for use as antimalarial drugs, but were found to have significant activity against a broad spectrum of bacteria.[21, 22]

A polymeric analog of these small molecules, poly(hexamethylene biguanide hydrochloride) (PHMB), was synthesized and found to have stronger biocidal activity than the small molecules (Figure 1.1).[23, 24] The first membrane investigations were performed by Ikeda et al.,[25] who demonstrated with fluorescence depolarization that the addition PHMB to lipid mixtures containing PG lipids increased fluidity of the bilayers. Simple binding of the polymer to anionic lipids in the membrane would create a local lipid–polymer complex that would be expected to have a slower rate of diffusion due to the increased mass and rigidity created by the binding. To explain the increase in fluidity, the authors suggest that the hexamethylene region inserts into the bilayer, increasing the spacing between PG lipids.

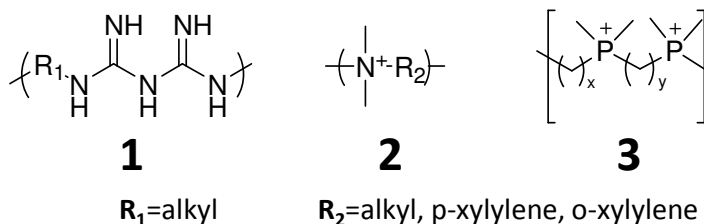


**Figure 1.1.** Polymers with cations in the main chain

In a separate paper, Ikeda et al.[20] used DSC to show that PHMB induced phase separation in PC–PG membranes, suggesting that the PHMB selectively bound to the anionic lipids. DSC gives the heat capacity of the polymer/lipid mixtures, showing distinct peaks at the melting point ( $T_m$ ) of the mixture. PHMB and its monomeric form, when added to pure PG lipid, reduced the melting temperature of the lipids, concurring with the earlier finding that PHMB increases membrane fluidity. This is in contrast to magnesium, which also binds lipids together but increases  $T_m$ , indicating a decrease in fluidity. The authors suggest that the hydrophobic regions of the polymer may insert into the bilayer, weakening the interactions between the acyl

tails. When PHMB is added to the lipid mixture, the characteristic peak for a mixture is present, as well as a peak that more closely resembles the peak seen for pure egg PG. This indicates that the polymer induces phase separation in the lipid, creating a PHMB/PG-complex region and a DPPC-rich region. Since neither the monomer form (which is less biocidal) nor divalent magnesium induces such phase separation, the authors hypothesized that this may be an important component of the biocidal activity. On the basis of the observed phase separation and the increased fluidity caused by the biocide, the authors hypothesized that a combination of hydrophobic and hydrophilic components were necessary for effective polymer biocides.

Ikeda et al.[26, 27] synthesized polymers with quaternary ammonium salts in the main chain. As with PHMB, the addition of DPH to bilayers containing anionic PA lipid caused increased fluidity. As with the biguanide polymers, the increase in fluidity was hypothesized to correlate with antimicrobial activity.

Similar synthetic methods were used to prepare a wide variety of quaternary cation structures with varying hydrophobicity and rigidity.[26] Antimicrobial activity was measured by the minimum inhibitory concentration (MIC), the lowest concentration of polymer needed to inhibit bacterial growth. Later literature often defines the term MIC<sub>90</sub> as the concentration at which 90% of bacterial growth is inhibited. MIC values for the polymers were lowest for the rigid, hydrophobic structures, and highest for the flexible, hydrophilic backbones. Polymers with flexible, hydrophobic backbones between charges had intermediate activity. There was also a small reduction in activity when p-xylylene spacers were exchanged for o-xylylene spacers, but this may be due to the change in MW (40–24 kg/mol) of the polymers more than the change in functionality. Hemolysis by these polymers was not measured, but activity against eukaryotic fungi was not substantially different than against bacteria. Extensive DSC studies were also performed on this polymer series. As with the biguanide polymers, the p-phenylene polymers

appeared to induce significant phase separation in mixed PA/PC lipid membranes. While evidence of phase separation was observed for the other, less effective polymers, it was less pronounced, and roughly correlated with antimicrobial activity. From this evidence, the authors hypothesized that antimicrobial activity was correlated with both the rigidity and hydrophobicity of the charged polymers.

Kanazawa et al.[28] synthesized polymers containing quaternary phosphonium cations with aromatic side groups on the phosphonium sites and aliphatic separators. Several different spacers were used, but their syntheses were similar. Polymers of varying MWs and spacer lengths were added to cultures of *Escherichia coli* and *Staphylococcus aureus* each containing ~10<sup>8</sup> cells/ml. Across the board, polymers had increased antibacterial activity with increasing MW and spacer length (hydrophobicity). The more effective samples needed <10 µg/ml polymer to kill both strains of bacteria.

### **1.2.2 Acrylic Polycations**

As a companion to the biguanide main-chain polymers, acrylic polymers with biguanide pendant groups were also synthesized (Figure 1.2) (polymer 4).[29] Polymers were synthesized by free radical polymerization, both as homopolymers and as copolymers of the biguanide monomer with acrylamide. MIC values for these polymers were substantially higher than for the monomer. The authors hypothesized that these results may be due to the fact that the polymers complex with anionic components in the culture media. As a comparison to this approach, the authors also performed killing assays in sterile solution. In these assays, a more expected result was shown: the monomers were significantly less effective than the polymers in killing *S. aureus*. Furthermore, the activity of the polymers was far higher, with the aniline homopolymer killing all *S. aureus* in culture in concentrations as low as 14 µg/mL. There was no significant difference

in activity between the homopolymer and copolymer (when measured by biguanide concentration), indicating that the acrylamide segments have no effect – positive or negative. This approach to bacterial testing eliminates the problem of polymer complexation with media; however, real-world use of these polymers would involve the presence of similar anions. Thus, while the data in sterile water may be simpler to explain from a mechanistic point of view, it may not correlate to real-world effectiveness.

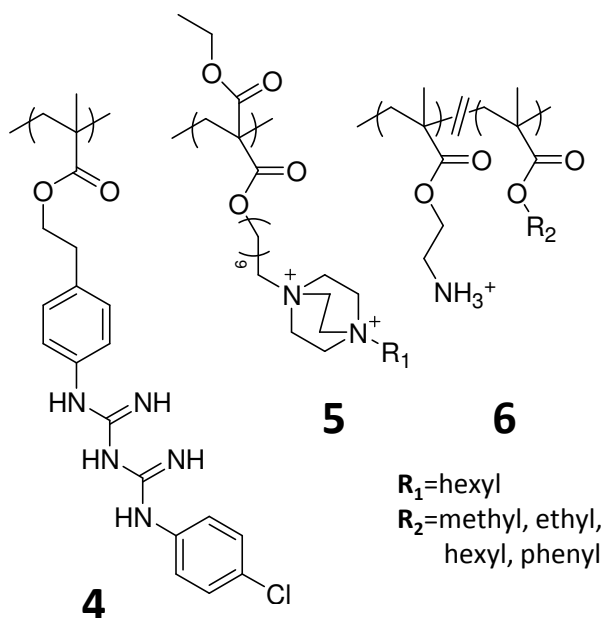


**Figure 1.2.** Acrylic Polymers

The most thorough examination of the interaction of cationic methacrylates and phospholipid membranes has been made by Kuroda et al.[30-34] Initial work combined butyl methacrylate and aminoethyl methacrylate monomers to generate a series of polymers with varying MWs and hydrophobic/cationic ratios (**6**).[30] Polymers with low MW and 17% butyl methacrylate content exhibited some selectivity ( $HC_{50}$  to MIC, or ratio of lysis to antimicrobial inhibition greater than 1), but relatively high MIC values of around 60  $\mu\text{g}/\text{mL}$ .

This repertoire of polymers was vastly expanded to include methyl, ethyl, hexyl, and phenyl side groups.[34] These polymers showed a step-like relationship between hydrophobic

content and MIC, but a more continuous trend in hemolytic data. Between these two extremes, there were some polymers with reasonable selectivity. Most notably, polymers with about 50% methyl methacrylate showed excellent antimicrobial activity, with a MIC of less than 10  $\mu\text{g}/\text{mL}$  and a selectivity index of around 10. The authors presumed that the amount of hemolysis caused by the polymers was directly related to the hydrophobic content of the polymers. To test this hypothesis, they used a theoretical octanol–water partition coefficient ( $P$ ) as a relative measure of hydrophobicity. As a scaling between the different alkyl side chains, the authors used the known linear  $P$  relationship between methanol, ethanol, butanol, and hexanol. To measure the relative hydrophobicity of an entire polymer, they added the logarithm of the partition coefficients for all of the polymers ( $\Sigma\log P$ ). The plot of  $\Sigma\log P$  against  $\text{HC}_{50}$  values provided remarkably consistent results across the series of polymers.

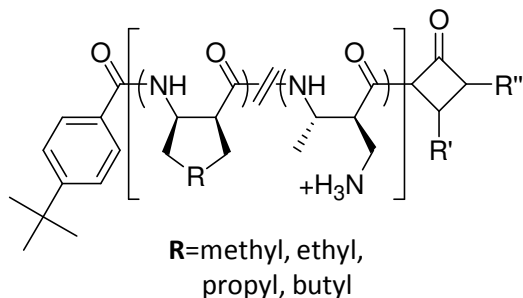
To understand the antimicrobial ability and selectivity of these polymers, Kuroda et al. looked at polymer binding affinity with membranes containing different lipid compositions. To determine the binding constants to lipid membranes, a fluorescent dansyl functional group was added to the end of the polymer. This group emits increased fluorescence in hydrophobic environments, so an increase in fluorescence is interpreted as a binding of the polymer to lipid vesicles. These data were fitted to a binding model to give a dissociation constant value. Binding to POPC vesicles increased with hydrophobic content of the polymer, which was expected. More surprising, however, was the ‘reduction’ of binding to both POPC/POPE and POPC/POPG vesicles compared to binding with POPC. Both lipids are far more common in bacteria than the outside of mammalian cells. Furthermore, POPG is anionic, which would be expected to have a stronger binding to a cationic polymer than the other zwitterionic lipids. This is also in stark contrast to some of the literature available for cationic peptides.[35-38]



Further work by Palermo and Kuroda[32] extended the library of molecules to include tertiary amine- and quaternary ammonium-functionalized methacrylates. For this series, cationic monomers were polymerized with methyl and butyl acrylate monomers. As with the styrene-based polymers of Gelman et al., the quaternary ammonium series was much less antimicrobial and somewhat less hemolytic than the primary and tertiary amine series. Again, titration of the polymers showed that there is partial deprotonation of the amine functionalities at neutral pH. The deprotonated moieties are more hydrophobic than the ammonium salts, and thus increase the membrane activity of the polymers. No explanation was given, however, for the increased activity of the primary amine polymers over the tertiary amine polymers.

### **1.2.3 Peptide-Based Polycations**

Similar to the work by Kuroda et al. with methacrylate polymers and Sambhy et al. with pyridinium polymers, Mowery et al.[39] created a series of random  $\beta$ -peptide copolymers containing cationic and hydrophobic residues (**7**). Polymers were synthesized by ring-opening polymerization using tert-butylbenzoyl chloride and lithium bis(trimethylsilyl) chloride. Polymers containing 30–100% cationic lactam were synthesized, and MIC and minimum hemolytic concentration (MHC) values were reported. MHC represents the lowest concentration of detectable hemolysis and is somewhat more sensitive than the  $HC_{50}$ . The polymers with the highest selectivity resided in the 60–65% cationic monomer range, with MIC values of 12–25  $\mu\text{g}/\text{mL}$  against *S. aureus* and *E. coli*. MHC values were in the 100–1000  $\mu\text{g}/\text{mL}$  range, depending on the exact monomer ratio.



## 7

**Figure 1.3.** Peptide-based antimicrobial polymers.

The polymer containing 60% cationic residues was used in studies with lipid vesicles mimicking mammalian and bacterial cell membranes by Epanand et al.[38] The authors loaded the vesicles with a dye (ANTS) and a concentration-dependant quencher (DPX). The released ANTS fluoresces, allowing determination of the extent of leakage. The 100% leakage level is set using a surfactant. The polymer permeabilized vesicles of DOPE:DOPG 80:20 (*E. coli* mimic), DOPG:CL 58:42 (*S. aureus* mimic), and DOPG:DOPE:CL 84:12:4 (*B. subtilis* mimic) at very low concentrations, but did not cause leakage from POPC (mammalian mimic) vesicles. The authors attribute the difference to the presence of anionic lipids in the bacterial membrane mimics. To demonstrate that the polymer binds to anionic lipids, ITC and DSC experiments were performed. ITC showed evidence of binding to DOPE:DOPG vesicles, but not to DOPC vesicles, indicating binding to the bacterial mimic, but not the mammalian mimic.

DSC was first run with a DPPG:CL lipid mixture. Pure DPPG has a gelation temperature of 65 °C which is reduced by the addition of cardiolipin. The DSC of the lipid mixture shows a broad peak at around 50 °C. With the addition of polymer, which does not have a thermodynamic transition in this range, two peaks become evident in the heating trace, indicating possible phase separation. The effect does not show up in subsequent traces, possibly because of

polymer degradation at high temperature. To remedy this, the experiment was attempted with POPE:CL, which has a gelation temperature of 20 °C. Addition of the polymer increased the gelation point on the heating curve, and created two peaks on the cooling curve. The authors argue that this is evidence that the polymer binds to cardiolipin and forces separation of the lipids into CL-rich and PE-rich phases.

To observe permeation through both the inner and outer membranes of gram-negative bacteria, Epanand et al. used two probes on a modified strain of *E. coli*. The *E. coli* strain was modified to lack lactose permease and express a  $\beta$ -lactamase. The first probe was a chromogenic  $\beta$ -lactam antibiotic. The antibiotic can only cross the outer membrane once the membrane is permeabilized, where it is then opened by the  $\beta$ -lactamase residing in the periplasm. The ring-opened form of the antibiotic absorbs at 486 nm which can be monitored. The cells show a gradual permeabilization of the outer membrane over the course of an hour. Melittin, by contrast, permeabilizes the outer membrane very quickly. To monitor inner membrane permeabilization, o-nitrophenyl-3-D-galactoside (ONPG) is used. ONPG cannot cross the inner membrane by itself but cleaves in the cytoplasm to o-nitrophenol, which absorbs at 420 nm. In the presence of melittin, the inner membrane is permeabilized quickly, with almost no delay from the outer membrane pore formation. With the antimicrobial polymer, however, the inner membrane was very slowly permeabilized, and only after a substantial delay from the outer membrane. Surprisingly, the inner membrane was only permeabilized at low polymer concentrations. The experiment was repeated with bacteria capable of actively transporting ONPG across the inner membrane, and the result was the same. ONPG was hydrolyzed in the cells at low polymer concentrations, but stopped at higher concentrations. The authors suggest that the polymer is somehow inhibiting transport of ONPG across the outer membrane at higher polymer concentrations.

Lastly, the authors used a SYTO 9/propidium iodide assay to test the overall membrane integrity after exposure to the polymer. At low doses, the membrane becomes more porous to the propidium iodide, but at high doses, the permeability of the membranes is again reduced. It should be noted, however, that this result did not correspond with cell death. Thus, it was suggested that some other method of cell toxicity must be at work for higher polymer concentrations.

#### **1.2.4 Imide-Based ROMP Polycations**

Ring-opening metathesis polymerization provides a platform on which to create living polymers with varied biologically active functionalities.[40-42] These polymers have been used both for antimicrobial and cell-penetrating peptide mimic purposes. The first class of ROMP polymers made used an imide-functionalized oxanorbornene structure.[40] Ilker et al.[43] designed a series of monomers with amine side chains and varying degrees of backbone hydrophobicity (Figure 1.4). This arrangement was meant to mimic the facially amphiphilic structure of magainin, an antimicrobial polymer found in frogs. Magainin has an  $\alpha$ -helical structure, with largely cationic residues displayed on one side and hydrophobic residues on another side.[44] Previous work had shown that small molecules containing a facially amphiphilic structure could be similarly antimicrobial without a helical structure.[45, 46] In this motif, each individual monomer is facially amphiphilic across the backbone, instead of using comonomers or placing both the hydrophobic and cationic regions on the same side chain (Figure 1.4).

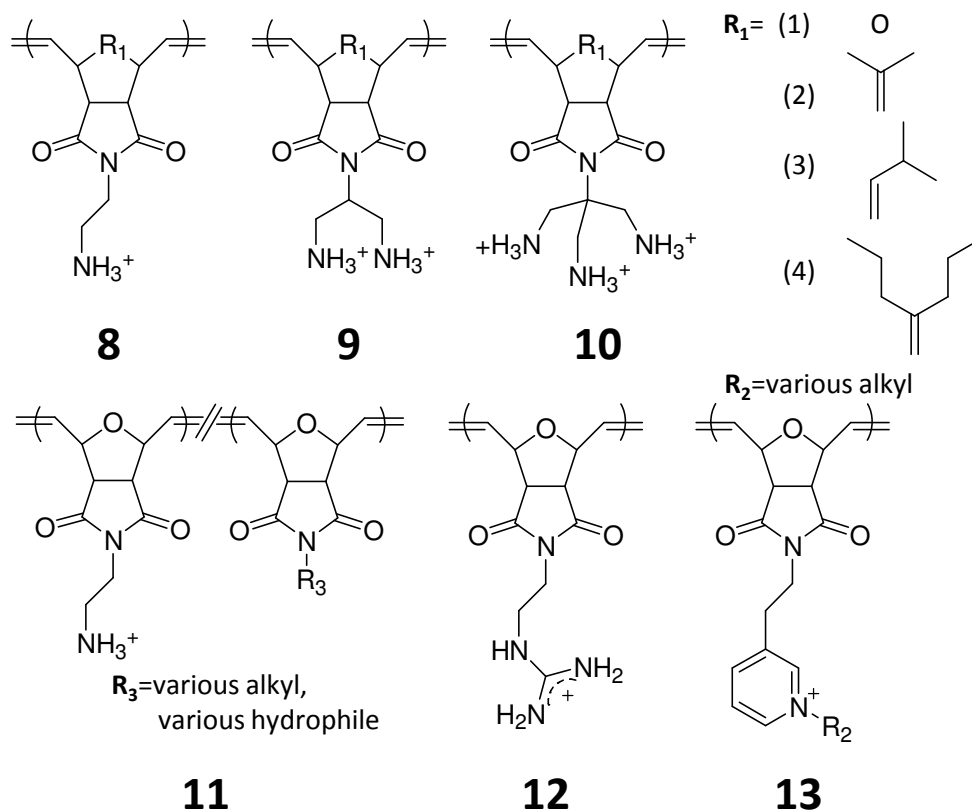


**Figure 1.4.** Imide-based ROMP antimicrobials.

The backbone was made with four different increasingly hydrophobic functionalities (series **8**). Polymerization by ring-opening metathesis polymerization used modified Grubbs' catalysts. The boc groups were removed postpolymerization with trifluoroacetic acid. Homopolymers made from the first monomer were relatively inactive against bacteria and nonhemolytic. Polymer **8-(2)** was only weakly antimicrobial, but still not hemolytic. Polymers made from the third monomer were somewhat effective against bacteria and very hemolytic. Polymers made from the most hydrophobic monomer were hemolytic but less antibacterial. None of the homopolymers were highly antibacterial and selective. Copolymers of **8-(2)** and **8-(3)**, however, were antimicrobial and strongly selective, suggesting that the proper degree of amphiphilicity was to be found between the two monomer types. The best performing of these

polymers had an MIC of 40  $\mu\text{g}/\text{mL}$  against both *B. subtilis* and *E. coli* and a selectivity ratio of over 100.

As an alternative to forming copolymers of **8-(2)** and **8-(3)**, both of which were partially active, Colak et al.[47] took the toxic **8-(3)** and introduced hydrophilic comonomers to increase the polymer selectivity. **8-(3)** was polymerized with different comonomers containing sugar, carbobetaine, and PEG functionalities, respectively. The 50:50 8-(3):carbobetaine copolymer had substantially improved selectivity, with MICs of 150  $\mu\text{g}/\text{mL}$  against *S. aureus* and 200  $\mu\text{g}/\text{mL}$  against *E. coli*.

The interaction of the homopolymers of this series with biomimetic vesicles was examined by Gabriel et al.[48] to understand the mechanism of antimicrobial activity and selectivity. Dye leakage of quenched calcein-filled vesicles was measured upon exposure to polymers of series 8. The vesicles consisted of 3:1 POPE:POPG lipids to mimic the composition of *E. coli* membranes. Across the series, dye leakage correlated with antimicrobial activity, suggesting the polymers may operate by permeabilizing the cell membranes. The interaction of the polymers with these vesicles was also examined under dynamic light scattering. Polymers **8-(2)** and **8-(3)**, which had some antimicrobial activity, caused the vesicles to aggregate, while polymer **8-(1)**, which was not antimicrobial, did not create any aggregation, despite its cationic nature. This aggregation behavior also contrasts with a detergent, which simply lyses vesicles and does not create vesicle aggregation. This aggregation behavior was also observed for both live *E. coli* and vesicles by fluorescence microscopy.

Binding of the polymers to *E. coli* vesicle mimics was measured quantitatively by ITC. Polymers **8-(1)** and **8-(4)**, which were not antimicrobial, showed little binding. Polymers **8-(2)** and **8-(3)**, which showed more activity, showed a strong binding endotherm. This indicates that the hydrophobic nature of the polymers is necessary to properly bury the polymer into the

membrane, while polymer **8-(4)** preferred self-association over membrane binding. From these studies, the antimicrobial polymers were shown to bind to *E. coli* vesicle mimics and insert into the membrane causing the vesicles to aggregate. The nonactive polymers shared none of these attributes.

This class of polymers was expanded by Al-Badri et al.[49] to include polymers with multiple cationic groups. It was found that for hydrophobic **9-(3)**, doubling the cationic content reduced hemolysis while leaving antibacterial activity unaffected. For the less hydrophobic polymer **9-(1)**, the increasing cationic nature improved activity against gram-positive *S. aureus*, but not gram-negative *E. coli*, while leaving hemolytic activity unaltered.

ROMP polymers with alkyl pyridinium moieties were also synthesized (**13**).[50] The ethyl and butyl pyridinium polymers were not only nonhemolytic but were also not strongly active against either *E. coli* or *B. subtilis*. Polymers with longer alkyl chains were not only antibacterial but also moderately hemolytic. The most selective polymer found was the hexyl polymer, with MIC values of 12.5  $\mu\text{g}/\text{mL}$  against *E. coli* and 4  $\mu\text{gml}^{-1}$  against *B. subtilis*, with an  $\text{HC}_{50}$  of 202  $\mu\text{g}/\text{mL}$ .

Similar to the above work with methacrylates and  $\beta$ -peptides, polymers containing random combinations of hydrophobic and hydrophilic side groups were created by Gabriel et al.[51] Both cationic and hydrophobic monomers possessed an oxanorbornene base. A large variety of hydrophobic alkyl side groups were used for the hydrophobic monomers. In contrast to the results for other polymers, none of the created copolymers showed selective antimicrobial activity. All of the created polymers were either nonantimicrobial or hemolytic. The authors suggest that the result stresses the importance of local over global amphiphilicity.

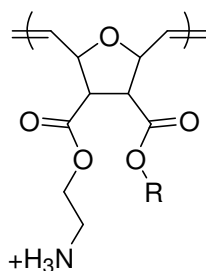
Gabriel et al.[52] also synthesized guanidine-rich oxanorbornene polymers (PGON) (**12**). Unlike the amine version of the same polymer, the PGON homopolymer was found to be both

antimicrobial and selective, with a selectivity ratio of 125 against *S. aureus* and 250 against *E. coli*. It was expected that like the other antimicrobial polymers described above, PGON would induce leakage in *E. coli* mimic POPE/POPG vesicles but not mammalian mimic POPC vesicles. Surprisingly, PGON did not induce leakage in the POPE/POPG vesicles, indicating that the antibacterial mode of action is not membrane disruption like the other polymers, but instead some other mechanism. The cause of PGON's antimicrobial activity is still being investigated.

### 1.2.5 Ester- and Amide-Based ROMP Polycations

In addition to the imide-based structures listed above, both single- and double-armed ester structures have been examined in contact with lipid membranes. Lienkamp et al.[41, 53, 54] introduced double-armed ester-based ROMP polymers (**14**) (Figure 1.5). The imide-based antimicrobial molecules have the disadvantage of requiring significant synthesis. Instead of giving the polymers amphiphilicity across the backbone, these polymers contain cationic and hydrophobic 'arms', which likely segregate in solution.[41]





R=methyl, ethyl, propyl  
butyl, ethylammonium

## 14

**Figure 1.5.** Ester-based ROMP antimicrobials.

Biological activity of the homopolymers was measured by inhibitory assays of *E. coli* and *S. aureus* bacteria and hemolysis of RBCs. The methyl polymers were inactive and nontoxic, the propyl polymers were active and toxic, and the ethyl polymers were selective but not impressively so. MW was found to be exceptionally important. Higher MW propyl polymers were more active against *E. coli* as well as more toxic, but were progressively less effective against *S. aureus*. This effect was attributed to stronger binding of longer polycations to the peptidoglycan layer of the gram-positive bacteria. Copolymers of methyl, ethyl, and propyl monomers were synthesized. The methyl/propyl copolymers were especially effective against *S. aureus*, with a selectivity of over 500. What was surprising (and previously unprecedented) was that while these polymers were very effective against *S. aureus*, they possessed no antimicrobial activity against *E. coli*.

This same synthetic approach was also used to create diamine ROMP monomers.[54] The homopolymers were again selective for *S. aureus*, but not for *E. coli*. Since the diamine monomers closely resembled the methyl monomers in terms of hydrophobicity, copolymers of these two monomers were used to examine the importance of charge density. There was a significant increase in *S. aureus* activity with increasing diamine content from 0% to 10%, but a

slow decrease in activity at higher ratios. It was thus hypothesized that the polymer needed to overcome a 'threshold' of cationic content to be active, but that additional cations do not improve antimicrobial activity.

The diamine polymers were used to investigate the cause of this 'double selectivity' further.[53] Gram-positive and gram-negative bacteria have significant differences in membrane composition. Gram-positive bacteria have a single phospholipid membrane containing significant amounts of cardiolipin (DPG), with a thick peptidoglycan layer on the outside. Gram-negative bacteria have two phospholipid membranes consisting of PE and PG lipids, with a thin peptidoglycan layer between them and a lipopolysaccharide (LPS) layer on the outside. There are thus features of *E. coli* which might inhibit activity: the number of membranes, membrane composition, and the LPS layer. The first possibility was tested by perforating the outer membrane of *E. coli* with EDTA and running the usual MIC<sub>90</sub> experiment. Removing the outer layer made the polymer antimicrobial, with an MIC<sub>90</sub> of 100 µg/mL. Dye leakage experiments were performed with CF-loaded vesicles of *E. coli*- and *S. aureus*-like lipid compositions and no significant differences were observed. In a similar dye leakage experiment, LPS was incubated with the polymer for varying lengths of time before injection in the vesicle solution. LPS did inhibit dye leakage, but only after 15 min of incubation with the polymer before injection into the vesicle solution. This means that the 'double selectivity' is likely due to the outer membrane limiting polymer exposure to the inner membrane, and possibly retarding LPS binding.

The study also approached the earlier question of why longer polymers had lower activity against *S. aureus*. To test the original hypothesis that the polymer was binding to the peptidoglycan layer, the polymer was incubated with peptidoglycan extract. Binding of the polymer to peptidoglycan does reduce dye leakage, but only after long incubation of the peptidoglycan with the polymer before injection into the vesicle solution. The conclusion is that

binding to the peptidoglycan layer is likely not the cause of the reduced activity of the larger molecules. The authors hypothesize that the reduction in activity may instead be due to the peptidoglycan layer acting as a sieve for larger molecules.

### **1.2.6 Conjugated Polycations**

The use of conjugated polymers has been thoroughly investigated by Schanze and Whitten. Chemburu et al.[55] created a series of polyphenylene ethynylene (PPE) biocidal polymers (Figure 1.6). Conjugated polymers containing quaternary ammonium and oligo-ethylene glycol side chains were made (**15**), as well as polymers containing doubly cationic DABCO-based side chains (**17**). Both classes of molecule were polymerized by Sonogashira coupling. These polymers were shown to have significant bactericidal activity at relatively low concentrations. They were less effective, however, when incubated without light exposure. Infrared spectroscopy showed the presence of singlet oxygen generated in solution by the polymer after exposure to visible light. The authors thus suggest that the polymer, upon light exposure, generates singlet oxygen that adds to the killing efficiency of the polymer. This process is not likely to be selective. As an expansion of this concept, the authors coated silica particles with the quaternary ammonium polymer using a grafting from process. The DABCO polymers were physisorbed onto negatively charged silica particles. These polymer beads were found to successfully attract and kill bacteria, causing the beads to quickly become coated in dead bacteria. The DABCO-PPE-coated beads were shown to be similarly effective when made by a layer-by-layer deposition when combined with an anionic PPE.[56]

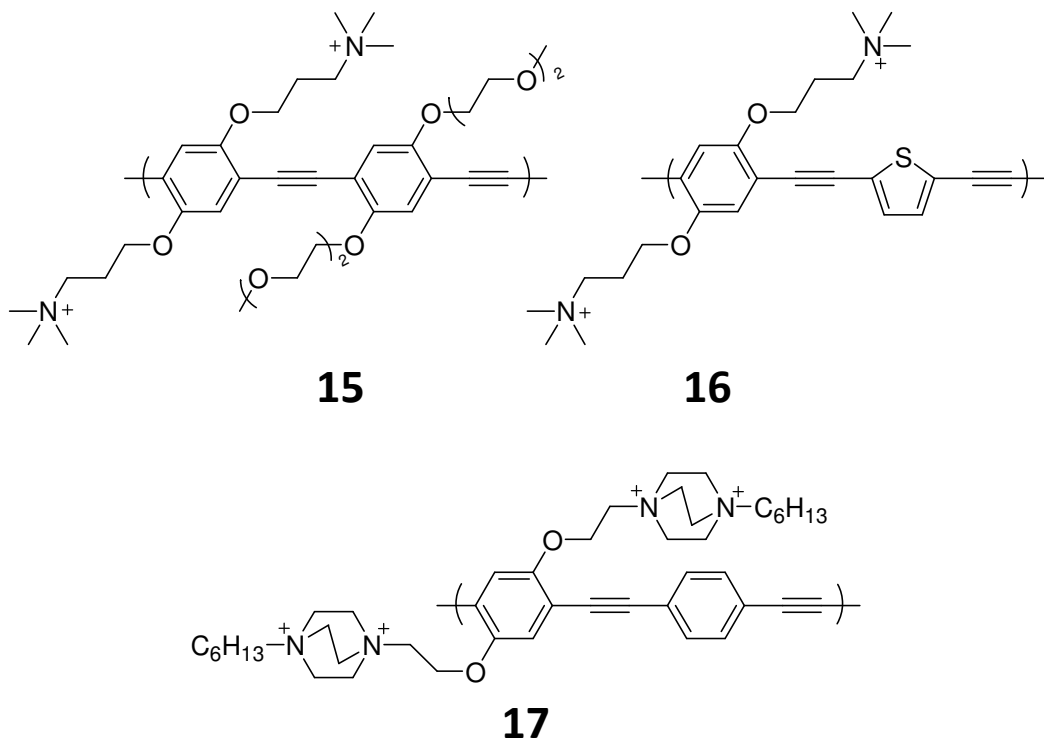


**Figure 1.6.** Conjugated Polycations

Further work involved the creation of a conjugated polymer with quaternary ammonium side chains and an alternating phenylene–ethynylene–thiophene–ethynylene backbone (**16**).<sup>[57]</sup> These polymers were also physisorbed onto silica beads. As with the other polymers, they showed the ability to attract and kill bacteria. Unlike previous polymers, however, light exposure appeared to inhibit bacterial growth. Furthermore, free polymer in solution appeared to be far more effective at killing *P. aeruginosa* than previous polymers. Infrared spectroscopy studies showed that the thiophene-containing polymer produced less singlet oxygen in water upon light exposure, an event attributed to reduced solubility of the polymer, and thus less exposure of the polymer to molecular oxygen dissolved in the water.

This hypothesis was tested by extensive examination of polymer–lipid interactions by Ding et al.<sup>[58]</sup> Both **16** and **17** showed an increase in fluorescence emission when combined with DOPG vesicles in solution, indicating that the polymer binds to the vesicle preferentially

over remaining in solution. An aqueous quencher was introduced to determine if the polymer sits on the inside or outside of the vesicles. Without vesicles, AQS quenched the fluorescence of both polymers almost completely. When **16** was combined with DOPG vesicles, very little quenching was seen, even after 5 min. With **17**, fluorescence was quenched for an hour. This indicates that **17** stays on the outside of the lipid membrane much longer and takes longer to insert itself. Studies of the interactions of both polymers with DMPG lipids at the air/water interface also suggested far stronger and kinetically faster interactions with **16** than **17**.

To examine polymer selectivity, the same tests were run with **16** and vesicles containing different lipid headgroups.[59] As before, the polymer was shown to bind and insert into DPPG vesicles. When the polymer was left in a solution of zwitterionic DPPE and DPPC vesicles, the fluorescence was strongly reduced by the aqueous quenching agent, indicating that the polymer does not insert into these vesicles. The fact that these polymers inserted into anionic lipids common in bacteria but not into zwitterionic lipids common in mammalian cells suggested possible selectivity. This was later confirmed by fluorescein leakage from vesicles.[60] DOPG/DOPE (bacterial mimic), *E. coli* lipid extract, and DOPC/cholesterol (mammalian mimic) vesicles were loaded with quenched fluorescein dye and exposed to all three polymers created above. All three polymers caused significant leakage in the DOPG/DOPE vesicles and very little leakage of the DOPC/cholesterol vesicles. For the *E. coli* lipid vesicles, **17** induced significant leakage, while the other two polymers induced only minor leakage. This further promotes the hypothesis that these polymers may indeed be selective towards killing bacteria and not mammalian cells.

### **1.2.7 The State of Antimicrobial and Biocidal Cationic Polymer Research**

As is clearly evident from the work above, there is a rich diversity of cationic polymer structures available, and strong structure-property relationships have been established. To be active antimicrobials, polymers need sufficient cationic content and hydrophobicity to penetrate bacterial lipid membranes. To be selective, however, there also needs to be a limit to those components so that they do not penetrate mammalian lipid membranes. This means that there is often a “sweet spot” or ideal balance of functional group content that leads to effective antimicrobial polymers.

Additionally, much headway has been made in understanding the nature of the interaction between these polymer and bacterial lipid membranes. Differences in lipid content are clearly linked to antimicrobial activity and selectivity. A selective antimicrobial polymer will induce dye release in a bacterial lipid membrane mimic (usually containing a phosphatidylethanolamine/phosphatidylglycerol mixture or cardiolipin), but not a mammalian one (usually phosphatidylcholine), suggesting that the differences between these lipid systems are critical to activity and selectivity. While bacterial membranes generally contain more anionic content than mammalian ones, binding studies often conflict over whether anion/polycation binding is critical to activity. The answer is more likely to be found in the work of Wong and colleagues, with small molecule- and peptide-based antimicrobials.[61-65] Here, there is a clearly established relationship between the formation of negative Gaussian curvature phases in bulk membrane systems and antimicrobial activity. The difference between activity in bacterial membranes and inactivity in mammalian ones lies in the negative intrinsic curvature contributed by phosphatidylethanolamine and cardiolipin.[61-63] This feature is discussed in more detail in section 1.3.2 of this introduction and chapters 4 and 5 of this work.

This work on cationic antimicrobials constitutes a framework for understanding PTDMs. A combination of binding studies, dye release experiments, and membrane curvature studies like those found in the antimicrobial literature above will be used in this thesis to better understand PTDM-membrane interactions.

### **1.3 Protein Transduction Domains and their Synthetic Mimics**

#### **1.3.1 Cell Studies of PTDs**

The protein transduction domain Tat was simultaneously and independently discovered by Frankel and Pabo[66] and Green and Loewenstein.[67] Tat had previously been well understood as a trans-activator protein that enhances the expression of HIV genes. As a method to quantifiably measure this trans-activation process, Frankel and Pabo scrape-loaded cells with purified Tat. The scrape loading damaged the cell membrane sufficiently to allow protein into the cells. As a control, however, they also simply introduced purified protein into an undamaged cell culture. To their surprise, Tat was able to induce trans-activation in the latter control case, although it required about an order of magnitude more protein to achieve the same result. This was relatively unheard of, as 86 base-pair molecules such as Tat are generally not capable of passing through cell membranes. Green and Loewenstein were similarly attempting to understand how trans-activation occurs, and were using microinjection to deliver both the HIV plasmid and purified Tat protein. Strong binding between the plasmid and Tat, however, limited the activity of the Tat protein. Rather than depend on sequential microinjections, the authors attempted to use microinjections for the plasmid and simply add Tat to the cell medium. To their surprise, much like Frankel and Pabo, they found that Tat was successfully able to cause trans-activation by simple introduction to the cell medium.

Furthermore, through the use of deletion mutants, they showed that region II (residues 38-48) and region III (residues 49-57) were both necessary and sufficient to cause trans-activation. The authors speculated that region II was the portion that caused trans-activation and that region III, which was highly basic and included 6 arginine residues, was necessary for membrane transport and nuclear localization.

Fawell et al.[68] subsequently determined that Tat<sub>37-72</sub>, was capable of carrying cargo into cells when covalently bound together. Truncated Tat was in separate experiments covalently bound to  $\beta$ -galactosidase and horseradish peroxidase (HRP). After exposure to the conjugate, the cells were then fixed and exposed to stains. Several different cell lines were tested, and all showed similar uptake, with punctuate endosomal uptake as well as diffuse staining in the cytosol. This was the first case of what would become the now-standard procedure of covalently bonding PTDs to desired cargo.

Vivès et al.[69] further narrowed the region of importance for cellular uptake. The authors used truncated peptides conjugated to fluorescein dye. HeLa cells were incubated with the dye-labeled peptides, fixed, and imaged under a confocal microscope. Peptides with only residues 48-60 showed no reduction in uptake, but others that truncated this region were unable to deliver to cells. Unlike previous studies, this was also the first case where Tat uptake in a cell was imaged directly. Most impressively, the imaged showed diffuse cytosolic uptake in addition to the regions concentrated inside endosomes. This uptake was maintained for cells both when the cells were cooled to 4°C and when endocytosis was chemically inhibited.

The major discovery in terms of understanding the necessary structural elements of this peptide was made by Wender et al. in 2000.[5] While previous studies all focused on small modifications and truncations of the natural peptide sequence, this study demonstrated that the major contributing element was the presence of arginine residues, and no other structural



or chemical contribution by other residues was necessary. Cellular uptake of fluorescein-labeled peptides was measured by flow cytometry. Deletion studies of Tat demonstrated that uptake was greatly diminished upon the deletion of any basic residue, but not the uncharged glutamine. Furthermore, oligomers of arginine showed improved uptake over Tat<sub>49-57</sub> and the non-natural D-oligomers showed higher uptake still. This latter attribute was due to the lack of enzymatic degradation of non-natural peptide, but was also an exceptionally important discovery. If natural peptides were unnecessary, then it is likely only the primary structure—more specifically, the presence of guanidinium side groups—that is required for polymer uptake.

This discovery of “arginine magic”, that all that was necessary for cellular uptake was a chain of guanidinium moieties, created an enormous boom of non-natural structures known as protein transduction domain mimics (PTDMs). Guanidinium-rich molecules in the form of peptides,  $\beta$ -peptides, peptoids, dendrimers, and polysaccharides were created to be used in delivery.[3] This array of molecules is too vast and wide ranging to be recounted in detail here, and is well-covered in the review listed. A more detailed review of synthetic polymer PTDMs is supplied in later sections of this introduction.

As mentioned above, most of the studies up to this point showing high cytosolic delivery in cells used a fixation step before determining the location of uptake. A 2003 study by Richard et al.[6] determined that much of the apparent cytosolic delivery was due to the use of formaldehyde as a fixing agent. The authors performed experiments similar to Vivès, except comparing uptake to that done without a fixation step. Cells that were not fixed showed polymer only in endosomes, an indication that uptake was limited largely to those regions. Furthermore, flow cytometry studies were performed with the use of trypsin to remove peptide accumulated on the surface of cells that has not been internalized. While cells incubated at 37°C still had significant uptake, cells incubated at 4°C or with depleted ATP levels had greatly

reduced uptake. This led the authors to conclude that cellular uptake was predominantly due to endocytosis.

This explanation was not wholly satisfying, however. In order for Tat to function in the way initially described by Frankel, Pabo, Green and Loewenstein, Tat must be definition be able to pass into the cytosol intact while the cell is still alive. There must be some amount of peptide, then, that is able to escape the endosome. Indeed, the continued use of Tat and related peptides as a delivery system belies this fact. This class of molecules has been widely used for the delivery of biologically active molecules,[4, 70, 71] which would not be possible without endosomal escape. It is also worth noting that in the Richard study, while the uptake of Tat at 4°C was nearly 0, the uptake of oligoarginine was still present (albeit only 10%).[6] This suggests that while only a small fraction of the uptake may be energy independent, it was still a possibility.

With a revised set of standards in mind, several studies confirmed that the majority of uptake of Tat and related peptides was by endocytosis. HeLa cell incubation, trypsinization and FACS of the oligoarginine peptide R8 showed a significant decrease in cellular uptake, much as in the Richard study.[72] In this case, however, a more substantial fraction (70%) of the activity remained. There is relatively little commentary on this difference, and it is uncertain whether the residual peptide uptake is due to energy-independent uptake incomplete inhibition of endocytosis. The authors also note that the macropinocytosis inhibitor EIPA reduces R8 uptake by a small but statistically significant amount, suggesting that at least some of the energy-dependent uptake is due to this process. Another study shows similar results, again showing that lowering cellular temperature to 4C causes a measurable drop in Tat uptake, although again not to 0.[73] Upon exposure to numerous macropinocytosis inhibitors, peptide uptake is

decreased by as much as 60%, suggesting that raft-mediated endocytosis. Macropinocytosis was cited in additional other studies as well, under similar circumstances.[74, 75]

This view, that the remaining activity after cooling cells to 4°C is due to energy-independent uptake, has persisted, as repeated tests have shown that some amount of activity remains. In fact, in two cases involving the bone marrow leukemia cell line KG1a, uptake was strangely shown to *increase* at 4°C.[7, 76] While this also calls into question the effectiveness of cooling cells to inhibit endocytosis (Chapter 2 of this thesis will focus on that), it also suggests that a substantial fraction of peptide uptake may indeed be independent of endocytosis and macropinocytosis. Attention then turned to precisely *how* these peptides are able to cross the cell membrane. Unfortunately, living cells presents complicated systems. Not only must energy-dependent processes like endocytosis be accounted for, but the membrane itself, as described earlier, contains proteins, sterols, polysaccharides, and other components that make direct, mechanistic observations difficult. Thus, much of the biophysical studies performed for this class of molecule involves model membrane systems, generally just consisting of phospholipids. While they do not encompass the full complexity of cell membranes, they are simple enough that real, mechanistic observations can be made with them.

### **1.3.2 Biophysical Studies of PTDs**

Some of the most pioneering work in this field came from the Matile Group of the Université de Genève.[77-79] Two general experimental frameworks were used to examine the transport of the polymers across the lipid bilayer. The first is what is called the “U-tube experiment”. Chloroform is placed in a U-shaped tube between two aqueous regions, so that the only way a substance could pass from one region to the other is through the hydrophobic chloroform phase. This region of chloroform was used as a model for the membrane. While

such a system lacks either the chemical composition or the dimension of a lipid bilayer, it has the advantage of a much larger distance, meaning that any the hydrophobic phase can be directly sampled in a way not possible with a bilayer. Carboxyfluorescein, a hydrophilic, anionic dye, was placed in one aqueous region, and diffusion into the hydrophobic phase was monitored. Not surprisingly, carboxyfluorescein alone did not move into chloroform, nor did it move in the presence of polyarginine.[77] However, when polyarginine was mixed with an amphiphilic anion before addition, dye was seen inside the chloroform phase. This did not occur for polylysine, suggesting that the bitentate nature and higher pKa of the cation contributed to complexation. Some chloroform was even found to transport across the hydrophobic phase into the *trans* aqueous region.

The second techniques used was dye release from vesicles. This is to some extent the simplest test of membrane activity possible. As had been shown in the section on antimicrobial polymers, this test provides a simple model for the permeation of the cellular membrane. Large unilamellar vesicles are filled with a quenched dye that becomes fluorescent upon escape. This allows for direct monitoring of activity in real time, but it does not directly make any mechanistic claims, except that said activity is purely energy-independent. Again, polyarginine alone did not cause much dye release, but adding instead a mixture of polyarginine and amphiphilic anions greatly increased dye release.[77, 78] Perhaps most interesting, activity for polyarginine was even increased in the presence of egg yolk phosphatidylglycerol (EYPG) in the bilayer (rather than mixed with the polymer). From this, the authors concluded that the polymer must bind to the anions, become integrated in the membrane, and the more hydrophobic mixture is allowed to pass through the hydrophobic bilayer. This process was called "adaptive translocation."

The use of these amphiphilic anions was applied to HeLa cells. Pyrenebutyrate was found to be particularly effective, and its combination with GFP and polyarginine allowed for rapid delivery to the cytosol.[79] While this approach is not practical, as competition with anions present in serum reduces the effectiveness of delivery, it suggests that the biophysical studies are an accurate descriptor of what happens in a cell culture.

Dye release was also used to examine the interaction of the amphiphilic PTD transportan with phospholipid membranes.[37] The kinetic data, along with measuring the change in tryptophan fluorescence upon interaction with the bilayer, allowed the authors to create a kinetic model for peptide interaction involving both surface binding and insertion of the peptide into the membrane. The authors found that while the peptide did bind more strongly to anionic 2:8 POPS:POPC membranes than to zwitterionic POPC membranes, this did not result in significantly different rates of dye release. This, they argue was because the limiting step to dye release was not surface association by insertion, and those rates were determined to be fundamentally similar. These results are fundamentally different from the above ones for polyarginine, though it is important to note that transportan contains fewer arginines and more lysines and hydrophobic monomers, meaning that its mechanism of activity may be fundamentally different from arginine-rich PTDs.

Similarly, penetratin and R9 were shown to bind more strongly to anionic lipid-containing membranes than purely zwitterionic ones. Plasmon waveguide resonance (PWR) spectroscopy of the amphiphilic PTD penetratin showed that it bound more than twice as strongly to EYPG vesicles as EYPC ones.[80] Isothermal titration calorimetry (ITC) gave strong binding traces for R9 with DSPG vesicles, but no measurable trace with DSPC vesicles.[81] Neither of these studies, though, are able to make more generalized statements about the

implications of this difference in binding for membrane activity. We thus have an incomplete story of the importance of anionic lipid in PTD activity.

Work examining the ability of PTDs to form negative Gaussian curvature phases has its roots in the antimicrobial literature. The formation of a toroidal pore in a phospholipid membrane is exceptionally difficult to observe directly, both because of the dimensions involved (the bilayer is ~5nm thick) and the fluid nature of the membrane. Such pores, though, do have geometric constraints. A bisection of the inside of a toroidal pore matches the shape of saddle, with orthogonal positive and negative curvatures. Since the product of these two signs is negative, such shapes are said to have *negative Gaussian curvature*. Much of the antimicrobial literature for a long time assumed it was the higher anionic content of bacterial cells that made them selectively susceptible to cationic antimicrobial compounds. Bacteria also differ in the intrinsic curvature content of their lipids, however. The lipid content of mammalian cells is dominated by the phosphatidylcholine, which has nearly zero intrinsic curvature.[82] (Figure 1.7) Bacteria, however, contain large quantities of phosphatidylethanolamine (PE) lipids and cardiolipin (CL), which have a negative intrinsic curvature. By creating bulk phases of these lipids, it can be shown that antimicrobials are able to form negative Gaussian curvature phases only in the presence of high negative intrinsic curvature lipid content.[61-63, 65] This means that the antimicrobials are capable of producing positive curvature, but not negative curvature, and that they are thus able to form pores in membranes containing high quantities of PE, but not those high in PC.

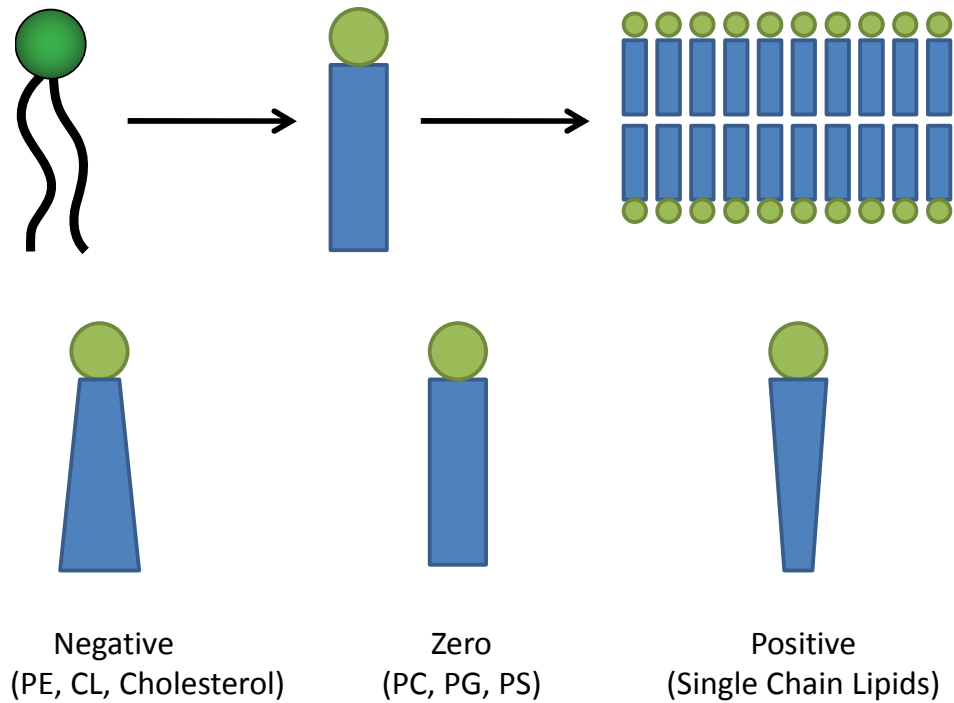


**Figure 1.7.** Lipids and intrinsic curvature.

It turns out that there is a strong resemblance between antimicrobial peptides (AMPs) and PTDs. A survey of both naturally-occurring PTDs and AMPs show that there is a general trade-off between the number of arginine residues in CPPS and the number of both lysine and hydrophobic residues.[83] It is perhaps not surprising, then, that PTDs like Tat and oligoarginine are able to induce negative Gaussian curvature phases in high-PE lipid systems.[11, 84] Less, clear, however, is the link between this behavior and activity in *mammalian* cells. As mentioned before, mammalian cells lack high quantities of PE, and PTDs do not form such phases in PC lipids.

### 1.3.3 Molecular Dynamics Simulations

While the molecular dynamics has only lightly explored the world of PTD-membrane interactions, some important contributions have been made. Of particular note is the work of

the Deserno group. The first work examines how the shape of particles influences how they interact with membranes.[85] Such work is important for understanding endocytotic processes, membrane protein aggregation, viral attachment, and lipid scavenging. Thirty-six spherical ‘caps’ were placed on a tensionless membrane. Small caps only cause a small perturbation, but larger caps cause clustering and then vesiculation of the membrane. For yet larger caps, vesiculation begins before the caps have aggregated into a single mass, leading to several vesiculations and the formation of sealed pockets beneath the new membrane containing the caps. When full, spherical capsids were tested, the effect was even more exaggerated. The authors comment that this type of aggregation and vesiculation is likely to be very common in cellular processes.

A separate study by Herce and Garcia[86] shows a similar mode of uptake of the Tat peptide in a simulated mammalian membrane. As with the antimicrobials, this model requires that multiple Tat peptides penetrate the membrane together. The crowding of peptides cause a thinning of the membranes, and then the peptides begin to insert into the membrane. The insertion of the peptides results in the formation of a narrow 3 nm pore.

#### **1.3.4 Polymer-Based PTDMs**

While the above works have provided some insight into the interaction of PTDs with cellular membranes, they are handicapped by a lack of structural diversity. While many of the studies alter peptide length and make individual sequence alterations, polymers allow for a vastly greater diversity of structures. As has been seen in earlier sections of this chapter, antimicrobial polymers have taken on enormously diverse structures and enormous insight into their function has been gained by subtle alterations in their composition. By comparison, the world of polymeric protein transduction domain mimics (PTDMs) is much smaller and less diverse. There are only a few groups actively pursuing polymer PTDMs and fewer still are



creating polymers with highly controlled functional and architectural properties. Using this kind of polymer template, we are able to more deeply understand the effects of hydrophobicity, charge, aromaticity, architecture, and length in a way not previously available, leading to both a better fundamental understanding of PTDM-membrane interactions as well as design rules for better delivery vectors.

The first polymer PTDMs were both based on ring-opening metathesis (ROMP) and were introduced by the Tew and Kiessling groups. Kolonko et al.[87] used a postpolymerization approach to create guanidine-rich norbornene-based polymers (**18**). An activated ester norbornene monomer was polymerized using a modified Grubbs' catalyst. The ester was substituted with a guanidine moiety postpolymerization. A dye was also added to the end of the polymer via a ketone-containing polymerization quenching agent attached to the end of the polymer. The interaction of the dye-labeled polymer with HeLa cells was tracked by confocal microscopy. The polymers were shown to both accumulate in endosomes and diffuse in the cytoplasm when incubated at room temperature. Cells were also incubated with the polymer at 4 °C to halt endocytosis, which the authors report demonstrated no intake. It was thus presumed that the polymer enters the cells only by energy-dependent pathways. This polymer template was expanded to include separately functionalizable random and block copolymers.[42] These polymers were shown to have similar uptake properties, suggesting viability as drug carriers.

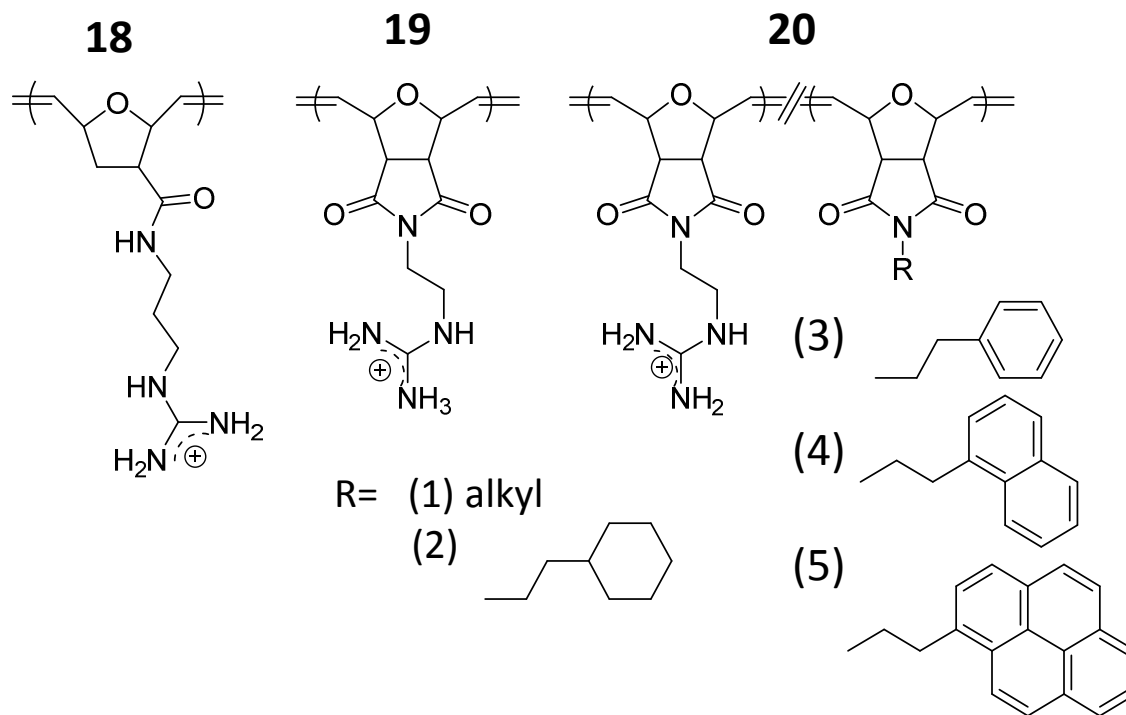


**Figure 1.8.** Amide and Imide-based ROMP PTDMs.

The poly(guanidinium-rich oxanorbornene) (PGON, **19**) had previously been introduced by the Tew group as an antimicrobial polymer capable of killing bacteria without causing substantial membrane disruption.[52] These polymers were shown by Hennig et al to also present many similar properties to polyarginine.[88] Similar to polyarginine, their ability to cross the lipid membrane and cause dye release from vesicles was greatly increased when the polymer was allowed to complex with activating counterions. An important distinction from polyarginine, however, was that the presence of EYPG inhibited dye release from the vesicles. The reason for this difference between polyarginine and PGON is unknown.

This library was expanded to include an ester based design similar to that used for antimicrobial polymers, but with a guanidinium functionality. The dual-armed nature of the monomer allowed for the comparison of the activity of a singly-functionalized polymer (**21-(1)**) to one with dual guanidinium moieties per residual monomer unit (**21-(3)**). Combining this with

length adjustments, it was possible to account for the relationship between membrane activity and guanidinium density. These polymers were labeled with NBD dye and their uptake was measured in HEK293T cells. To distinguish between polymer simply accumulated on the surface of the cell and polymer inside the cell proper, the cell cultures were washed with sodium dithionite solution. Overall cell association scaled with polymer length, but the di-functionalized polymers outperformed similar-length mono-functionalized ones with lower toxicity at 4°C. This suggested that high guanidinium density improved overall cellular uptake.

While the ability of polyarginine to cross phospholipid membranes requires complexation with amphiphilic anions, polymers can incorporate hydrophobic moieties directly into the main chain.[89] Furthermore, these hydrophobic moieties can themselves be tuned, allowing for easily scalable hydrophobicities. Both imide and ester structures were examined. **(20-(1), 21-(1))** Their activity was measured as a function of dye release from vesicles. In both series, activity was improved by additional hydrophobicity only up to a point. Once the hydrophobic moieties was stronger than a butyl group, the polymer began to have reduced activity, most likely due to precipitation in solution.

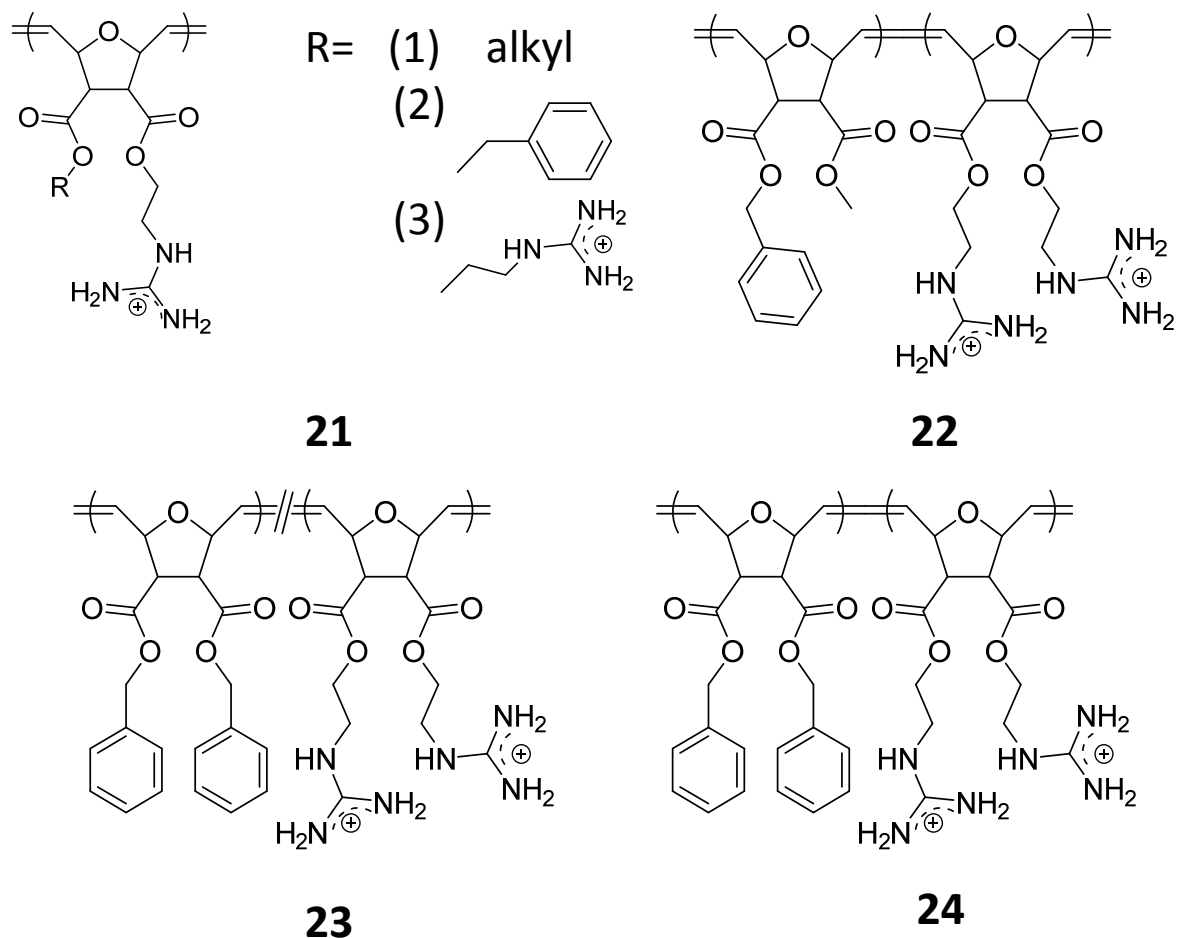


**Figure 1.9.** Ester-based ROMP PTDMs.

The importance of aromatic functionality was also examined. Trans membrane proteins generally have unusually high quantities of aromatic residues, especially concentrated in so-called “aromatic belts” at either end of the transmembrane region.[90-92] Additionally, aromatic peptide residues interact more strongly with phospholipid bilayers than would be expected based purely upon their hydrophobicity. A comparison of octanol-water to phospholipid-water partitioning demonstrated that aromatic residues associate unusually strongly with phospholipids.[93] This suggests that there is some important interaction between the aromatic residues and the polar regions of the phospholipid membrane. The exact cause of this favorability is uncertain, although NMR studies[92] suggested that it may be due to

a combination of the flat geometry of the aromatic ring as well as the shared electronic structure and its various interactions with charged and polar molecules. Dye release studies of similarly hydrophobic aromatic and non-aromatic PTDMs (**20(2-5)**) suggested that the aromatic structures may have slightly higher activity.[94]

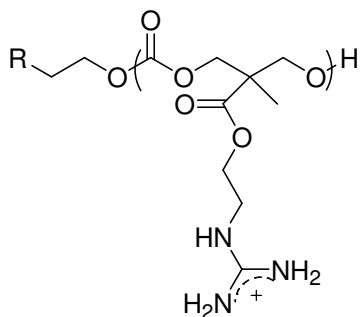
A fundamentally new class of polymer PTDM was created for the purpose of non-covalent delivery of PTDMs. Most delivery schemes for the delivery of biomolecules by PTDM involve covalently bonding the peptide to the desired delivery component.[4] This is not convenient, however, as it requires specialized synthesis of your cargo and delivery vector. Much preferable would be a system where the PTDM and cargo could simply be mixed in solution in preparation for delivery. This is much the way Pep-1, a chimeric peptide, functions.[95] Similar to that, a PTDM block copolymer structure containing a guanidinium-rich region and a hydrophobic region was created.[96] (**22**) The unique construction allows the polymer to combine with the cargo in solution, while maintaining its capacity for uptake. First, uptake of FITC-labeled siRNA was measured, and it was shown that dye was present in cells both at 37°C and at 4°C (although greatly reduced in the latter). Uptake of the FITC-siRNA was also an order of magnitude higher for the block copolymer than the homopolymer. More impressive was the actual knockdown data. The block copolymer-siRNA combination was able to knock down NOTCH1 expression in Jurkat T cells by 50%, while no other delivery system was able to achieve any knockdown at all.

One strong difference between the homopolymer and the block copolymer was that the homopolymer was far less hydrophobic than the block copolymer. Was the improved activity really due to the architecture, or was it due to the hydrophobicity? Sgolastra et al. created a series of polymers with identical hydrophobic content but different polymer architectures.[97] A block copolymer structure was similar to the one studied above, (**24**) but alongside that were

examined a homopolymer where one arm was hydrophobic and the other a guanidinium moiety **(21-(2))** and a “gradient” copolymer, where guanidinium and hydrophobic moieties were polymerized together to give a partially segregated system.**(23)** While dye release of these polymers generated similar EC<sub>50</sub> values, the maximum amount of dye released varied widely. For some reason, the block copolymer only release about 50% dye at maximum, while the homopolymer released 90%, with the gradient polymer was in-between. Similar results were seen in cellular uptake studies, where the block copolymer was the least effective of the three. It should be cautioned, however, that uptake is different than active cargo delivery, and as-yet unpublished data shows that the block copolymer is still superior to the homopolymer for protein delivery.[98]

In addition to the ROMP-based structures described above, ring-opened carbonate polymers containing guanidine functionality have also been synthesized by Cooley et al. (C31).[99] The fluorescently labeled oligomer was shown to have comparable uptake to oligoarginine in Jurkat cells by flow cytometry.

Confocal microscopy showed that the oligomer was internalized into the cells, though it did not show definitive evidence of escape of the polymer into the cytosol. To verify the ability of this drug delivery system to introduce cargo to the cytosol, luciferin was attached to the initiator thiol group. In the cell, if the system is effective, the thiol bond is broken, and luciferin is converted to oxyluciferin, releasing light. Thus, by measuring the light output of the system, the kinetics of drug release can be measured. While the delivery was shown to be effective, drug release was not as quick as with similarly fashioned octaarginine peptides. Delivery appeared to be hindered by high potassium salt concentrations.



**25**

**Figure 1.10.** Carbonate-Based PTDMs.

#### **1.4 The Scope of this Thesis**

The combination of cell and biophysical studies using both peptide and polymer systems has led to important progress in the understanding of PTDMs and their interactions with cell membranes. At the core, guanidinium-rich peptides have high uptake in cells, much higher than for other charged macromolecules. This activity is generally not driven by exact secondary structure or receptor-specific activity, and is transferrable to guanidinium-containing polymers with different backbones. Membrane activity of these polymers is increased in biophysical experiments by the addition of hydrophobicity to the polymer, either through the complexation of amphiphilic anions, or by the addition of hydrophobic moieties to the backbone. The use of block copolymers allowed for the transport of large macromolecular cargo into cells without the use of covalent bonding.

Despite this progress, however, there is still a lack of detailed understanding of how this PTDM uptake occurs, and how features such as hydrophobicity and charge contribute to polymer activity. How much of PTDM uptake is energy-dependent versus energy-independent is still hotly debated, and the intermolecular driving force for such energy-independent uptake is

still unknown. This thesis will focus on three important aspects of PTDM-membrane interactions: membrane phase, anionic lipid content, and negative curvature generation. Cooling cells to 4°C is a widely used technique in distinguishing between energy dependent and energy-independent uptake processes. Between 4°C and 37°C, however, mammalian lipid membranes undergo a phase transition, and the effect of that transition on PTDM activity is unknown. Previous work has not critically examined this relationship, and instead simply assumes that the change in temperature has no measurable effect on energy-independent uptake. Chapter 2 examines the activity of a range of polymers against membranes both in the fluid as well as gel phases, demonstrating that cooling lipid membranes has a substantial effect on their permeability to PTDMs, and that these considerations must be taken into account when considering the prevalence of energy-independent uptake.

As mentioned above, the literature discussing the importance of anionic lipid content is not straightforward. While anionic lipid content is generally seen as necessary for “adaptive translocation”, empirical evidence supporting this claim is conflicting for different classes of PTDM (as shown in section 1.3.2). Additionally, while peptide systems have been examined, the effect of anionic lipids in polymer PTDM activity has not been determined. Chapter 3 will examine the effect of anionic lipid content on ROMP-based PTDM activity. The results contradict the adaptive translocation model for this subset of polymers and instead suggest that anionic lipid content inhibits PTDM activity. This has important implications both for our mechanistic understanding as well as for the design of improved molecules.

The final two chapters examine the ability of ROMP-based PTDMs to induce negative Gaussian curvature in bulk lipid systems. The variables of polymer length, hydrophobicity, aromaticity, and architecture are all examined. It is shown that all but aromaticity play key roles



in determining how these polymers are able to induce curvature. It is still unclear, however, how much this ability is linked to membrane activity.

This thesis, then, presents a step forward in our understanding of the interaction of guanidinium-rich polymers with phospholipid membranes. The final section describes some of the remaining gaps in our knowledge, and suggests approaches to explore and fill those gaps.

## 1.5 References

1. Schwarze, S.R., K.A. Hruska, and S.F. Dowdy, *Protein transduction: unrestricted delivery into all cells?* Trends in Cell Biology, 2000. **10**(7): p. 290-295.
2. Stanzl, E.G., et al., *Fifteen Years of Cell-Penetrating, Guanidinium-Rich Molecular Transporters: Basic Science, Research Tools, and Clinical Applications*. Accounts of Chemical Research, 2013.
3. Wender, P.A., et al., *The design of guanidinium-rich transporters and their internalization mechanisms*. Advanced Drug Delivery Reviews, 2008. **60**(4-5): p. 452-472.
4. Heitz, F., M.C. Morris, and G. Divita, *Twenty years of cell-penetrating peptides: from molecular mechanisms to therapeutics*. British Journal of Pharmacology, 2009. **157**(2): p. 195-206.
5. Wender, P.A., et al., *The design, synthesis, and evaluation of molecules that enable or enhance cellular uptake: Peptoid molecular transporters*. Proceedings of the National Academy of Sciences of the United States of America, 2000. **97**(24): p. 13003-13008.
6. Richard, J.P., et al., *Cell-penetrating Peptides*. Journal of Biological Chemistry, 2003. **278**(1): p. 585-590.
7. Al-Taei, S., et al., *Intracellular Traffic and Fate of Protein Transduction Domains HIV-1 TAT Peptide and Octaarginine. Implications for Their Utilization as Drug Delivery Vectors*. Bioconjugate Chemistry, 2006. **17**(1): p. 90-100.
8. Futaki, S., *Membrane-permeable arginine-rich peptides and the translocation mechanisms*. Advanced Drug Delivery Reviews, 2005. **57**(4): p. 547-558.
9. Kosuge, M., et al., *Cellular Internalization and Distribution of Arginine-Rich Peptides as a Function of Extracellular Peptide Concentration, Serum, and Plasma Membrane Associated Proteoglycans*. Bioconjugate Chemistry, 2008. **19**(3): p. 656-664.
10. Drin, G., et al., *Studies on the Internalization Mechanism of Cationic Cell-penetrating Peptides*. Journal of Biological Chemistry, 2003. **278**(33): p. 31192-31201.
11. Mishra, A., et al., *Translocation of HIV TAT peptide and analogues induced by multiplexed membrane and cytoskeletal interactions*. Proceedings of the National Academy of Sciences of the United States of America, 2011. **108**(41): p. 16883-16888.
12. Räägel, H., P. Säälük, and M. Pooga, *Peptide-mediated protein delivery--Which pathways are penetrable?* Biochimica et Biophysica Acta (BBA) - Biomembranes, 2010. **1798**(12): p. 2240-2248.
13. Gabriel, G.J., et al., *Infectious disease: Connecting innate immunity to biocidal polymers*. Materials Science and Engineering: R: Reports, 2007. **57**(1-6): p. 28-64.

14. Gabriel, G.J. and G.N. Tew, *Conformationally rigid proteomimetics: a case study in designing antimicrobial aryl oligomers*. *Organic & Biomolecular Chemistry*, 2008. **6**(3): p. 417-423.
15. Simon, S.A. and T.J. McIntosh, *Peptide-Lipid Interactions* 2002: Academic Press. 606.
16. Nelson, D.L. and M.M. Cox, *Lehninger Principles of Biochemistry, Fourth Edition*. 4th edition ed2004, New York: W. H. Freeman. 1100.
17. Israelachvili, J., *Intermolecular and surface forces*. 3rd ed. ed2011, Burlington MA: Academic Press.
18. Cevc, G. and D. Marsh, *Phospholipid bilayers: physical principles and models* 1987: Wiley. 472.
19. Gunstone, F., *The Lipid handbook*. 2nd ed. ed1994, London ;;New York: Chapman and Hall.
20. Ikeda, T., et al., *Interaction of a polymeric biguanide biocide with phospholipid membranes*. *Biochimica et Biophysica Acta (BBA) - Biomembranes*, 1984. **769**(1): p. 57-66.
21. Davies, G.E., et al., *1:6-di-4'-chlorophenyldiguanidohexane ("hibitane")*. *Laboratory investigation of a new antibacterial agent of high potency*. *British Journal of Pharmacology and Chemotherapy*, 1954. **9**(2): p. 192-196.
22. Rose, F.L. and G. Swain, *850. Bisbiguanides having antibacterial activity*. *Journal of the Chemical Society (Resumed)*, 1956.
23. Davies, A., M. Bentley, and B.S. Field, *Comparison of the Action of Vantocil, Cetrimide and Chlorhexidine on Escherichia coli and its Spheroplasts and the Protoplasts of Gram Positive Bacteria*. *Journal of Applied Microbiology*, 1968. **31**(4): p. 448-461.
24. Davies, A. and B.S. Field, *Action of Biguanides, Phenols and Detergents on Escherichia coli and its Spheroplasts*. *Journal of Applied Microbiology*, 1969. **32**(2): p. 233-243.
25. Ikeda, T., S. Tazuke, and M. Watanabe, *Interaction of biologically active molecules with phospholipid membranes: I. Fluorescence depolarization studies on the effect of polymeric biocide bearing biguanide groups in the main chain*. *Biochimica et Biophysica Acta (BBA) - Biomembranes*, 1983. **735**(3): p. 380-386.
26. Ikeda, T., H. Yamaguchi, and S. Tazuke, *Phase separation in phospholipid bilayers induced by biologically active polycations*. *Biochimica et Biophysica Acta (BBA) - Biomembranes*, 1990. **1026**(1): p. 105-112.
27. Ikeda, T., et al., *Time-resolved fluorescence anisotropy studies on the interaction of biologically active polycations with phospholipid membranes*. *Biochimica et Biophysica Acta (BBA) - Biomembranes*, 1990. **1021**(1): p. 56-62.
28. Kanazawa, A., T. Ikeda, and T. Endo, *Polymeric phosphonium salts as a novel class of cationic biocides. IV. Synthesis and antibacterial activity of polymers with phosphonium salts in the main chain*. *Journal of Polymer Science Part A: Polymer Chemistry*, 1993. **31**(12): p. 3031-3038.
29. Ikeda, T., H. Yamaguchi, and S. Tazuke, *New polymeric biocides: synthesis and antibacterial activities of polycations with pendant biguanide groups*. *Antimicrobial Agents and Chemotherapy*, 1984. **26**(2): p. 139-144.
30. Kuroda, K. and W.F. DeGrado, *Amphiphilic Polymethacrylate Derivatives as Antimicrobial Agents*. *Journal of the American Chemical Society*, 2005. **127**(12): p. 4128-4129.
31. Ivanov, I., et al., *Characterization of Nonbiological Antimicrobial Polymers in Aqueous Solution and at Water-Lipid Interfaces from All-Atom Molecular Dynamics*. *Journal of the American Chemical Society*, 2006. **128**(6): p. 1778-1779.

32. Palermo, E.F. and K. Kuroda, *Chemical Structure of Cationic Groups in Amphiphilic Polymethacrylates Modulates the Antimicrobial and Hemolytic Activities*. *Biomacromolecules*, 2009. **10**(6): p. 1416-1428.
33. Palermo, E.F., I. Sovadinova, and K. Kuroda, *Structural Determinants of Antimicrobial Activity and Biocompatibility in Membrane-Disrupting Methacrylamide Random Copolymers*. *Biomacromolecules*, 2009. **10**(11): p. 3098-3107.
34. Kuroda, K., G.A. Caputo, and W.F. DeGrado, *The Role of Hydrophobicity in the Antimicrobial and Hemolytic Activities of Polymethacrylate Derivatives*. *Chemistry – A European Journal*, 2009. **15**(5): p. 1123-1133.
35. Wenk, M.R. and J. Seelig, *Magainin 2 Amide Interaction with Lipid Membranes: Calorimetric Detection of Peptide Binding and Pore Formation<sup>†</sup>*. *Biochemistry*, 1998. **37**(11): p. 3909-3916.
36. Wieprecht, T., M. Beyermann, and J. Seelig, *Binding of Antibacterial Magainin Peptides to Electrically Neutral Membranes: Thermodynamics and Structure<sup>†</sup>*. *Biochemistry*, 1999. **38**(32): p. 10377-10387.
37. Yandek, L.E., et al., *Mechanism of the Cell-Penetrating Peptide Transportan 10 Permeation of Lipid Bilayers*. *Biophysical Journal*, 2007. **92**(7): p. 2434-2444.
38. Epand, R.F., et al., *Dual Mechanism of Bacterial Lethality for a Cationic Sequence-Random Copolymer that Mimics Host-Defense Antimicrobial Peptides*. *Journal of Molecular Biology*, 2008. **379**(1): p. 38-50.
39. Mowery, B.P., et al., *Mimicry of Antimicrobial Host-Defense Peptides by Random Copolymers*. *Journal of the American Chemical Society*, 2007. **129**(50): p. 15474-15476.
40. Ilker, M.F., H. Schule, and E.B. Coughlin, *Modular Norbornene Derivatives for the Preparation of Well-Defined Amphiphilic Polymers: Study of the Lipid Membrane Disruption Activities*. *Macromolecules*, 2004. **37**(3): p. 694-700.
41. Lienkamp, K., et al., *Antimicrobial Polymers Prepared by ROMP with Unprecedented Selectivity: A Molecular Construction Kit Approach*. *Journal of the American Chemical Society*, 2008. **130**(30): p. 9836-9843.
42. Kolonko, E.M., et al., *General Synthetic Route to Cell-Permeable Block Copolymers via ROMP*. *Journal of the American Chemical Society*, 2009. **131**(21): p. 7327-7333.
43. Ilker, M.F., et al., *Tuning the Hemolytic and Antibacterial Activities of Amphiphilic Polynorbornene Derivatives*. *Journal of the American Chemical Society*, 2004. **126**(48): p. 15870-15875.
44. Zasloff, M., *Magainins, a class of antimicrobial peptides from *Xenopus* skin: isolation, characterization of two active forms, and partial cDNA sequence of a precursor*. *Proceedings of the National Academy of Sciences of the United States of America*, 1987. **84**(15): p. 5449-5453.
45. Tew, G.N., et al., *De novo design of biomimetic antimicrobial polymers*. *Proceedings of the National Academy of Sciences of the United States of America*, 2002. **99**(8): p. 5110-5114.
46. Liu, D., et al., *Nontoxic Membrane-Active Antimicrobial Arylamide Oligomers<sup>13</sup>*. *Angewandte Chemie International Edition*, 2004. **43**(9): p. 1158-1162.
47. Colak, S., et al., *Hydrophilic Modifications of an Amphiphilic Polynorbornene and the Effects on its Hemolytic and Antibacterial Activity*. *Biomacromolecules*, 2009. **10**(2): p. 353-359.
48. Gabriel, G.J., et al., *Interactions between Antimicrobial Polynorbornenes and Phospholipid Vesicles Monitored by Light Scattering and Microcalorimetry*. *Langmuir*, 2008. **24**(21): p. 12489-12495.

49. Al-Badri, Z.M., et al., *Investigating the Effect of Increasing Charge Density on the Hemolytic Activity of Synthetic Antimicrobial Polymers*. *Biomacromolecules*, 2008. **9**(10): p. 2805-2810.
50. Eren, T., et al., *Antibacterial and Hemolytic Activities of Quaternary Pyridinium Functionalized Polynorbornenes*. *Macromolecular Chemistry and Physics*, 2008. **209**(5): p. 516-524.
51. Gabriel, G.J., et al., *Comparison of Facially Amphiphilic versus Segregated Monomers in the Design of Antibacterial Copolymers*. *Chemistry - A European Journal*, 2009. **15**(2): p. 433-439.
52. Gabriel, G.J., et al., *Synthetic Mimic of Antimicrobial Peptide with Nonmembrane-Disrupting Antibacterial Properties*. *Biomacromolecules*, 2008. **9**(11): p. 2980-2983.
53. Lienkamp, K., et al., *"Doubly Selective" Antimicrobial Polymers: How Do They Differentiate between Bacteria?* *Chemistry - A European Journal*, 2009. **15**(43): p. 11710-11714.
54. Lienkamp, K., et al., *Antimicrobial Polymers Prepared by Ring-Opening Metathesis Polymerization: Manipulating Antimicrobial Properties by Organic Counterion and Charge Density Variation*. *Chemistry - A European Journal*, 2009. **15**(43): p. 11715-11722.
55. Chemburu, S., et al., *Light-Induced Biocidal Action of Conjugated Polyelectrolytes Supported on Colloids*. *Langmuir*, 2008. **24**(19): p. 11053-11062.
56. Corbitt, T.S., et al., *Conjugated Polyelectrolyte Capsules: Light-Activated Antimicrobial Micro "Roach Motels"*<sup>†</sup>. *ACS Applied Materials & Interfaces*, 2009. **1**(1): p. 48-52.
57. Corbitt, T.S., et al., *Light and dark biocidal activity of cationic poly(arylene ethynylene) conjugated polyelectrolytes*. *Photochemical & Photobiological Sciences*, 2009. **8**(7).
58. Ding, L., et al., *Insight into the Mechanism of Antimicrobial Poly(phenylene ethynylene) Polyelectrolytes: Interactions with Phosphatidylglycerol Lipid Membranes*<sup>††</sup> *Langmuir 25th Year: Molecular and macromolecular self-assemblies*. *Langmuir*, 2009. **25**(24): p. 13742-13751.
59. Ding, L., et al., *Insight into the Mechanism of Antimicrobial Conjugated Polyelectrolytes: Lipid Headgroup Charge and Membrane Fluidity Effects*. *Langmuir*, 2010. **26**(8): p. 5544-5550.
60. Wang, Y., et al., *Membrane Perturbation Activity of Cationic Phenylene Ethynylene Oligomers and Polymers: Selectivity against Model Bacterial and Mammalian Membranes*. *Langmuir*, 2010. **26**(15): p. 12509-12514.
61. Yang, L., et al., *Synthetic Antimicrobial Oligomers Induce a Composition-Dependent Topological Transition in Membranes*. *Journal of the American Chemical Society*, 2007. **129**(40): p. 12141-12147.
62. Yang, L., et al., *Mechanism of a prototypical synthetic membrane-active antimicrobial: Efficient hole-punching via interaction with negative intrinsic curvature lipids*. *Proceedings of the National Academy of Sciences*, 2008. **105**(52): p. 20595-20600.
63. Som, A., et al., *Divalent Metal Ion Triggered Activity of a Synthetic Antimicrobial in Cardiolipin Membranes*. *Journal of the American Chemical Society*, 2009. **131**(42): p. 15102-15103.
64. Schmidt, N.W., et al., *Criterion for amino acid composition of defensins and antimicrobial peptides based on geometry of membrane destabilization*. *Journal of the American Chemical Society*, 2011. **133**(17): p. 6720-6727.

65. Schmidt, N.W., et al., *Arginine in  $\alpha$ -defensins: differential effects on bactericidal activity correspond to geometry of membrane curvature generation and peptide-lipid phase behavior*. The Journal of biological chemistry, 2012. **287**(26): p. 21866-21872.
66. Frankel, A.D. and C.O. Pabo, *Cellular uptake of the tat protein from human immunodeficiency virus*. Cell, 1988. **55**(6): p. 1189-1193.
67. Green, M. and P.M. Loewenstein, *Autonomous functional domains of chemically synthesized human immunodeficiency virus tat trans-activator protein*. Cell, 1988. **55**(6): p. 1179-1188.
68. Fawell, S., et al., *Tat-mediated delivery of heterologous proteins into cells*. Proceedings of the National Academy of Sciences, 1994. **91**(2): p. 664-668.
69. Vivès, E., P. Brodin, and B. Lebleu, *A Truncated HIV-1 Tat Protein Basic Domain Rapidly Translocates through the Plasma Membrane and Accumulates in the Cell Nucleus*. Journal of Biological Chemistry, 1997. **272**(25): p. 16010-16017.
70. Mäe, M. and Ü. Langel, *Cell-penetrating peptides as vectors for peptide, protein and oligonucleotide delivery*. Current Opinion in Pharmacology, 2006. **6**(5): p. 509-514.
71. Snyder, E.L. and S.F. Dowdy, *Cell Penetrating Peptides in Drug Delivery*. Pharmaceutical Research, 2004. **21**(3): p. 389-393.
72. Nakase, I., et al., *Cellular Uptake of Arginine-Rich Peptides: Roles for Macropinocytosis and Actin Rearrangement*. Molecular Therapy, 2004. **10**(6): p. 1011-1022.
73. Kaplan, I.M., J.S. Wadia, and S.F. Dowdy, *Cationic TAT peptide transduction domain enters cells by macropinocytosis*. Journal of Controlled Release, 2005. **102**(1): p. 247-253.
74. Fretz, M., et al., *Effects of Na<sup>+</sup>/H<sup>+</sup> exchanger inhibitors on subcellular localisation of endocytic organelles and intracellular dynamics of protein transduction domains HIV-TAT peptide and octaarginine*. Journal of Controlled Release, 2006. **116**(2): p. 247-254.
75. Nakase, I., et al., *Interaction of Arginine-Rich Peptides with Membrane-Associated Proteoglycans Is Crucial for Induction of Actin Organization and Macropinocytosis<sup>†</sup>*. Biochemistry, 2007. **46**(2): p. 492-501.
76. Fretz, Marjan M., et al., *Temperature-, concentration- and cholesterol-dependent translocation of L- and D-octa-arginine across the plasma and nuclear membrane of CD34<sup>+</sup> leukaemia cells*. Biochemical Journal, 2007. **403**(2).
77. Sakai, N. and S. Matile, *Anion-Mediated Transfer of Polyarginine across Liquid and Bilayer Membranes*. Journal of the American Chemical Society, 2003. **125**(47): p. 14348-14356.
78. Nishihara, M., et al., *Arginine magic with new counterions up the sleeve*. Organic & Biomolecular Chemistry, 2005. **3**(9): p. 1659-1669.
79. Takeuchi, T., et al., *Direct and Rapid Cytosolic Delivery Using Cell-Penetrating Peptides Mediated by Pyrenebutyrate*. ACS Chemical Biology, 2006. **1**(5): p. 299-303.
80. Alves, I.D., et al., *Relationships between Membrane Binding, Affinity and Cell Internalization Efficacy of a Cell-Penetrating Peptide: Penetratin as a Case Study*. PLoS ONE, 2011. **6**(9).
81. Walrant, A., et al., *Different membrane behaviour and cellular uptake of three basic arginine-rich peptides*. Biochimica et Biophysica Acta (BBA) - Biomembranes, 2011. **1808**(1): p. 382-393.
82. Zimmerberg, J. and M.M. Kozlov, *How proteins produce cellular membrane curvature*. Nature Reviews Molecular Cell Biology, 2006. **7**(1): p. 9-19.

83. Mishra, A., et al., *Translocation of HIV TAT peptide and analogues induced by multiplexed membrane and cytoskeletal interactions*. Proceedings of the National Academy of Sciences, 2011. **108**(41): p. 16883-16888.
84. Mishra, A., et al., *HIV TAT Forms Pores in Membranes by Inducing Saddle-Splay Curvature: Potential Role of Bidentate Hydrogen Bonding*. Angewandte Chemie International Edition, 2008. **47**(16): p. 2986-2989.
85. Reynwar, B.J., et al., *Aggregation and vesiculation of membrane proteins by curvature-mediated interactions*. Nature, 2007. **447**(7143): p. 461-464.
86. Herce, H.D. and A.E. Garcia, *Molecular dynamics simulations suggest a mechanism for translocation of the HIV-1 TAT peptide across lipid membranes*. Proceedings of the National Academy of Sciences, 2007. **104**(52): p. 20805-20810.
87. Kolonko, E.M. and L.L. Kiessling, *A Polymeric Domain That Promotes Cellular Internalization*. Journal of the American Chemical Society, 2008. **130**(17): p. 5626-5627.
88. Hennig, A., et al., *Stimuli-Responsive Polyguanidino-Oxanorbornene Membrane Transporters as Multicomponent Sensors in Complex Matrices*. Journal of the American Chemical Society, 2008. **130**(31): p. 10338-10344.
89. Som, A., et al., *Self-Activation in De Novo Designed Mimics of Cell-Penetrating Peptides*. Angewandte Chemie International Edition, 2011. **50**(27): p. 6147-6150.
90. Killian, J.A. and G. von Heijne, *How proteins adapt to a membrane–water interface*. Trends in Biochemical Sciences, 2000. **25**(9): p. 429-434.
91. White, S.H. and W.C. Wimley, *MEMBRANE PROTEIN FOLDING AND STABILITY: Physical Principles*. Annual Review of Biophysics and Biomolecular Structure, 1999. **28**(1): p. 319-365.
92. Yau, W.-M., et al., *The Preference of Tryptophan for Membrane Interfaces†*. Biochemistry, 1998. **37**(42): p. 14713-14718.
93. Wimley, W.C. and S.H. White, *Experimentally determined hydrophobicity scale for proteins at membrane interfaces*. Nature Structural & Molecular Biology, 1996. **3**(10): p. 842-848.
94. Som, A., A. Reuter, and G.N. Tew, *Protein Transduction Domain Mimics: The Role of Aromatic Functionality*. Angewandte Chemie International Edition, 2012. **51**(4): p. 980-983.
95. Deshayes, S., et al., *Delivery of proteins and nucleic acids using a non-covalent peptide-based strategy*. Advanced Drug Delivery Reviews, 2008. **60**(4–5): p. 537-547.
96. Tezgel, A.Ö., et al., *Novel Protein Transduction Domain Mimics as Nonviral Delivery Vectors for siRNA Targeting NOTCH1 in Primary Human T cells*. Molecular Therapy, 2013. **21**(1): p. 201-209.
97. Sgolastra, F., et al., *The Importance of Sequence Specific Hydrophobicity in Synthetic Protein Transduction Domain Mimics*. Biomacromolecules, 2014. **15**(3): p. 812-820.
98. Sgolastra, F., et al., *Sequence Segregation Improves Non-covalent Protein Delivery*, 2014, University of Massachusetts--Amherst: Amherst, MA.
99. Cooley, C.B., et al., *Oligocarbonate Molecular Transporters: Oligomerization-Based Syntheses and Cell-Penetrating Studies*. Journal of the American Chemical Society, 2009. **131**(45): p. 16401-16403.

## CHAPTER 2

### THE LOW TEMPERATURE UPTAKE OF PROTEIN TRANSDUCTION DOMAIN MIMICS IS AFFECTED BY LIPID PHASE

#### 2.1 Introduction

Protein transduction domains (PTDs), also known as cell-penetrating peptides, are cation-rich protein segments capable of high uptake into cells.[1-3] Several varieties of these molecules, including the arginine-rich Tat peptide from HIV, have been extensively used as vectors for protein, DNA, and siRNA delivery into cells.[4] For Tat-based systems, it has been shown that guanidine functionality, but not specific secondary structure, is critical for uptake,[5] providing a set of basic parameters for a variety of synthetic mimics. These include discrete oligomers and macromolecules based on oligoarginines,  $\beta$ -peptides, peptoids, dendrimers, polysaccharides, and synthetic polymers, comprising a class of protein transduction domain mimics (PTDMs).[3] To this wide array of designs, our research group has contributed a library of polyoxanorbornene-based polymers.[6-10]

Despite the wide-ranging utility of PTDs and their mimics, their uptake mechanism is still under considerable debate.[11-17] Most critically, there has been much research comparing the amount of cellular uptake by energy-dependent (endocytosis, macropinocytosis) and energy-independent (pore formation, membrane diffusion, translocation) mechanisms.[8, 11, 12, 15, 18, 19] This is an important distinction because molecules internalized by energy-dependent means are entrapped in endosomes, potentially limiting their value as carriers. One common method for distinguishing between these two forms of internalization is to compare PTDM uptake in cells at physiological conditions to that in cells with inhibited endocytotic pathways, either by ATP depletion or by cooling the cells to 4°C. Sodium azide inhibits mitochondrial

oxidative phosphorylation, reducing the amount of available ATP in the cell, thus retarding cellular metabolism.[20] Cooling cells to 4°C also reduces cellular metabolism.[21] While both approaches are fairly common, there is little data directly comparing the two, particularly within the realm of PTDMs.[11] Without such a direct comparison, it is difficult to tell if either experiment is influencing the purported outcome beyond simply reducing endocytosis. As demonstrated here, however, these two methods produce inconsistent results, suggesting that indeed reducing membrane temperature also affects energy-independent uptake.

Of particular concern is the effect temperature plays on the ability of PTDMs to interact with the cell membrane. Phospholipid membranes undergo phase transitions at temperatures specific to their lipid composition (acyl chain lengths and degrees of unsaturation). The reduction in lipid lateral mobility that occurs below the liquid-to-gel transition causes an increase in membrane rigidity, as well as a decrease in the amount of penetration by non-ionic pluronics.[22, 23]

Reports show that Chinese hamster lung cells have a broad liquid-to-gel transition between 7 and 37°C, while bovine oocytes have their temperature transition in the 10 to 20°C range.[24, 25] Since the process of cooling cells from 37°C to 4°C crosses both of these temperature regions, it is important to understand the effect of these temperature transitions on PTDM-membrane interactions. The effects of temperature and membrane phase on vector internalization are not well studied, but it is reasonable to consider that molecules whose uptake is primarily driven by membrane interactions would be more strongly affected by lipid phase transitions.

These experiments establish that reducing membrane temperature greatly reduces the membrane activity of ROMP-based PTDMs. While increased polymer hydrophobicity is able to



overcome this barrier, this effect of temperature must be taken into account in experiments designed to distinguish energy-dependent and energy-independent uptake.

## 2.2 Materials and Methods

### 2.2.1 Materials

Maleic anhydride, maleimide, furan, 4-dimethyl aminopyridine (DMAP), 1-(3-Dimethylaminopropyl)-3-ethylcarbodiimide hydrochloride (EDC), methanol, 1,3-Di-Boc-2-(2-hydroxyethyl)guanidine, benzyl alcohol, ethyl vinyl ether and trifluoroacetic acid (TFA) were obtained as reagent grade from Aldrich, Fluka or Acros and used as received. 3<sup>rd</sup> generation Grubbs catalyst (Dichloro-di(3-bromopyridino)-N,N'-Dimesitylenoimidazolino-Ru=CHPh; G3) was synthesized as described previously by Grubbs *et al.*[26] The HPLC grade solvents, ethyl acetate, pentane and hexane, were purchased from Aldrich, Fisher Scientific or Acros and used as received. Tetrahydrofuran (THF) (HPLC grade, Fisher Scientific) was distilled from sodium/benzophenone under nitrogen. Dichloromethane (DCM) (HPLC grade, Fisher Scientific) was distilled from CaH<sub>2</sub> under nitrogen. Spectra/Por<sup>®</sup> Biotech Cellulose Ester (CE) dialysis membranes with the molecular weight cut off (MWCO) of 100-500 and 1000 were purchased from Spectrum Medical Industries. Egg yolk phosphatidylcholine (EYPC) and dipalmitoylphosphatidylcholine (DPPC) were purchased from Avanti Polar Lipids Inc. and 5(6)-carboxyfluorescein (CF) was purchased from Fluka. Pen/Strep antibiotics were purchased from Lonza. 2-Deoxy-D-glucose was from Sigma-Aldrich.

### 2.2.2 Instrumentation

<sup>1</sup>H and <sup>13</sup>C NMR spectra were recorded at 300 MHz and 75 MHz respectively, using a Bruker DPX-300 NMR spectrometer. Chemical shifts ( $\delta$ ) are reported in ppm and coupling

constants ( $J$ ) in Hz. The abbreviations for splitting patterns are: s, singlet; d, doublet; dd, doublet of doublets; t, triplet; q, quartet; m, multiplet; br, broad. Mass spectral data were obtained at the University of Massachusetts, Mass Spectrometry Facility from a JEOL JMS 700 instrument (JEOL, Peabody, MA). Gel permeation chromatography was measured on an Agilent 1260 series GPC setup with a PL Gel 5  $\mu\text{m}$  guard column, two 5  $\mu\text{m}$  analytical Mixed-C columns and a 5  $\mu\text{m}$  analytical Mixed-D column (Agilent), incubated at 40  $^{\circ}\text{C}$ . THF was used as the eluent at a flow rate of 1.0 mL/min. Polystyrene standards were used for the calibration and toluene as flow marker. Vesicle experiments were performed using a Biotek SynergyMx fluorescence plate reader and an Horiba Scientific FluoroLog-3 spectrophotometer.

### 2.2.3 Monomer Synthesis

Figure 2.1 shows the monomers used to synthesize the polymers for this study. All procedures have been previously been reported in the literature. [8, 9, 27-29]

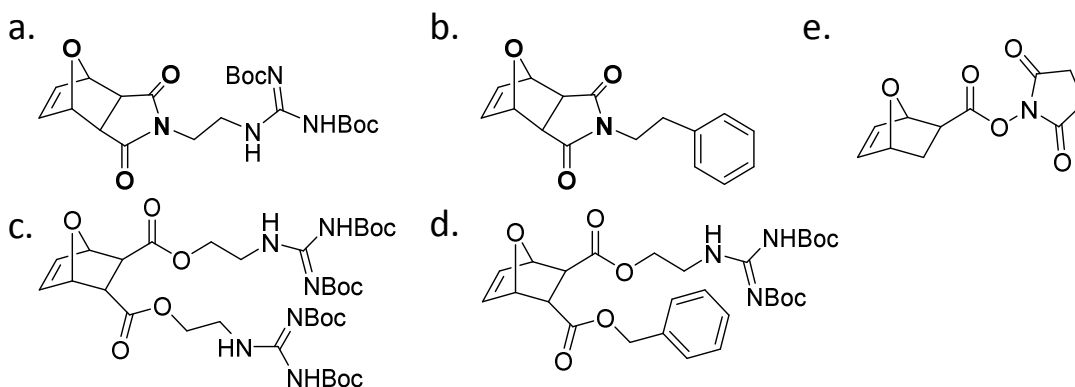


**Figure 2.1.** Monomers used in this study.

### 2.2.4 Polymer Synthesis

Unlabeled polymers were synthesized by ring-opening metathesis polymerization with Grubbs 3<sup>rd</sup> generation catalyst using previously reported methods.[7, 8, 27, 29] As a general

procedure, 200 mg of monomer and the desired amount of catalyst were separately dissolved in dry dichloromethane and placed in Schlenk flasks. The flasks were flooded with nitrogen and the solutions degassed by the freeze-pump-thaw method. The degassed monomer was transferred to the catalyst flask and the reaction was allowed to proceed for 40 minutes at 25°C, after which time the reaction was quenched by 1 mL of ethyl vinyl ether. The imide monomer-based polymers were then precipitated in ether or an ether-pentane mix to separate the polymer from the catalyst, while the diester polymers were precipitated in pentane.

The boc-protected polymers were deprotected in 5 mL 1:1 trifluoroacetic acid (TFA):dichloromethane overnight. TFA was removed by repeated azeotropic distillation with methanol. All polymers were suspended in water and lyophilized for three days, with diester polymers first being dialyzed in water using dialysis membranes with MWCO 100-500 Da.

Dye-labeled polymers were prepared by a similar method, with minor variations. One molar equivalent activated ester monomer was placed in a Schlenk flask with dichloromethane and freeze-pump-thawed, the same as the monomer and catalyst solutions. The activated ester monomer was added to one molar equivalent of Grubbs 3<sup>rd</sup> generation catalyst. After five minutes, 10 equivalents of the desired diester monomer were added to the polymerization reaction. After 60 minutes, the polymerization was quenched with 1 mL of ethyl vinyl ether. The resulting polymer was then precipitated in pentane.

The activated ester polymer was then dissolved in DMF with the TFA salt of [2-(7-nitrobenz-2-oxa-1,3-diazole)-aminoethyl] ammonium (NBD-ethylenediamine) at a molar ratio of 1:1.5 and allowed to stir overnight protected from light.[8] The modified polymer was then precipitated in water, filtered, subsequently deprotected as previously described while protected from light.

**Boc-Protected G<sub>16</sub>**: <sup>1</sup>H-NMR (300 MHz, CD<sub>2</sub>Cl<sub>2</sub>): δ=11.49 (1H, br), 8.45 (1H, br), 7.27 (0.3H, m), 6.08 (trans) and 5.80 (cis) (2H total, br), 5.02 (cis) and 4.48 (trans) (2H total, br), 1.52 (9H, s), 1.47 (9H, br)

**G<sub>16</sub>**: <sup>1</sup>H-NMR (300 MHz, DMSO-*d*<sub>6</sub>): δ=7.88 (1H, br), 7.36 (4H, br), 5.96 (1H, br), 5.74 (1H, br), 4.92 (1H, br), 4.43 (1H, br) 3.47 (4H, br).

**Boc-Protected G<sub>16</sub>-*r*-Ph<sub>4</sub>**: <sup>1</sup>H NMR (300 MHz, CD<sub>2</sub>Cl<sub>2</sub>): δ=11.46 (16H, br), 8.44 (16H, br), 7.21 (20H, br), 6.05 (trans), 5.76 (cis) (40H total, br), 4.99 (40H, br), 4.46 (32H, br), 4.08 (8H, br), 3.73 (48H, br), 3.38 (40H, br) 2.91 (8, br) 1.52 (144H, br), 1.47 (144H, br)

**G<sub>16</sub>-*r*-Ph<sub>4</sub>**: <sup>1</sup>H NMR (300 MHz, DMSO-*d*<sub>6</sub>): δ = 7.27 (20H, br), 5.96-5.72 (40H, br), 4.88 (32H, br), 4.43 (8H, br), 4.10 (8H, br), 2.85 (8H, br)

**Boc-Protected G<sub>16</sub>-*r*-Ph<sub>8</sub>**: <sup>1</sup>H NMR (300 MHz, CD<sub>2</sub>Cl<sub>2</sub>): δ=11.46 (16H, br), 8.44 (16H, br), 7.21 (48H, br), 6.05 (trans), 5.76 (cis) (48H total, br), 4.99 (48H, br), 4.46 (16H, br), 4.08 (8H, br), 3.73 (80H, br), 3.38 (48H, br) 2.91 (16, br) 1.52 (144H, br), 1.47 (144H, br)

**G<sub>16</sub>-*r*-Ph<sub>8</sub>**: <sup>1</sup>H NMR (300 MHz, DMSO-*d*<sub>6</sub>): δ = 7.27 (20H, br), 5.96-5.72 (48H, br), 4.88 (32H, br), 4.43 (16H, br), 4.10 (16H, br), 2.85 (16H, br)

**Boc-Protected, Unlabeled dG<sub>9</sub>**: <sup>1</sup>H NMR (300 MHz, CD<sub>3</sub>CN): 11.52 (br, 2H), 8.35 (br, 2H), 7.31 (br, 0.47H, end group), 5.86 (br, 1H), 5.05 (br, 1H), 4.65 (br, 1H), 4.17 (br, 4H), 3.55 (br, 4H), 3.15 (br, 2H), (2.76, 0.4H), (1.44, 36H)

**Unlabeled dG<sub>9</sub>:** <sup>1</sup>H NMR (300 MHz, DMSO-*d*<sub>6</sub>): δ = 7.99 (br, 2H), 7.43 (br, 4H), 5.83 (br, 1H), 5.60 (br, 1H), 4.96 (br, 1H) and 4.62 (br, 1H), 4.05 (br, 4H), 3.40 (br, 4H), 3.27 (br, 2H), 2.92 (br, 0.4H).

**Boc-Protected, Activated Ester-Labeled dG<sub>9</sub>:** <sup>1</sup>H NMR (300 MHz, CD<sub>3</sub>CN): 11.52 (br, 2H), 8.35 (br, 2H), 7.31 (br, 0.47H, end group), 5.86 (br, 1H), 5.05 (br, 1H), 4.65 (br, 1H), 4.17 (br, 4H), 3.55 (br, 4H), 3.15 (br, 2H), (2.76, 0.4H), (1.44, 36H)

**Dye-Labeled dG<sub>9</sub>:** <sup>1</sup>H NMR (300 MHz, DMSO-*d*<sub>6</sub>): δ = 7.99 (br, 2H), 7.43 (br, 4H), 5.83 (br, 1H), 5.60 (br, 1H), 4.96 (br, 1H) and 4.62 (br, 1H), 4.05 (br, 4H), 3.40 (br, 4H), 3.27 (br, 2H), 2.92 (br, 0.4H).

**Boc-Protected, Unlabeled PhG<sub>10</sub>:** <sup>1</sup>H NMR (300 MHz, CD<sub>2</sub>Cl<sub>2</sub>): δ 11.48 (br, 1H), 8.38 (br, 1H), 7.32 (br, 5.5H, Ph + end group), 5.85 (br, 1H), 5.58 (br, 1H), 5.08 (br, 3H), 4.64 (br, 1H), 4.03 (br, 2H), 3.47 (br, 2H), 3.12 (br, 2H), 1.44 (d, *J* = 5.3 Hz, 18H).

**Unlabeled PhG<sub>10</sub>:** <sup>1</sup>H NMR (300 MHz, CD<sub>3</sub>CN): δ 7.82 (br, 1H), 7.33 (br, 5.5H, Ph + end group), 7.08 (br, 3H), 5.83 (br, 1H), 5.61 (br, 1H), 5.07 (br, 3H), 4.63 (br, 1H), 3.97 (d, *J* = 41.8 Hz, 2H), 3.26 (br, 4H), 2.73 (br, 0.1H).

**Boc-Protected, Activated Ester-Labeled PhG<sub>10</sub>:** <sup>1</sup>H NMR (300 MHz, CD<sub>2</sub>Cl<sub>2</sub>): δ 11.48 (br, 1H), 8.38 (br, 1H), 7.32 (br, 5.5H, Ph + end group), 5.85 (br, 1H), 5.58 (br, 1H), 5.08 (br, 3H), 4.64 (br, 1H), 4.03 (br, 2H), 3.47 (br, 2H), 3.12 (br, 2H), 2.78 (br, 0.4H), 1.44 (d, *J* = 5.3 Hz, 18H).

**Dye-Labeled PhG<sub>10</sub>:** <sup>1</sup>H NMR (300 MHz, CD<sub>3</sub>CN): δ 7.82 (br, 1H), 7.33 (br, 5.5H, Ph + end group), 7.08 (br, 3H), 5.83 (br, 1H), 5.61 (br, 1H), 5.07 (br, 3H), 4.63 (br, 1H), 3.97 (d, *J* = 41.8 Hz, 2H), 3.26 (br, 4H), 2.73 (br, 0.1H).

### 2.2.5 Cell Culture and Uptake Studies

Jurkat T cells (human T lymphocyte leukemia cell line) were grown in RPMI 1640 + Glutamax1 (GIBCO-Invitrogen), supplemented with 10% (v/v) FBS (GIBCO-Invitrogen), 100 U/mL penicillin and 100 U/mL streptomycin (Lonza). Cells were incubated at 37 °C with 5% CO<sub>2</sub> and passaged the day before the treatment.

On the day of the experiment, Jurkat T cells were harvested, centrifuged, counted, and resuspended in complete growth medium to a density of 1x10<sup>6</sup> cells/mL (1 mL final volume, 12-well plate). Cells were incubated with the specific reagent at 37°C for 30 min. Then cells were harvested, centrifuged and washed 2 times with ice-cold PBS, resuspended in 500µL of ice-cold FACS buffer (PBS with 0.2% BSA) and analyzed by flow cytometry (Becton Dickinson LSR II, BD Biosciences). Cell-associated fluorophores were excited at 488 nm, and fluorescence was measured at 530 nm. The fluorescence signal was collected for 10,000 cells exhibiting a normal morphology to obtain a histogram of fluorescence intensity per cell. The calculated median fluorescence intensity (MFI) of the distribution represented the amount of total cell-associated molecules.

For measuring fluorescence from internalized molecules exclusively, after the last washing step, cells that were treated with 50 nM of fluorescein conjugate **transferrin** (Molecular Probes-Invitrogen) or 4 µM of nonarginine **R<sub>9</sub>** (FAM-GRRRRRRRR-NH<sub>2</sub>, customized from Peptide 2.0) were incubated with 0.1% trypsin at 37 °C for 5 min then washed and resuspended in 500µL ice-cold FACS buffer for flow cytometric analysis., Cells that were treated with 4 µM of NBD-

labeled **D<sub>9</sub>** or **H<sub>10</sub>** were incubated with 1 mM of freshly prepared sodium dithionite solution (in 1M TRIS, pH=10) for 5 min at room temperature to quench NBD. Cells were subsequently washed and resuspended in 500 $\mu$ L ice-cold FACS buffer for flow cytometric analysis. The MFI measured after trypsin or dithionite treatment represented the amount of internalized cell-associated molecules.

For cellular uptake experiments in energy-depleted conditions, the cells were harvested, centrifuged and resuspended in either ATP-depleting media (RPMI without glucose, 10% FBS, 25 mM 2-deoxy-D-glucose and 10mM NaN<sub>3</sub>) at 37°C or in standard complete RPMI media at 4°C and let equilibrate for 30 min before the addition of the reagents.

## **2.2.6 Dye Release Studies**

### **2.2.6.1 Vesicle Preparation**

25mg egg yolk phosphatidylcholine (EYPC) or dipalmitoylphosphatidylcholine (DPPC) lipid in 3 mL of chloroform was evaporated onto the wall of a 10 mL flask using a rotary evaporator, then placed under vacuum overnight. The lipid film was resuspended in buffer containing 10 mM Tris and 50 mM carboxyfluorescein dye, titrated to pH 7.5. The buffer was allowed to sit for an hour, vortexing every 15 minutes. The DPPC vesicles were swelled in a water bath set to 50°C during this time. The vesicle solution was then put through six freeze-thaw cycles. The solution was then extruded nine times through a 100 nm pore membrane. The DPPC vesicles were warmed with a heat gun during the extrusion process. Dye-loaded vesicles were separated from free dye by size exclusion chromatography (Sephadex G-50 superfine, Sigma Aldrich) in Tris saline buffer (10 mM Tris, 107 mM NaCl, pH 7.5).

### 2.2.6.2 Vesicle Concentration Calibration

Lipid concentration for a serial dilution of vesicles was measured using a Wako Phospholipids C diagnostic kit. The same serial dilution was also measured for fluorescence in Tris buffer with 0.05% Triton-X 100. 68,000 counts in the Biotek Synergy Mx fluorescence plate reader was found to correspond to an in-well phosphatidylcholine concentration of 2.5  $\mu\text{M}$ . This was the standard for further fluorescence measurements.

### 2.2.6.3 DPPC and EYPC Dye Release at 25°C

Experiments similar to those published previously[27] were performed using a Biotek Synergy Mx fluorescence plate reader. All Fluorescence measurements were taken at an excitation wavelength of 492 nm and emission wavelength of 517 nm. 1,960  $\mu\text{L}$  Tris buffer (10 mM Tris, 107 mM NaCl, pH 7.5) was added to the wells of a 12-well plate. 20  $\mu\text{L}$  of 250  $\mu\text{M}$  vesicle solution (as defined above) was added to each well, creating an in-well concentration of 2.5  $\mu\text{M}$ . The plate reader was heated to 25°C before continuing. The plates were shaken at 25°C and after three minutes a baseline fluorescence measurement,  $F_0$ , was taken. 20  $\mu\text{L}$  polymer/DMSO solutions containing varying concentrations (0.01-1000  $\mu\text{L}$ ) of polymer were added to wells with stirrers, and the plate was returned to the reader for 10 minutes of shaking. After 10 minutes, another reading,  $F_{10}$ , was taken. 20  $\mu\text{L}$  5% Triton X-100 in DMSO was added to the wells and after three minutes a final measurement,  $F_T$ , was taken.  $F_T$  and  $F_0$  allowed use to normalize fluorescence to measure the fractional dye release:

$$Y = (F_{10} - F_0)/(F_T - F_0)$$

The fractional dye release  $Y$  was then fitted as a function of concentration,  $c$ , to the Hill equation by a least-squares method:



$$Y = Y_m \frac{(c/EC_{50})^n}{1 + (c/EC_{50})^n}$$

Where  $EC_{50}$  is the concentration of 50% of maximal dye release and  $n$  is a fitting parameter.

#### **2.2.6.4 DPPC Dye Release at 50°C**

Experiments were performed similar to the above except that the plates were allowed to incubate in the plate reader at 50°C for 10 minutes before proceeding, to ensure that the vesicles were at the desired temperature.

#### **2.2.6.5 EYPC Dye Release at 4°C**

Experiments were performed using an Horiba Scientific FluoroLog-3 spectrophotometer. Experiments were similar the ones above and to previously reported work,[7, 9] but adjusted to match the equipment and experimental conditions. 20  $\mu$ L 250 $\mu$ M vesicle solution was added to 1,960  $\mu$ L Tris buffer in a cuvette with a stir bar. The solution was allowed to cool for 20 minutes before proceeding. Fluorescence was continually measured over the 800s experiment, as 20  $\mu$ L polymer/DMSO solution was added at 100 s and Triton X-100 was added at 700 s. From this kinetic curve, we have  $F_0=F(t=0s)$ ,  $F_{10}=F(t=700s)$ , and  $F_T=F(t=800s)$  and we can use these values to get the fractional dye release  $Y$ . Repeated experiments allow us to build the previously described Hill plot.

## 2.3 Results and Discussion

### 2.3.1 Polymer Design

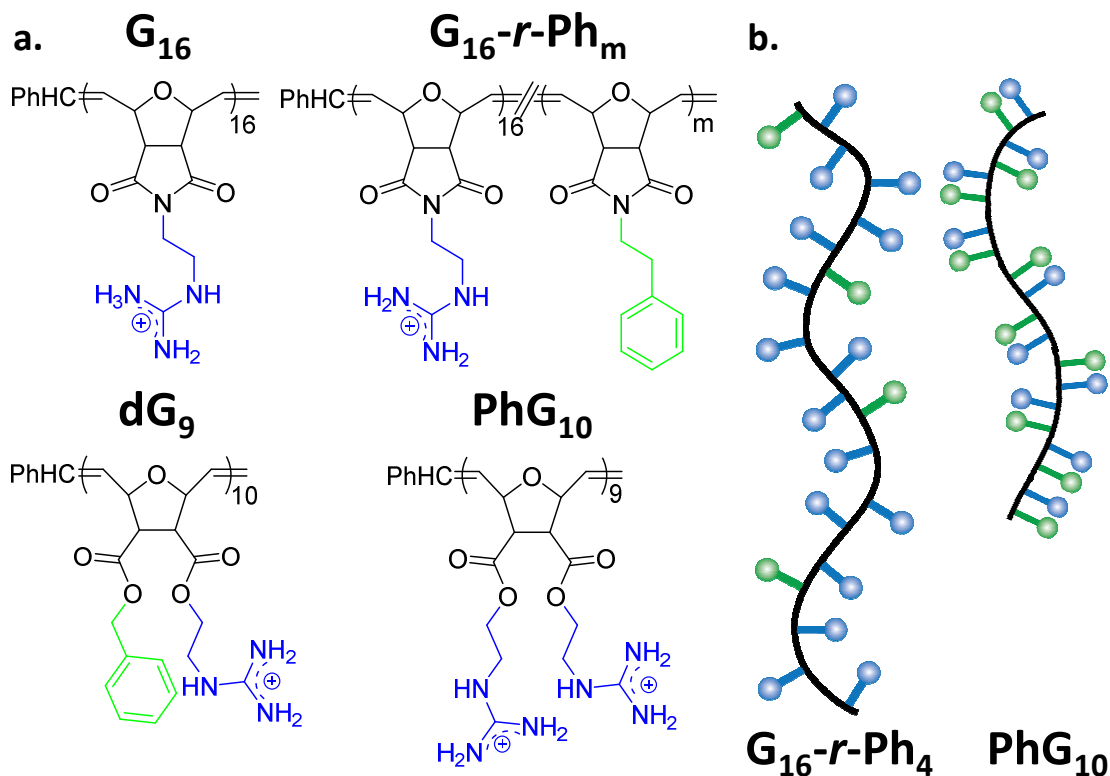


**Figure 2.2.** PTDMs used for this study. a) Polymer structures, with guanidinium moieties colored blue and aromatic/hydrophobic moieties colored green.  $m=4$  or  $8$ . b) Cartoon representations of **G<sub>16</sub>-r-Ph<sub>4</sub>** (left) and **PhG<sub>10</sub>** (right) with the same coloring scheme. Dye-labeled analogs of **PhG<sub>10</sub>** and **dG<sub>10</sub>** were also synthesized.

Our diverse library of polymer structures (Figure 2.2), combined with biophysical and *in vitro* cell experiments, provided us a unique framework for understanding how cooling cells to 4°C alters PTDM-membrane interactions. We first compared the effects of ATP depletion and temperature changes on uptake in cellular experiments by measuring the degree of dye-labeled PTDM internalization in Jurkat T-cells. Next, we measured PTDM-promoted dye release from

single-component lipid vesicles of dipalmitoylphosphatidylcholine (DPPC) in both their gel and liquid phases, to show clearly how changes in lipid phase alter polymer-membrane interactions. DPPC vesicles provide the simplest possible model for membrane transitions, as they contain just one type of head group (the zwitterionic phosphatidylcholine) as well as a single acyl tail type. This latter feature ensures a narrow, well-defined set of phase transitions. It was thus expected that any alterations to membrane activity would be most evident in this system. As a bridge between the simple DPPC system and the more complicated cell membrane, we also measured PTDM-promoted dye release from egg yolk PC (EYPC). EYPC contains a mixture of lipid tails and thus has a very broad phase transition, but also more closely resembles the lipid composition found in cell membranes.[30] Through these three lipid systems (DPPC, EYPC, cell membranes), we are able to examine the connection between a trait seen in a simple, single component systems and the more nuanced response of cell membranes.

The representative polymer library used in this study spans two important design parameters: hydrophobicity and guanidinium density. While guanidine content alone is enough to produce some amount of activity, additional hydrophobicity has been shown to greatly increase activity when either complexed with the PTDM[31, 32] or incorporated directly into the chain.[7, 10, 27] Additionally, although it has not yet been demonstrated for such systems, it was hypothesized that more hydrophobic polymers might more readily cross gel-phase membranes, as they would have a stronger insertion potential. The imide series (**G<sub>16</sub>**, **G<sub>16</sub>-*r*-Ph<sub>m</sub>**) consists of repeat units bearing either guanidinium or phenyl moieties. Polymers were synthesized with a fixed number of guanidinium groups (16) and varying numbers of hydrophobic groups (0, 4, and 8) randomly interspersed throughout the polymer chain. This allowed us to vary hydrophobicity across a series of polymers with the same charge content. The di-ester series (**dG<sub>9</sub>**, **PhG<sub>10</sub>**) consists of dual-functional repeat units containing either a

guanidinium and a phenyl group or two guanidinium groups. This allowed us to exchange guanidinium for aromatic groups while maintaining constant chain length. Between these two series, we can account for the effects of polymer chain length, charge content, and hydrophobicity (Figure 2.2b). All polymers were synthesized by ring-opening metathesis polymerization (ROMP) using previously reported protocols[7, 8, 27, 29] and were labeled with NBD dye for cellular experiments or left unlabeled for the liposomal dye release experiments.

### 2.3.2 Cellular Uptake Studies

To measure the effect of ATP depletion and reduced temperature on cellular internalization, we measured the uptake of dye-labeled macromolecules into Jurkat T cells, a hard-to-transfect cell line, in a manner similar to previous reports.[8, 10, 29] As a positive control for endocytotic inhibition, we used Transferrin (**Tf**), a non-PTD protein which enters exclusively by endocytosis.[33, 34] As our reference to the PTD literature, we used nonaarginine (**R9**), one of the most widely explored PTDs.[3] Both **Tf** and **R9** were labeled with FITC dye and detailed procedures are provided in the Supporting Information (SI). Briefly, cells were incubated for 30 minutes either with sodium azide or at 4°C in order for them to equilibrate, and then treated with a dye-labeled reagent for another 30 minutes. To eliminate any fluorescence response from molecules on the outer layer of cells, cells were then exposed to either trypsin (for **Tf** and **R9**) or sodium dithionite (for PTDMs). Trypsin digests any protein outside the cell, while sodium dithionite quenches the NBD dye on the polymers. The median fluorescence intensity (MFI) of the cells, representing molecular uptake, was then measured by flow cytometry (Figure 2.3a).

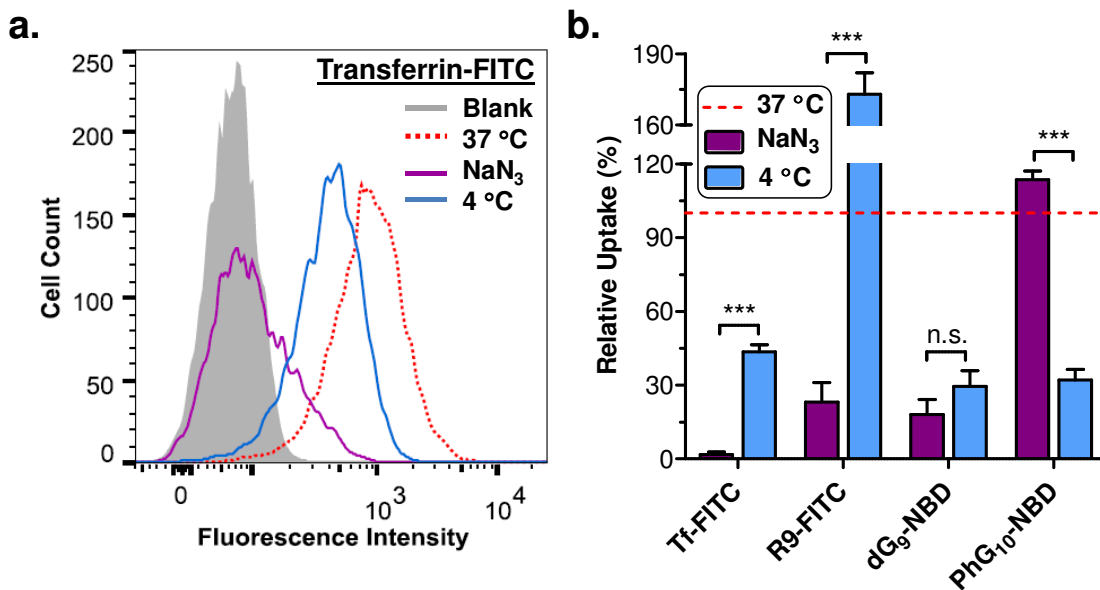


**Figure 2.3.** Internalization studies. Jurkat T cells ( $1 \times 10^6$  cells/mL) were incubated for 30 min with the indicated compound either after cellular ATP depletion (with 10 mM  $\text{NaN}_3$ , purple) or at 4 °C (blue) and compared to uptake under normal conditions (37 °C, red dotted line). a)

Representative flow cytometry analysis for the cellular uptake of 50 nM Transferrin-FITC (Tf-FITC), as a control, at the indicated conditions; b) Relative uptake values are normalized to the cellular uptake (in MFI) at 37 °C in normal growth media. Each point represents the mean  $\pm$  SE (standard error) of three independent experiments. \*\*\* ( $p < 0.001$ ); n.s. ( $p > 0.05$ ), as calculated by unpaired two-tailed student t-test.

Figure 2.3b shows relative uptake after ATP-depletion (purple bars) and temperature reduction (blue bars) as a percentage of the uptake measured under normal conditions (red dotted line). Raw MFI values are reported in the SI. Transferrin, our negative control for energy-independent uptake, showed a decrease in uptake under both ATP-depleted and 4 °C conditions.

However there was significantly lower uptake in ATP-depleted cells (2%) than in cells at 4°C (43%), suggesting that cooling did not entirely inhibit endocytosis. These data are consistent with results previously reported for K562 Leukemia cells.[15] The results for **R9**, **dG<sub>9</sub>**, and **PhG<sub>10</sub>** further highlight the discrepancies between these two methods. While the relative uptake of **dG<sub>9</sub>** was similar for both methods (18% and 29%), the uptake for the other two molecules was significantly different. Uptake for **R9** in ATP-depleted conditions was very low (23%) while uptake at 4°C (173%) was even higher than at 37°C. While these results appear anomalous, **R9** has a history of strongly cell-type-dependent uptake. The acute myelogenous leukemia cell line KG1 similarly showed an increase in the total MFI of internalized peptide at 4°C.[12, 35, 36] Most cell lines, however, have shown a decrease in uptake at 4°C. Another leukemia-based suspension cell line, K562, shows dramatically reduced uptake under the same conditions.[12, 36] Likewise, the adherent HeLa and A549 cell lines,[19, 36] along with the wild-type Chinese hamster ovary (CHO-K1) cells,[18] showed a significant drop-off in activity at 4°C. Since this anomaly was not present for the polymers presented here, it is likely that there is some interaction specific to both the peptide and the cell line. By contrast, uptake of **PhG<sub>10</sub>** under ATP-depleted conditions was 114% relative to normal conditions, suggesting it is ATP-independent, but its internalization was significantly reduced at 4°C (32%). If both methods only inhibited endocytosis, then they would be expected to produce similar results. As that is distinctly not the case, these results strongly suggest that the two methods do not create the same set of cellular conditions.

### 2.3.3 DPPC Dye Release

A reasonable explanation for this discrepancy is that cooling cells to 4°C causes changes beyond simply inhibiting endocytosis. One possible change is that the energy-independent

transport across the membrane is also altered at lower temperatures. The phase diagram for phospholipids reveals many different phase states, including the gel and liquid phases.[30] The gel phase is more rigid and individual lipid molecules have far less lateral mobility than in membranes above the transition temperature. To understand the effect of this phase transition on PTDM membrane activity, we looked at dye release from single-component dipalmitoylphosphatidylcholine (DPPC) vesicles. In the dye release experiment, large unilamellar vesicles (LUVs) containing a high concentration (50mM) of carboxyfluorescein dye were exposed to varying concentrations of polymer. Inside the vesicle, the dye is self-quenched due to high concentration so that any dye released becomes fluorescent upon dilution. This approach is well established as an analog for energy-independent membrane activity.[6, 32] Dye release data was then fit to the Hill equation.

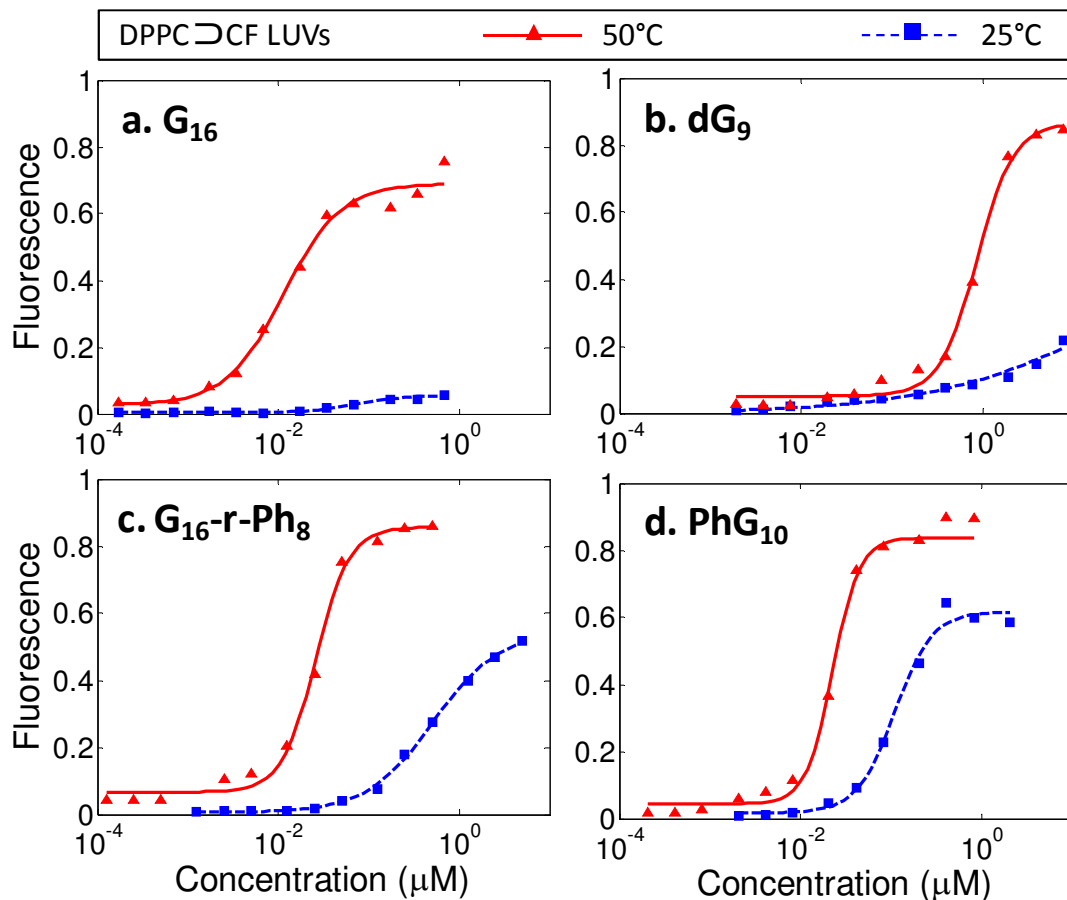


**Figure 2.4.** Dye release from single-component DPPC/CF LUVs. Values represent fraction of dye released from vesicles at 600s after the addition of PTDM. Red triangles were taken at 50°C, which is above the liquid-to-gel transition. Blue squares were taken at 25°C, which is below the liquid-to-gel transition. Red lines and blue dashes are least-squares fits to the Hill Equation.

DPPC has two well-defined, narrow phase transitions: a gel-to-ripple phase transition at 34°C and a ripple-to-liquid transition at 42°C.[37, 38] We therefore measured dye release at a temperature firmly in the gel phase (25°C) and another well into the liquid phase (50°C). **R9**, as shown in the SI, did not induce more than 20% dye release under either condition. This is not particularly surprising, given previous literature.[9] Transferrin was not tested, as its uptake is



exclusively by endocytosis.[33, 34] Figure 2.4 shows results and Hill plot fits for our PTDM series. The largest discrepancy between PTDM-membrane activity in gel phase and liquid phase occurred with **G<sub>16</sub>**. In the liquid phase **G<sub>16</sub>** induced 70% dye release with an EC<sub>50</sub> of 0.011μM, while in the gel phase it never exceeded 10% release. **dG<sub>9</sub>** showed similar results, with substantial differences above and below the phase transition. It is difficult, however, to assess the exact maximum release and EC<sub>50</sub> in the gel phase since the curve did not reach a plateau even at very high concentrations (>>10μM). The magnitude of the effect decreased with increasing PTDM hydrophobicity. The intermediately hydrophobic polymer **G<sub>16</sub>-r-Ph<sub>4</sub>** had a gel phase EC<sub>50</sub> (0.006μM) that was 70 times higher than in the liquid phase EC<sub>50</sub> (0.12μM, Figure 2.5). Continuing this trend of decreasing EC<sub>50</sub> ratios (gel phase EC<sub>50</sub>/liquid phase EC<sub>50</sub>), the most hydrophobic polymers were less sensitive to changes in lipid phase. The copolymer **G<sub>16</sub>-r-Ph<sub>8</sub>** had an EC<sub>50</sub> in the gel phase (0.52μM) that was 20 times higher than the one in the liquid phase (0.026μM), and the homopolymer **PhG<sub>10</sub>** had an EC<sub>50</sub> in the gel phase (0.11μM) that was only 4.8 times larger than that in the liquid phase (0.023μM). It is also noteworthy that with the exception of **dG<sub>9</sub>**, the EC<sub>50</sub> values in the liquid phase, but not in the gel phase, were roughly independent of hydrophobic content.

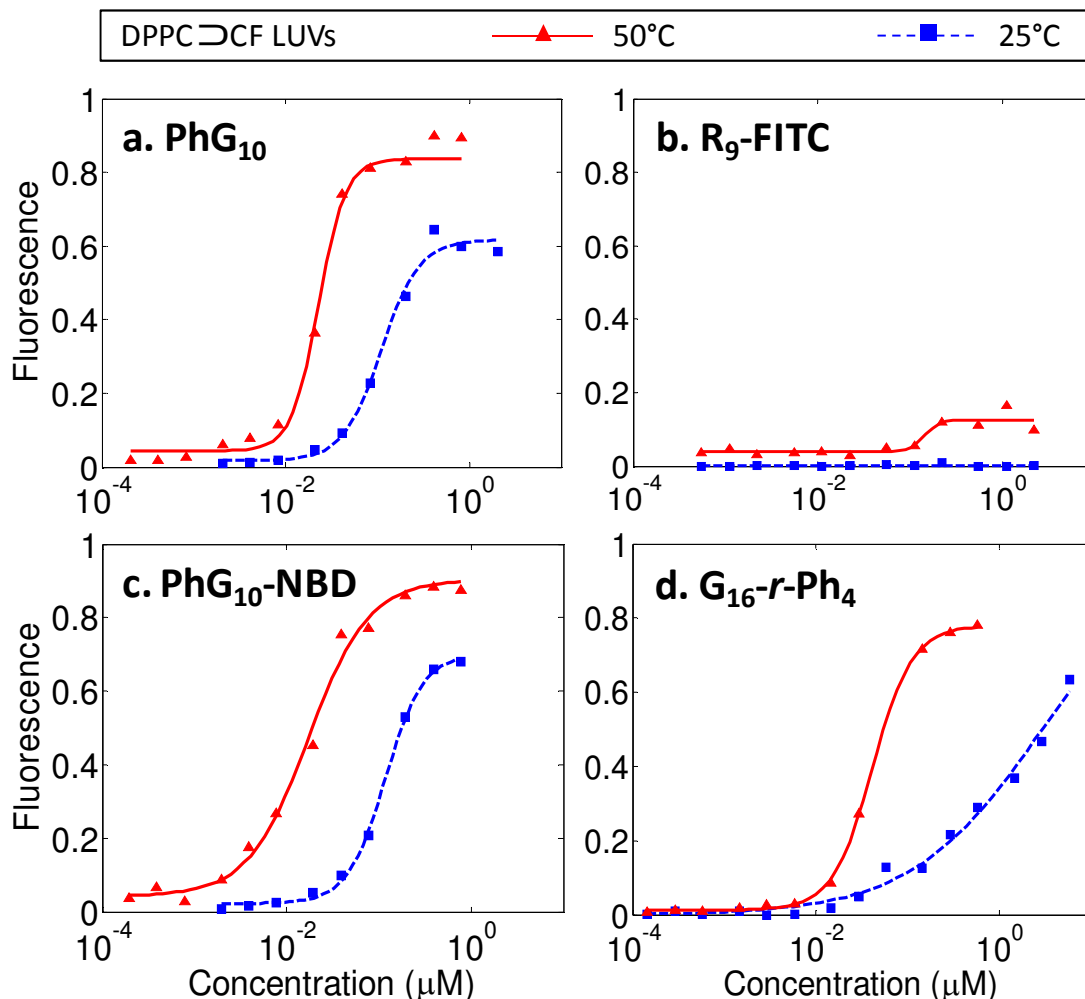


**Figure 2.5.** Dye release from DPPC/CF LUVs. Values represent fraction of dye released from vesicles at 600s. Red triangles were taken at 50°C, above  $T_g$ . Blue squares were taken at 25°C, below  $T_g$ . Red lines and blue dashes are least-squares fits to the Hill Equation. a) and c) compare the same polymer with and without dye, showing little difference in their release profile.

These sets of data suggest that all of the polymers used in this study were able to penetrate the DPPC vesicle membrane in the liquid phase, but increased hydrophobic content was necessary to induce efficient dye release below the transition temperature. *In vitro* study results also suggest that, since cooling cells to 4°C has an effect on the overall membrane rigidity, the cellular internalization efficiency would be expected to differ from other methods

that inhibit endocytosis without inducing phase transitions. The cellular membrane is extremely complicated, including but not limited to the presence of proteins, cholesterol, mixed acyl lipids and other components that lead to broad phase transitions that produce multiple phases and lipid rafts. This makes it challenging to directly compare to much simpler single-lipid systems. While the effects of the membrane transition on dye release are obvious for DPPC, we wanted to better understand whether a mixed-acyl system which better resembles the biological membrane displayed similar behavior. To this end, we created dye-filled vesicles consisting of mixed-acyl chain egg yolk PC (EYPC), which shows a broad transition ranging from -7 to 25°C.[38-40] Dye release was measured for these vesicles at 4°C and 25°C, representing both bounds for the temperature transition.

### 2.3.4 EYPC Dye Release

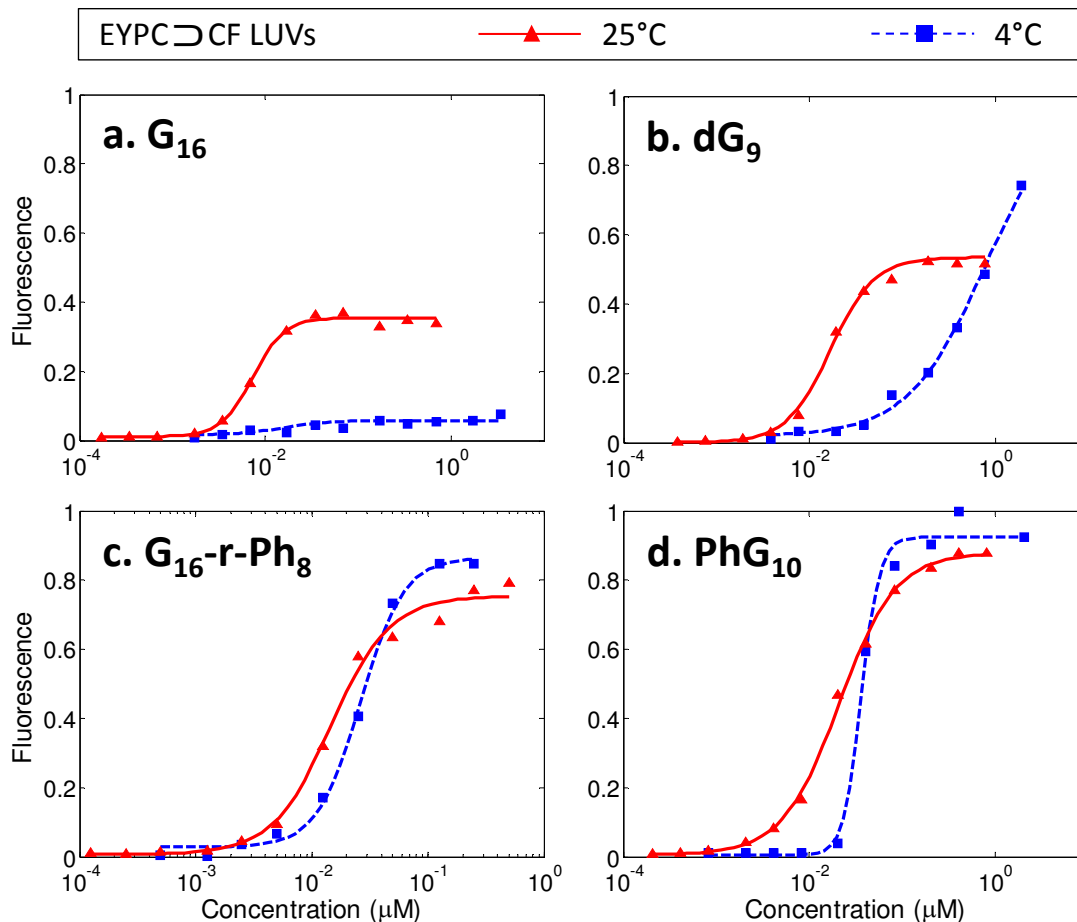


**Figure 2.6.** Dye release from mixed-acyl chain EYPC=CF LUVs. Values represent fraction of dye released from vesicles at 600s after the addition of PTDM. Red triangles were taken at 25°C. Blue squares were taken at 4°C. Red lines and blue dashes are least-squares fits to the Hill Equation.

The EYPC dye release curves shown in Figure 2.6 globally resemble those collected from experiments with DPPC, with some reduction in separation across the temperature range. As with DPPC,  $\text{G}_{16}$  showed substantial dye release at 25°C, while release never rose above 10% at 4°C.  $\text{dG}_9$  showed release at both temperatures, with an  $\text{EC}_{50}$  ratio greater than 25. The more hydrophobic polymers  $\text{G}_{16}\text{-r-Ph}_8$  and  $\text{PhG}_{10}$  had little measurable differences between dye release at 4°C and 25°C (each having  $\text{EC}_{50}$  ratios of just 1.8). Also in line with the DPPC data, the

intermediate polymer  $\mathbf{G}_{16}\text{-}r\text{-Ph}_4$  showed behavior between  $\mathbf{G}_{16}$  and  $\mathbf{G}_{16}\text{-}r\text{-Ph}_8$ , with an  $\text{EC}_{50}$  ratio of 19 (Figure 2.7). All polymer samples showed similar  $\text{EC}_{50}$  values at 25°C (from 0.0073 $\mu\text{M}$  for  $\mathbf{G}_{16}$  to 0.021 $\mu\text{M}$  for  $\mathbf{PhG}_{10}$ ), while the  $\text{EC}_{50}$  values at 4°C showed a sizable structure-property relationship across varying hydrophobicities. There was little difference between the dye release behavior of a shorter polymer with fewer charges ( $\mathbf{PhG}_{10}$ ) and a longer polymer with more charges ( $\mathbf{G}_{16}\text{-}r\text{-Ph}_8$ ), suggesting that neither of these factors were critical to membrane behavior within the range examined.

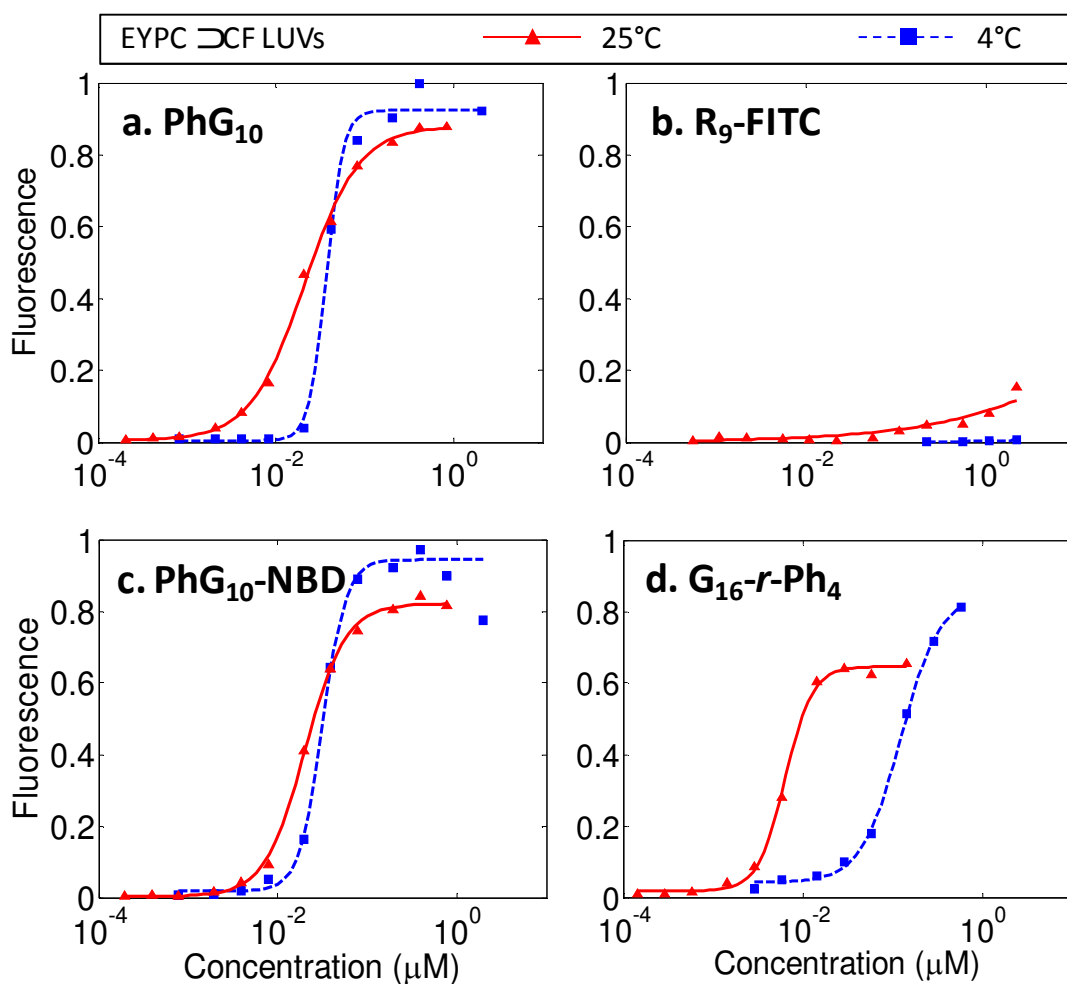


**Figure 2.7.** Dye release from EYPC∩CF LUVs. Values represent fraction of dye released from vesicles at 600s. Red triangles were taken at 25°C, above  $T_g$ . Blue squares were taken at 4°C, below  $T_g$ . Red lines and blue dashes are least-squares fits to the Hill Equation. a) and c)

compare the same polymer with and without dye, showing little difference in their release profile.

**Table 2.1.** Compiled dye release data for all polymers. With increasing hydrophobic content, the EC<sub>50</sub> values above and below T<sub>g</sub> converge. The ratios are larger for the single-lipid DPPC system than the mixed-acyl EYPC

Polymer	Dye Release EC <sub>50</sub> Values (μM)					
	4C	EYPC 25C	Ratio	25C	DPPC 50C	Ratio
R9-FITC	>10	>10	n/a	>10	>10	n/a
G <sub>16</sub>	>10	0.0073	>1300	>10	0.011	>900
dG <sub>9</sub>	0.77	0.017	45	>10	0.86	>11
G <sub>16</sub> -r-Phi <sub>4</sub>	0.12	0.006	19	2.9	0.041	>25
G <sub>16</sub> -r-Phi <sub>8</sub>	0.026	0.015	1.8	0.52	0.026	20
PhG <sub>10</sub>	0.037	0.021	1.8	0.11	0.023	4.8
PhG <sub>10</sub> -NBD	0.032	0.020	1.6	0.118	0.017	6.8

## 2.4 Conclusions

It is clear that for hydrophilic polymers like G<sub>16</sub> and dG<sub>9</sub>, the stark reduction in membrane activity caused by altering the lipid phase conditions through cooling is robust across both single- and mixed-acyl lipid systems. In both cases, lowering temperature across the vesicle phase transition greatly altered dye release. This effect decreased with increasing polymer hydrophobicity. It is likely that increased lipid packing and reduced mobility heightened the barrier for polymer insertion into the membrane, a barrier that could be overcome by increasing the number of hydrophobic moieties. This conclusion, while intuitive, has implications for both PTDM design and the methodology used in measuring cellular uptake.

For PTDM design, it makes clear that energy-independent uptake requires polymers hydrophobic enough to insert into the membrane. While dG<sub>9</sub> releases dye in liquid-phase vesicles, it still only has minimal uptake in Jurkat T cells under ATP-depleted conditions. This

suggests that while the polymer is able to insert into pure liquid phase phospholipids, the multi-component cell membrane requires a higher hydrophobicity threshold for insertion. Indeed, the more hydrophobic **PhG<sub>10</sub>** has a much higher uptake under ATP-depleted conditions, but still struggles below the membrane transition at 4°C. We would then hypothesize that a still more hydrophobic PTDM would be required for energy-independent uptake at 4°C. Since gel-phase lipids are not like present in cells at 37°C, **PhG<sub>10</sub>** can be considered sufficiently hydrophobic for energy-independent uptake under most procedures.

On the characterization side, chilling cells to 4°C has been a popular method for differentiating between energy-independent and energy-dependant uptake mechanisms, but has potential pitfalls. The claim that measurements at 4°C represent only energy-independent uptake presupposes that chilling does not alter membrane activity. As our vesicle studies show, this is not necessarily the case. The clear change of membrane behavior in dye release studies, when combined with the difference in activity between cellular uptake at 4°C and in ATP-depleted media strongly suggest that chilling alters the membrane properties and thus the ability of the polymers to cross the membrane. This may bias uptake tests towards favoring polymers with increased hydrophobicity. In order to avoid this kind of bias, we recommend that future studies use ATP depletion over cooling as a means of more accurately measuring energy-independent uptake.

## 2.5 References

1. Schwarze, S.R., K.A. Hruska, and S.F. Dowdy, *Protein transduction: unrestricted delivery into all cells?* Trends in Cell Biology, 2000. **10**(7): p. 290-295.
2. Stanzl, E.G., et al., *Fifteen Years of Cell-Penetrating, Guanidinium-Rich Molecular Transporters: Basic Science, Research Tools, and Clinical Applications*. Accounts of Chemical Research, 2013.
3. Wender, P.A., et al., *The design of guanidinium-rich transporters and their internalization mechanisms*. Advanced Drug Delivery Reviews, 2008. **60**(4-5): p. 452-472.

4. Heitz, F., M.C. Morris, and G. Divita, *Twenty years of cell-penetrating peptides: from molecular mechanisms to therapeutics*. British Journal of Pharmacology, 2009. **157**(2): p. 195-206.
5. Wender, P.A., et al., *The design, synthesis, and evaluation of molecules that enable or enhance cellular uptake: Peptoid molecular transporters*. Proceedings of the National Academy of Sciences of the United States of America, 2000. **97**(24): p. 13003-13008.
6. Hennig, A., et al., *Stimuli-Responsive Polyguanidino-Oxanorbornene Membrane Transporters as Multicomponent Sensors in Complex Matrices*. Journal of the American Chemical Society, 2008. **130**(31): p. 10338-10344.
7. Som, A., et al., *Self-Activation in De Novo Designed Mimics of Cell-Penetrating Peptides*. Angewandte Chemie International Edition, 2011. **50**(27): p. 6147-6150.
8. Tezgel, A.O., J.C. Telfer, and G.N. Tew, *De Novo Designed Protein Transduction Domain Mimics from Simple Synthetic Polymers*. Biomacromolecules, 2011. **12**(8): p. 3078-3083.
9. Som, A., A. Reuter, and G.N. Tew, *Protein Transduction Domain Mimics: The Role of Aromatic Functionality*. Angewandte Chemie International Edition, 2012. **51**(4): p. 980-983.
10. Tezgel, A.Ö., et al., *Novel Protein Transduction Domain Mimics as Nonviral Delivery Vectors for siRNA Targeting NOTCH1 in Primary Human T cells*. Molecular Therapy, 2013. **21**(1): p. 201-209.
11. Richard, J.P., et al., *Cell-penetrating Peptides*. Journal of Biological Chemistry, 2003. **278**(1): p. 585-590.
12. Al-Taei, S., et al., *Intracellular Traffic and Fate of Protein Transduction Domains HIV-1 TAT Peptide and Octaarginine. Implications for Their Utilization as Drug Delivery Vectors*. Bioconjugate Chemistry, 2006. **17**(1): p. 90-100.
13. Futaki, S., *Membrane-permeable arginine-rich peptides and the translocation mechanisms*. Advanced Drug Delivery Reviews, 2005. **57**(4): p. 547-558.
14. Kosuge, M., et al., *Cellular Internalization and Distribution of Arginine-Rich Peptides as a Function of Extracellular Peptide Concentration, Serum, and Plasma Membrane Associated Proteoglycans*. Bioconjugate Chemistry, 2008. **19**(3): p. 656-664.
15. Drin, G., et al., *Studies on the Internalization Mechanism of Cationic Cell-penetrating Peptides*. Journal of Biological Chemistry, 2003. **278**(33): p. 31192-31201.
16. Mishra, A., et al., *Translocation of HIV TAT peptide and analogues induced by multiplexed membrane and cytoskeletal interactions*. Proceedings of the National Academy of Sciences of the United States of America, 2011. **108**(41): p. 16883-16888.
17. Räägel, H., P. Säälük, and M. Pooga, *Peptide-mediated protein delivery--Which pathways are penetrable?* Biochimica et Biophysica Acta (BBA) - Biomembranes, 2010. **1798**(12): p. 2240-2248.
18. Walrant, A., et al., *Different membrane behaviour and cellular uptake of three basic arginine-rich peptides*. Biochimica et Biophysica Acta (BBA) - Biomembranes, 2011. **1808**(1): p. 382-393.
19. Nakase, I., et al., *Cellular Uptake of Arginine-Rich Peptides: Roles for Macropinocytosis and Actin Rearrangement*. Molecular Therapy, 2004. **10**(6): p. 1011-1022.
20. Schmid, S.L. and L.L. Carter, *ATP is required for receptor-mediated endocytosis in intact cells*. Journal of Cell Biology, 1990. **111**(6 Pt 1): p. 2307-2318.
21. Silverstein, S.C., R.M. Steinman, and Z.A. Cohn, *Endocytosis*. Annual Review of Biochemistry, 1977. **46**(1): p. 669-722.



22. Needham, D. and E. Evans, *Structure and mechanical properties of giant lipid (DMPC) vesicle bilayers from 20.degree.C below to 10.degree.C above the liquid crystal-crystalline phase transition at 24.degree.C*. Biochemistry, 1988. **27**(21): p. 8261-8269.
23. Wu, G., et al., *Effects of bilayer phases on phospholipid-poloxamer interactions*. Soft Matter, 2009. **5**(7): p. 1496-1503.
24. Arav, A., et al., *Phase Transition Temperature and Chilling Sensitivity of Bovine Oocytes*. Cryobiology, 1996. **33**(6): p. 589-599.
25. Lepock, J.R., et al., *Thermotropic lipid and protein transitions in chinese hamster lung cell membranes: relationship to hyperthermic cell killing*. Canadian journal of biochemistry and cell biology = Revue canadienne de biochimie et biologie cellulaire, 1983. **61**(6): p. 421-427.
26. Love, J.A., et al., *A practical and highly active ruthenium-based catalyst that effects the cross metathesis of acrylonitrile*. Angew Chem Int Ed, 2002. **41**(21): p. 4035-7.
27. Schmidt, N.W., et al., *Molecular Basis for Nanoscopic Membrane Curvature Generation from Quantum Mechanical Models and Synthetic Transporter Sequences*. Journal of the American Chemical Society, 2012. **134**(46): p. 19207-19216.
28. Kolonko, E.M., et al., *General Synthetic Route to Cell-Permeable Block Copolymers via ROMP*. Journal of the American Chemical Society, 2009. **131**(21): p. 7327-7333.
29. Sgolastra, F., et al., *The Importance of Sequence Specific Hydrophobicity in Synthetic Protein Transduction Domain Mimics*. Biomacromolecules, 2014. **15**(3): p. 812-820.
30. Chapman, D., *Phase transitions and fluidity characteristics of lipids and cell membranes*. Quarterly Reviews of Biophysics, 1975. **8**(2): p. 185-235.
31. Nishihara, M., et al., *Arginine magic with new counterions up the sleeve*. Organic & Biomolecular Chemistry, 2005. **3**(9): p. 1659-1669.
32. Sakai, N. and S. Matile, *Anion-Mediated Transfer of Polyarginine across Liquid and Bilayer Membranes*. Journal of the American Chemical Society, 2003. **125**(47): p. 14348-14356.
33. Dautry-Varsat, A., A. Ciechanover, and H.F. Lodish, *pH and the recycling of transferrin during receptor-mediated endocytosis*. Proceedings of the National Academy of Sciences of the United States of America, 1983. **80**(8): p. 2258-2262.
34. Klausner, R.D., et al., *Receptor-mediated endocytosis of transferrin in K562 cells*. Journal of Biological Chemistry, 1983. **258**(8): p. 4715-4724.
35. Fretz, Marjan M., et al., *Temperature-, concentration- and cholesterol-dependent translocation of L- and D-octa-arginine across the plasma and nuclear membrane of CD34+ leukaemia cells*. Biochemical Journal, 2007. **403**(2).
36. Watkins, C.L., et al., *Low concentration thresholds of plasma membranes for rapid energy-independent translocation of a cell-penetrating peptide*. Biochemical Journal, 2009. **420**(2): p. 179-189.
37. Jacobson, K. and D. Papahadjopoulos, *Phase transitions and phase separations in phospholipid membranes induced by changes in temperature, pH, and concentration of bivalent cations*. Biochemistry, 1975. **14**(1): p. 152-161.
38. Koynova, R. and M. Caffrey, *Phases and phase transitions of the phosphatidylcholines*. Biochimica et Biophysica Acta (BBA) - Reviews on Biomembranes, 1998. **1376**(1): p. 91-145.
39. Ladbrooke, B.D., R.M. Williams, and D. Chapman, *Studies on lecithin-cholesterol-water interactions by differential scanning calorimetry and X-ray diffraction*. Biochimica et Biophysica Acta (BBA) - Biomembranes, 1968. **150**(3): p. 333-340.

40. Huang, C. and J.T. Mason, *Structure and properties of mixed-chain phospholipid assemblies*. *Biochimica et Biophysica Acta*, 1986. **864**(3-4): p. 423-470.

## CHAPTER 3

### ANIONIC LIPID CONTENT PRESENTS A BARRIER TO ROMP-BASED PTDM ACTIVITY

#### 3.1 Introduction

The mechanism of cellular uptake of PTDs and their synthetic mimics is a widely debated and still largely uncertain topic. As described in the previous chapter, the fraction of the polymer that enters cells through energy independent means is a matter of intense study.[1-6] However, there is compelling evidence that at least some polymer is able to cross the lipid bilayer, either from outside the cells or to escape endosomal entrapment. Primary among this evidence is that it is possible to deliver functional biomolecules to the interior of a cell. Our group has previously demonstrated siRNA knockdown of the NOTCH1 protein through the delivery of sequence-specific siRNA.[7] More recent work has also demonstrated delivery of fully-functional CRE recombinase enzyme for the knockout of a GFP reporter gene located between two loxP sites.[8] Studies by other research groups have also demonstrated the delivery of functional biomolecules by covalently-bound PTDs.[9-12] Such delivery would only be possible in a system where the cargo, at least, is able to cross the bilayer membrane and enter the cytosol. Further supporting this position are biophysical and simulation studies that demonstrated the ability of these polymers to cross lipid bilayers without the need for endocytosis.[13-21] These studies were outlined in more detail in the introduction of this manuscript.

Among those biophysical studies, there is a strong consensus of the importance of the interaction between the cationic nature of the polymer and the anionic surface of the cell. Matile and coworkers have demonstrated that oligo- and polyarginine has dramatically increased membrane activity when the polymers are complexed with amphiphilic anions.[4, 13-

15] This even applies to polyarginine even when the amphiphiles are lipids integrated into the vesicle bilayer, as an increase of anionic egg yolk phosphatidylglycerol (EYPG) content in otherwise zwitterionic EYPC membranes leads to a dramatic increase in dye release activity.[13] Isothermal calorimetry studies of the binding energy associated with nonaarginine show that while the peptide has a strong association with anionic DSPG vesicles, they do not measure any such association with zwitterionic DSPC vesicles.[21] Similarly, plasmon waveguide resonance studies of the PTD penetratin with EYPC and EYPG lipid bilayers shows a higher affinity for the anionic EYPG membrane.[18] Small-angle x-ray scattering studies with PTDs and PTDMs have assumed anionic content as necessary, and examinations of their pore-forming activity have focused on bi-dentate hydrogen bonding interactions of the guanidinium group with anionic phosphate groups on anionic lipids.[22, 23]

There are also exceptions to this notion, however. Detailed kinetic analysis of the interaction of the PTDM tp10 with vesicle systems revealed that while the tp10 has stronger binding to anionic vesicles, the actual rate of dye efflux was not measurably different.[24] This is because the rate of dye efflux was more dependent on the amount of time the polymer spend integrated into the bilayer, which was similar for both anionic and zwitterionic systems. It is worth noting, however, that tp10 is an amphiphilic, helical peptide that is lysine, rather than arginine, rich. Perhaps most relevant to this investigation is work by Henning et. al. with a polymer very similar to polymer **1** used in this study.[15] As with polyarginine, dye release was measured against a series of vesicles with progressively increasing amounts of EYPG. Unlike the previous study, however, dye release dramatically *decreased* with increasing anionic content. This clearly suggested that this class of guanidinium-rich ROMP polymers interacted fundamentally differently with lipid bilayers than arginine-rich peptides, and required its own, separate analysis of its interaction with lipid bilayers.

There then seem to be two separate classes of PTDs and PTDMs; those, like polyarginine, that have an increased uptake in the presence of anionic lipids and those, like tp10 and ROMP PTDMs that have a decreased activity in their presence. It is not understood why this latter class of polymers is different in this way, nor is it clear why this class of polymers is fundamentally different from the first. This chapter will use a combination of polymer chemistry and biophysical experiments to explore these questions.

The following study examines the effect of anion lipid content on the interaction of a series of guanidinium-rich ring-opening metathesis (ROMP) polymers with phospholipid membranes. It begins with more complete dye release studies characterizing the effect of anionic lipid content on membrane permeabilization. Next, the surface charge and aggregation of polymer-vesicle mixtures is examined, demonstrating that surface association is independent of anionic lipid content. Lastly, surface plasmon resonance (SPR) experiments quantify the relative effects of anionic lipid content and polymer hydrophobicity on membrane association.

## **3.2 Materials and Methods**

### **3.2.1 Polymer Synthesis**

Polymers in this study are the same as the imide series in chapter 2. Synthetic details are provided therein.

## **3.2.2 Dye Release Studies**

### **3.2.2.1 Vesicle Preparation**

#### **3.2.2.1.1 EYPC and DOPC Vesicles**

25mg egg yolk phosphatidylcholine (EYPC) or dioleoylphosphatidylcholine (DOPC) lipid in 3 mL of chloroform was evaporated onto the wall of a 10 mL flask using a rotary evaporator, then placed under vacuum overnight. The lipid film was resuspended in buffer containing 10 mM Tris and 50 mM carboxyfluorescein dye, titrated to pH 7.5. The buffer was allowed to sit for an hour, vortexing every 15 minutes. The DPPC vesicles were swelled in a water bath set to 50°C during this time. The vesicle solution was then put through six freeze-thaw cycles. The solution was then extruded nine times through a 100 nm pore membrane. The DPPC vesicles were warmed with a heat gun during the extrusion process. Dye-loaded vesicles were separated from free dye by size exclusion chromatography (Sephadex G-50 superfine, Sigma Aldrich) in Tris saline buffer (10 mM Tris, 107 mM NaCl, pH 7.5).

#### **3.2.2.1.2 80:20 EYPC:Brain PS and 80:20 DOPC:DOPS Vesicles**

20mg EYPC or DOPC was combined with 5mg porcine brain phosphatidylserine (brain PS) or dioleoylphosphatidylserine (DOPS), respectively, in 3mL chloroform. The mixture was rotary evaporated onto the wall of a 10mL flask and placed under vacuum overnight. The rest of the vesicle formation was performed as above.

### 3.2.2.2 Vesicle Concentration Calibration

Lipid concentration for a serial dilution of vesicles was measured using a Wako Phospholipids C diagnostic kit. The same serial dilution was also measured for fluorescence in Tris buffer with 0.05% Triton-X 100. 68,000 counts in the Biotek Synergy Mx fluorescence plate reader was found to correspond to an in-well phosphatidylcholine concentration of 2.5  $\mu\text{M}$ . This was the standard for further fluorescence measurements.

### 3.2.2.3 Dye Release Experiments

Experiments similar to those published previously[23] were performed using a Biotek Synergy Mx fluorescence plate reader. All Fluorescence measurements were taken at an excitation wavelength of 492 nm and emission wavelength of 517 nm. 1,960  $\mu\text{L}$  Tris buffer (10 mM Tris, 107 mM NaCl, pH 7.5) was added to the wells of a 12-well plate. 20  $\mu\text{L}$  of 250  $\mu\text{M}$  vesicle solution (as defined above) was added to each well, creating an in-well concentration of 2.5  $\mu\text{M}$ . The plate reader was heated to 25°C before continuing. The plates were shaken at 25°C and after three minutes a baseline fluorescence measurement,  $F_0$ , was taken. 20  $\mu\text{L}$  polymer/DMSO solutions containing varying concentrations (0.01-1000  $\mu\text{L}$ ) of polymer were added to wells with stirrers, and the plate was returned to the reader for 10 minutes of shaking. After 10 minutes, another reading,  $F_{10}$ , was taken. 20  $\mu\text{L}$  5% Triton X-100 in DMSO was added to the wells and after three minutes a final measurement,  $F_T$ , was taken.  $F_T$  and  $F_0$  allowed use to normalize fluorescence to measure the fractional dye release:

$$Y = (F_{10} - F_0)/(F_T - F_0)$$

The fractional dye release  $Y$  was then fitted as a function of concentration,  $c$ , to the Hill equation by a least-squares method:

$$Y = Y_m \frac{(c/EC_{50})^n}{1 + (c/EC_{50})^n}$$

Where  $EC_{50}$  is the concentration of 50% of maximal dye release and  $n$  is a fitting parameter.

### **3.2.3 Dynamic Light Scattering and Zeta Potential Measurements**

#### **3.2.3.1 Vesicle Preparation**

Vesicles were prepared in a similar manner to the dye release experiments above, but without carboxyfluorescein dye and omitting the size exclusion step. For DOPC vesicles, 25mg DOPC lipid dissolved in chloroform was added to a flask that was then rotary evaporated to form a lipid film on the inner wall. After placing the film under high vacuum overnight, the film was hydrated with a 1mL buffer solution containing 107mM NaCl, 10mM Tris, and titrated to pH 7.5. After an hour of periodic vortex agitation, the vesicles were subjected to six freeze-thaw cycles and then extruded nine times through a 100nm membrane. The resulting 25mg/mL was then appropriately diluted in the same buffer for use. 80:20 DOPC:DOPS vesicles were prepared identically, except with 20mg DOPC and 5mg DOPS.

#### **3.2.3.2 Particle Mean Size and Zeta Potential Measurement**

Measurements were made using a Malvern Zetasizer Nano Z. As with the dye release experiments above, varying concentrations of polymer were added to a vesicle solution containing 2.5 $\mu$ M lipid under constant agitation. After 10 minutes, the solution was injected into a Malvern DTS 1061 folded capillary cell and dynamic light scattering measurements were immediately made and the number average mean size of the particles in solution was made. Zeta potential was then measured on the same sample.



### 3.2.3.3 Surface Plasmon Resonance Experiments

#### 3.2.3.4 Materials

HEPES, sodium chloride and 1 M NaOH solution were obtained from Sigma Aldrich(Germany). Polycarbonate membranes (0.2  $\mu\text{m}$  and 0.05  $\mu\text{m}$ ) and the lipids 1,2-dioleoyl-*sn*-glycero-3-phosphocholine (DOPC) and 1,2-dioleoyl-*sn*-glycero-3-phospho-L-serine (sodium salt) (DOPS) were obtained as solutions (10 mg/ mL chlorofom) from Avanti Polar-Lipids (Alabaster/AL, USA). Filter with a hydrophilic PTFE membrane and 0.2  $\mu\text{m}$  pore size were obtained from Millipore.

#### 3.2.3.5 Working conditions and apparatus:

Experiments were performed at 20 °C. All SPR measurements were performed on a RES-TEC RT2005 (Res-Tec, Mainz, Germany) with SF10 sensor chips (unmodified gold on high refractive index glass, XanTec bioanalytics, Duesseldorf, Germany) equipped with a flow cell (10  $\mu\text{L}$ , teflon, Res-Tec, Mainz, Germany) and a peristaltic pump IsmatecReglo ICC (Idex, Wertheim, Germany). Plasmon excitation was effected in Kretschmann configuration[25] with a He-Ne-Laser ( $\lambda= 632.8 \text{ nm}$ ).

Injection of vesicles as well as polymer-lipid interactions was followed by measuring the intensity of the reflected laser beam every 0.5 seconds. The incidence angle was between 55.35 and 55.60° for the formation of the lipid film and between 55.85 and 56.77° for the polymer-lipid interaction. The angles were chosen to obtain the same initial intensity of the signal. Signal measurements are given in reflectance units (RU).

### 3.2.3.6 Lipid vesicles

All manipulations were performed with immaculately clean, grease-free glassware. 2.5 mL lipid solution (10 mg/mL pure DOPC or DOPC/DOPS 4:1 by volume in chloroform) was placed in a small vial. The solvent was evaporated under reduced pressure and the vial was gently shaken until a lipid film was formed on the vial walls. The film was then dried at high vacuum ( $10^{-3}$  mbar) for at least 4 h. The lipid film was then hydrated with 1.0 mL HEPES buffer (10 mM, 107 mM NaCl, pH = 7.4) and shortly vortexed (4 times, every 15 min). The vesicle solution was then subjected to seven freeze-thaw cycles, which yielded unilamellar vesicles. To obtain small vesicles with even size distribution, this solution was extruded six times through a polycarbonate membrane with 200 nm pore-size and seven times through a polycarbonate membrane with 50 nm pore-size at 65 °C. Prior to use, the solution was diluted with HEPES to 1 mM vesicle concentration (0.05 mL vesicle solution + 1.45 mL buffer).

### 3.2.3.7 Polymer solutions

Polymer ( $4 \cdot 10^{-4}$  mmol) was dissolved in 100  $\mu$ L DMSO and diluted with HEPES buffer to a concentration of 10  $\mu$ M.

### 3.2.3.8 SPR

Prior to use, all solutions were freshly prepared and filtered (0.20  $\mu$ m). The SPR chip was mounted into the SPR flow cell and connected to the peristaltic pump. The lipid film on the SPR chip was produced by flowing the vesicles solution over the chip (3  $\mu$ L/min) until a plateau was reached (at least 3600s contact time, which corresponds to 18x the flow cell volume). A short injection of 10 mM NaOH (30  $\mu$ L/min, 240 s, 12x flow cell volume) was used to remove loose

vesicles, followed by rinsing with HEPES buffer (30  $\mu\text{L}/\text{min}$ , 240 s and 5  $\mu\text{L}/\text{min}$ , 300 s) to obtain a stable signal. The surface was kept under buffer. In a control measurement, it was tested that injection of DMSO in buffer at the same concentrations as in the polymer solution does not influence the lipid film. For each measurement, a fresh chip was used. HEPES buffer was pumped over the vesicle surface to obtain a stable signal (5  $\mu\text{L}/\text{min}$ , 600 s), followed by the polymer solution (5  $\mu\text{L}/\text{min}$ , 1200 s, 10x flow cell volume). Finally, HEPES buffer was injected until a stable signal was reached (5  $\mu\text{L}/\text{min}$ , at least 3600 s). The amount of bound polymer was measured in RU under the same conditions as with the lipid measurements.

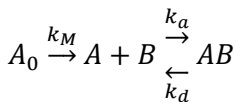
### 3.2.3.9 Curve Fitting

To fit the SPR data to a transport-limited kinetic model both the binding and unbinding curves were used. First, the dissociation curve was fit to a simple exponential:

$$[AB] = ([AB]_0 - [AB]_\infty)e^{-k_d[AB]} + [AB]_\infty$$

Where  $[AB]$  is the bound polymer concentration (proportional to the signal response),  $[AB]_0$  is the initial bound polymer concentration,  $[AB]_\infty$  is the bound polymer after infinite time, and  $k_d$  is the dissociation constant. The data from the dissociation curve was fit to this function but a least-squares method in Mathematica.

To fit the binding curves, the approximation used by Myszka et al.[26] was implemented. In this two compartment model, polymer concentration within a distance  $h_i$  from the surface ( $C(t)$ ) is seen as the polymer concentration available for binding. This creates a to-stage binding relation:



Where  $A_0$  is the polymer concentration in the injected solution,  $A$  is the polymer concentration near the surface,  $B$  is the number of binding sites available,  $k_a$  is the association constant, and  $k_M$  is the transport coefficient.

Under this system, the binding behavior can be described by a pair of differential relations:

$$h_i \frac{d[A]}{dt} = -k_a[A]([B] - [AB]) + k_d[AB] + k_M([A_0] - [A])$$

$$\frac{d[AB]}{dt} = k_a[A]([B] - [AB]) - k_d[AB]$$

Here, we assume a state of quasi-equilibrium where  $d[A]/dt=0$ , in which case the values of  $k_a$ ,  $k_d$  and  $k_M$  become independent of  $h_i$ . [26, 27] For ease of calculation, then, we set  $h_i=1\text{RU/M}$  and measure  $[AB]$  in RU. This gives us the similar relationship:

$$\frac{d[A]}{dt} = -k_a[A]([\tilde{B}] - [\tilde{AB}]) + k_d[\tilde{AB}] + \tilde{k}_M([A_0] - [A])$$

$$\frac{d[\tilde{AB}]}{dt} = k_a[A]([\tilde{B}] - [\tilde{AB}]) - k_d[\tilde{AB}]$$

Where  $[\tilde{B}] = [B]/h_i$ ,  $[\tilde{AB}] = [AB]/h_i$ , and  $\tilde{k}_M = k_M/h_i$ . These differential equations are solved analytically and fit to the data using a least-squares method in Mathematica.

### 3.3 Results and Discussion

#### 3.3.1 Polymer Design

The polymer library used for this study (Figure 3.1) is identical to the imide series presented in chapter 2. These polymers present a sequence of varying hydrophobicity with an average of 16 charges per polymer molecule. Polymer **1** consists of only guanidinium-containing polymer with no additional hydrophobic moieties. Polymer **2** has an additional average of four phenyl-containing monomer units, for a hydrophobic residue fraction of 20%. Polymer **3**

contains an average of 8 phenyl-containing units, for a hydrophobic fraction of 33%. As a result, all polymers in this system would be expected to have similar electrostatic interactions with anionic surfaces but different water and lipid solubilities.

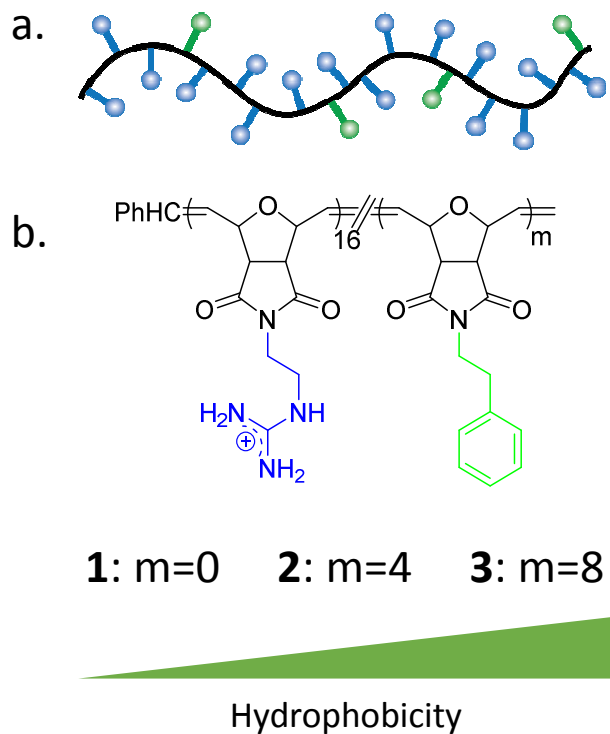


**Figure 3.1.** The polymer design used for this study. (Top) Cartoon representation of random copolymer 2. (Middle) Generic polymer structure for the series.

### 3.3.2 Dye Release Studies

The dye release profile of polymer **1** with EYPC (Figure 3.2a, Table 3.1) has a clearly-defined  $EC_{50}$  value (7.3nM), unlike dye release from 80:20 EYPC:Brain PS vesicles, which has some small amount of dye release (less than 15% at 7 $\mu$ M) but no defined  $EC_{50}$ . This result runs counter to conventional wisdom for most guanidinium-rich PTD(M)s, where anionic lipid content is generally deemed necessary for membrane activity. Indeed, the opposite effect has

previously been noted for polyarginine, where addition of anionic EYPG to an otherwise zwitterionic EYPC vesicle system increased dye release.[13] That polymer **1** has reduced membrane activity upon the addition of anionic lipid content was previously reported, but no further study of such behavior was made.[15] Polymers **2** and **3** (Figures 3.2b and 3.2c) demonstrate how this effect changes with increased polymer hydrophobicity. Polymer **2** has a similar  $EC_{50}$  to polymer **1** against EYPC vesicles (6.4nM), with a higher maximum fluorescence (65% vs. 35%). Against 80:20 EYPC:Brain PS vesicles, however, the  $EC_{50}$  for polymer **2** (85nM) is much closer to the EYPC value. This trend of convergence continues with polymer **3**, where the  $EC_{50}$  values (14nM for EYPC, 67nM for 80:20 EYPC:Brain PS) are closer to one another than for the other polymers. It is thus clear that for the most hydrophilic polymer **1**, the presence of anionic lipid in lipid vesicles strongly reduces membrane activity, but that this effect decreases with increasing polymer hydrophobic content. This effect was also examined for polymer **2** against DOPC and 80:20 DOPC:DOPS vesicles to ensure lipid phase was not causing this difference. (Figure 3.3) Both DOPC and DOPS have very low spontaneous curvature values,[28] so it is unlikely that the addition of 20% DOPS has any meaningful effect on the ability of these membranes to form negative Gaussian curvature.[22]

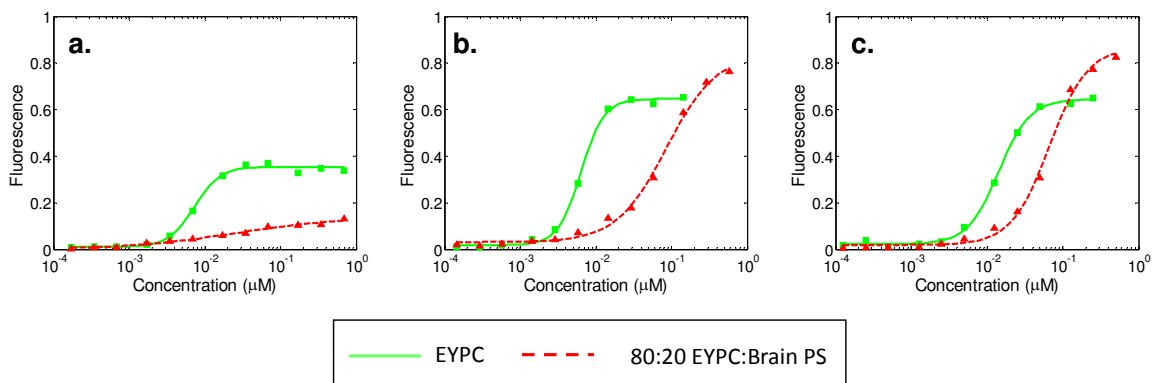


**Figure 3.2.** Dye release for the polymers a) **1** b) **2** and c) **3** from carboxyfluorescein-loaded EYPC (green squares) and 80:20 EYPC:Brain PS (red triangles) vesicles. Green lines and red dashes are fits to the Hill Equation.

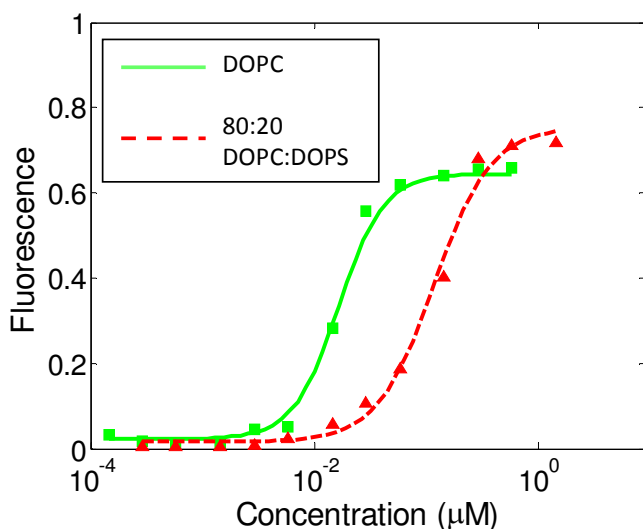


**Figure 3.3.** Dye release of polymer 2 from DOPC (green squares) and 80:20 DOPC:DOPS (red triangles) vesicles. Green lines and red dashes are fits to the Hill Equation.

**Table 3.1.** EC<sub>50</sub> values for the dye release experiments.

Polymer	EC <sub>50</sub> (μM)			EC <sub>50</sub> (μM)		
	EYPC	80:20 EYPC/Brain PS	Ratio	DOPC	80:20 DOPC/DOPS	Ratio
1	0.0073	>7	>900			
2	0.0064	0.085	13.4	0.016	0.117	7.12
3	0.014	0.067	4.68			

### 3.3.3 Size and Zeta Potential

The “adaptive translocation” model generally supposes that cation-anion binding is critical to membrane activity.[1] To compare surface association behavior with membrane activity, we looked at size and zeta potential of vesicles under similar conditions to those used in the dye release experiments. (Figure 3.4) 100nm vesicles at the same concentration as used in the dye release experiments (2.5 $\mu$ M lipid) were exposed to varying quantities of polymer **2**, and both zeta potential and dynamic light scattering mean size were measured. The isoelectric point (IEP) and the aggregation behavior of the vesicles can be used to demonstrate the point at which surface charge neutralization occurs, while the high-concentration plateau of the zeta potential gives the surface-association saturation point. For reference to these data points, the EC50 values for DOPC (green dashed line) and 80:20 DOPC:DOPS (red dashed line) are shown.

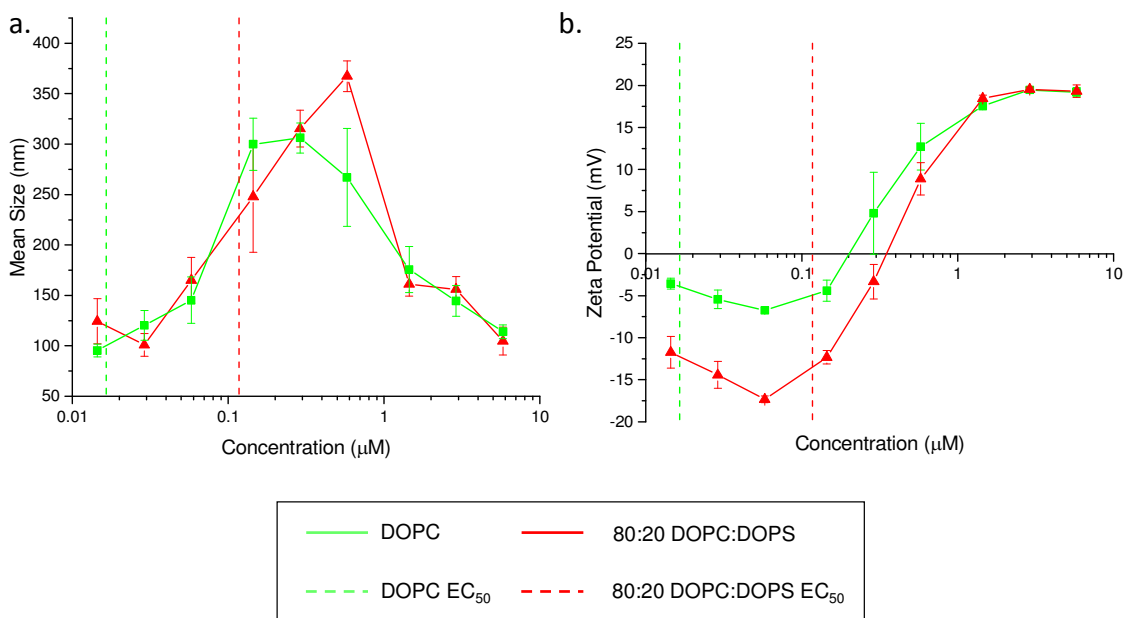


**Figure 3.4.** a) Number mean particle size by dynamic light scattering and b) zeta potential measurements for the interaction of varying concentrations of polymer **2** with phospholipid vesicles. Green squares represent data for zwitterionic DOPC vesicles, while red triangles



represent data for anionic 80:20 DOPC:DOPS vesicles. Green and red dashes represent the dye release EC<sub>50</sub> values for the DOPC and 80:20 DOPC:DOPS vesicle systems, respectively.

Several clear, important trends become noticeable. The first is that the both the zwitterionic and anionic lipid systems have a typical sigmoidal zeta potential response to the addition of polymer. This is typical of polyelectrolyte adsorption onto an oppositely-charged surface.[29, 30] The zwitterionic vesicles appear to maintain some small amount of negative charge before the addition of polymer, although this level is considerably lower than for the anionic lipid system. The isoelectric points of these two systems is similar; 0.2  $\mu$ M for the zwitterionic system and 0.4  $\mu$ M for the anionic system. Perhaps more importantly, the zeta potential for both systems reaches a plateau at around the same concentration (2  $\mu$ M) and at the same zeta potential value (20mV), suggesting that the total accumulated amount of polymer on the surface is similar. The mean size data (Figure 3.4a) supports the notion of similar binding behavior, as the two vesicles systems demonstrate similar aggregation properties, with maximum aggregation around the isoelectric point. This is consistent with studies of the interaction of cationic polymers with anionic particles, which show a maximum rate of vesicle aggregation at charge neutralization, with reduced rates at both lower and higher polymer concentrations.[29-31] These two data sets combined mean that while membrane activity (as shown through dye release) is highly differentiated between anionic and zwitterionic lipid systems, the initial binding behavior is not. For DOPC vesicles, the EC<sub>50</sub> value is an order of magnitude below the isoelectric point, while for 80:20 DOPC:DOPS, the EC<sub>50</sub> and isoelectric points are only a factor of 2 apart, suggesting that the difference in activity is due to membrane interaction aspects other than surface association rates.

Light scattering data also tells us two other important features. The first is that while the dye release studies do not distinguish between dye released by membrane permeabilization

and dye released by vesicle disruption, the light scattering data suggests that these vesicles remain largely intact at concentrations relevant to dye release. This suggests that the dye release studies function by some process other than simple membrane disruption. Secondly, light scattering of the polymer in buffer solution alone (Figure 3.5) demonstrates that some amount of aggregate material is present for each polymer used. The aggregates are larger for polymer 3, though, indicating that this polymer is less soluble in solution than the others.

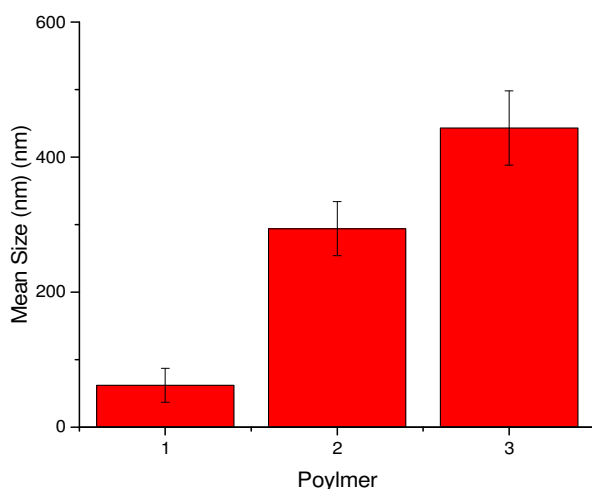


**Figure 3.5.** Dynamic light scattering of 10 $\mu$ M polymer in buffer solution.

### 3.3.4 Surface Plasmon Resonance

To examine the relationship between binding, bilayer insertion, and membrane activity, we turn to surface plasmon resonance (SPR). SPR relies on the plasmon resonance phenomenon, where for a specific incidence angle light cast on to a gold-plated chip is adsorbed in an evanescent wave.[32-34] When material accumulates on the surface of the chip, the refractive index of the chip is altered and the incidence angle changes. By monitoring the reflectivity at a single angle on the leading slope of the reflectivity dip, it is possible measure the real-time surface adsorption of an analyte. While the dye release and zeta potential

experiments had identical lipid and polymer concentrations, SPR is performed fundamentally differently. The concentration of polymer in solution remains fixed due to continuous flow, meaning that the only limits on the amount of polymer interaction with the lipid bilayer is the kinetics of interaction and the amount of polymer that is able to adsorb onto the lipid layer.

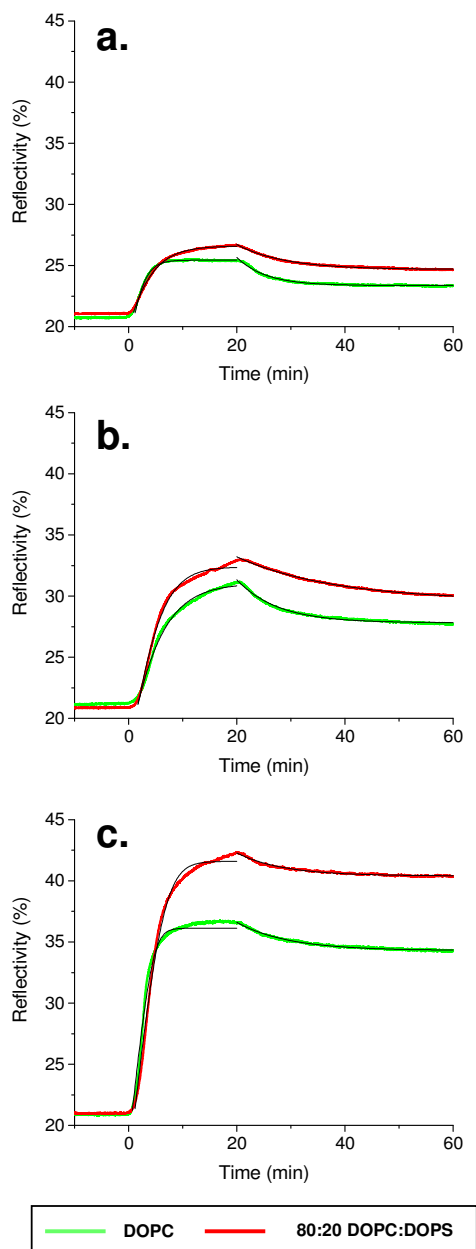


**Figure 3.6.** Surface plasmon resonance binding and unbinding curves for 10 $\mu$ M of polymer (a) **1**, (b) **2** and (c) **3**. Green lines represent binding to the zwitterionic DOPC lipid system, while red

lines represent binding to the anionic DOPC:DOPS system. The bilayer was exposed to a continuous flow of polymer solution starting at t=0 and then flushed with buffer starting at t=20 minutes. Black lines represent model fits.

**Table 3.2.** Peak and final change in reflectance for SPR experiments.

Polymer	DOPC		DOPC:DOPS	
	Peak (RU)	After Buffer (RU)	Peak (RU)	After Buffer (RU)
1	4.7	2.5	5.7	3.7
2	10.6	7.2	12.1	9.1
3	15.8	13.3	21.3	19.4

The SPR data here (Figure 3.6, Table 3.2) corroborates the size and zeta potential data from Figure 3.4. In each case, a phospholipid bilayer is exposed to a continuous flow of 10 $\mu$ M polymer. While for all three polymers the polymer binds slightly more strongly to the anionic lipid system than the purely zwitterionic one, this effect is dwarfed by the increase in binding due to the differences in polymer hydrophobicity. After 20 minutes, polymer **1** increases the SPR signal by a total of 4.7 reflectance units (RU) on the DOPC bilayer, and by 5.7 RU for the 80:20 DOPC:DOPS bilayer, for an increase of 21%. Polymer **2** shows a signal of 10.6 RU with the DOPC bilayer, a 126% increase in signal over polymer **1**. While polymer **2** is 12.1 RU with the DOPC:DOPS bilayer, this is only a 14% increase over the signal with the DOPC bilayer. For polymer **3** with the DOPC bilayer, there is a signal of 15.8 RU, and increase of 48% over that for polymer **2**. For the DOPC:DOPS bilayer, polymer **3** contributes 21.3 RU, an increase of 34% over the signal for the zwitterionic DOPC bilayer. It's worth noting, however, that the amount of polymer removed from the membrane after a prolonged buffer flow was relatively independent of both membrane composition and polymer hydrophobicity. In each case, a drop of 1.9-3.4 RU was recorded, with the largest drops occurring for polymer **2**.

**Table 3.3.** Fitting parameters for transport ( $k_M$ ), association ( $k_a$ ), and disassociation ( $k_d$ ) for all three polymers. Fitting was performed using a transport-limited rate model.

Polymer	DOPC			DOPC:DOPS		
	$k_M$ (RU cm $M^{-1} s^{-1}$ )	$k_a$ ( $M^{-1} s^{-1}$ )	$k_d$ ( $s^{-1}$ )	$k_M$ (RU cm $M^{-1} s^{-1}$ )	$k_a$ ( $M^{-1} s^{-1}$ )	$k_d$ ( $s^{-1}$ )
1	8517	984	$3.09 \times 10^{-3}$	8517	351	$1.89 \times 10^{-3}$
2	8517	255	$2.19 \times 10^{-3}$	8517	549	$9.22 \times 10^{-4}$
3	8517	2192	$1.75 \times 10^{-3}$	8517	1229	$1.94 \times 10^{-3}$

The kinetic curves from the SPR data were fitted to a mathematical model. The unbinding curve gave the dissociation constant  $k_d$ , which was then folded into a transport-limited binding model,[26] where the transport rate constant ( $k_M$ ) was fitted to a single value over the series. The data for this fitting is shown in Table 3.3, and the curves themselves are shown in Figure 3.6. There is a fair bit more variation in the kinetic data than there was in the peak and final reflectance values. Additionally, the quality of the fits is very high for polymer **1**, but polymers **2** and **3** show poorer fits. Two trends are evident, however. One is that the dissociation constants are fairly similar across the board, not changing within a series by much more than a factor of two. The dissociation values are also slightly higher as a whole for the DOPC lipid system than the DOPC:DOPS system. The association values are less consistent with the DOPC system, but in both sets polymer 3 shows much stronger binding than polymers 1 or 2.

From the SPR data, it is clear that while anionic content increases the membrane association of all polymers, this effect is far smaller than the effect of increased polymer hydrophobicity. After flushing with buffer for 40 minutes, there is 5.3 times as much polymer **3** bound to the DOPC membrane as polymer **1**. By comparison, polymer 1 shows the largest fractional increase of binding due to anionic content, with the DOPC:DOPS layer containing 1.5 times as much polymer as DOPC alone. It is then reasonable to state that membrane association is primarily driven by hydrophobic interactions with electrostatics playing a

secondary, ancillary role. This has major implications for how we consider PTDM-membrane interactions for this class of polymer. The first is that while it is clear from the dye release data that anionic lipid content acts as a barrier to membrane activity, it does not greatly affect initial association of the polymer to the membrane. This means that the anionic content must affect other stages of membrane interaction—namely, the ability of the polymer to transport across the membrane and provide release for the dye. This is in direct contradiction to the “adaptive translocation” model that is frequently proposed for PTDs and PTDMs. Instead of the anionic lipid assisting in polymer transport across the membrane, they instead pin the polymer to one side and prevent movement across the bilayer.

The second implication is that cationic nature of these polymers may not be critical for energy-independent transport. Net positive charge has previously been assumed to be necessary to allow anionic amphiphiles to assemble around the polymer and integrate it into the membrane.[13] It has also been proposed that the special bidentate hydrogen bonding capabilities of guanidinium ions with phosphate groups allows for improved membrane integration.[13, 14, 22, 23] However, if the polycation-anionic surface interactions are detrimental to membrane transport, it is possible that a neutral polymer containing a similar balance of water and lipid solubility could be equally if not more effective at membrane transport. Neutral polymers have the advantage of generally being considered less toxic than cationic polymers.[35-37] In particular, a polymer containing a guanidinium group and overall zwitterionic nature may provide the optimum balance of activity and low toxicity.

The association kinetics of the polymers **1** and **3** to the membrane in the SPR experiments are so rapid that they are transport limited, meaning that their kinetic profile is limited by the rate of polymer introduction to the surface. A transport-limited rate model was introduced to account for this effect. While this model generated excellent fits for polymer **1**, it

is apparent that this model is still not an excellent fit for polymers **2** or **3**. This suggests further complexity. This is particularly noticeable when looking at the kinetic traces for polymer **2**. While the association of polymers **1** and **3** to the membrane is very rapid, approaching saturation before 10 minutes, polymer **2** shows a slower kinetic trace. All three polymers have very narrow polydispersities and show no tailing or shoulders, (Figure 3.7, Table 3.3) so this difference isn't likely due to synthetic irregularity or defect. The most likely explanation of the difference in these traces can be found in a two-step binding model. Polymer **1** shows rapid surface binding—the first step—but saturates quickly as very little of the polymer sits in the lipid layer. Polymer **3** shows rapid surface binding and rapid integration into the membrane, allowing it a much higher binding capacity but still rapid kinetics. Polymer **2**, on the other hand, still has a rapid first step, but a slow second step, resulting in the high total membrane association but slower kinetics.

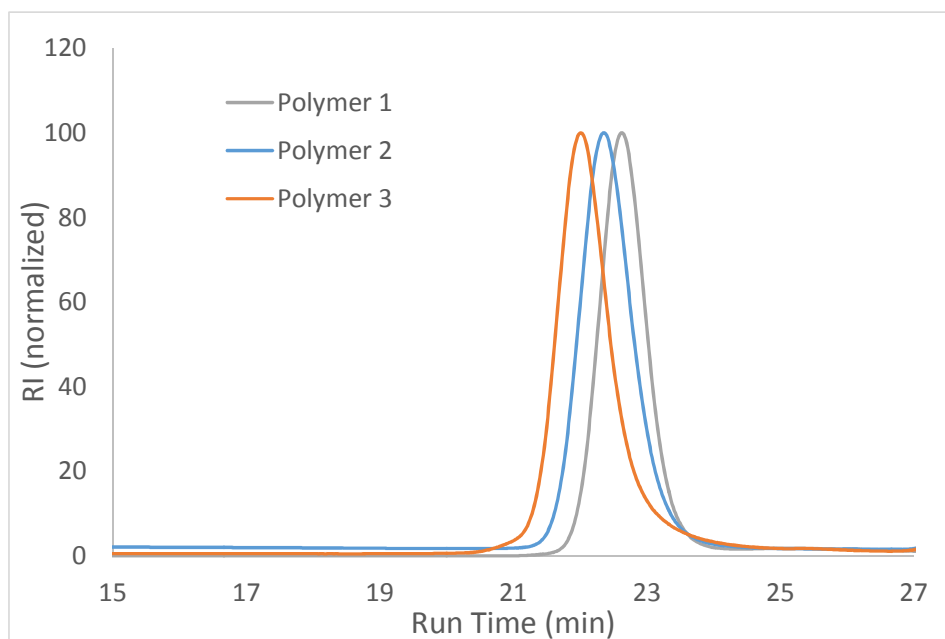


**Figure 3.7.** GPC traces of polymers 1, 2, and 3.

**Table 3.4.** GPC molecular weights of the polymers.

Polymer	Mn (g/mol)	$\bar{D}$
1	7400	1.08
2	8050	1.10
3	8400	1.06

### 3.4 Conclusions

The dye release data demonstrates conclusively that the introduction of anionic lipid to phospholipid membranes presents a barrier to ROMP-based PTDM activity, but that this barrier can overcome with the addition of hydrophobic moieties to the polymer. Light scattering and zeta potential showed that polymer 2 had similar surface-association behavior with both anionic and zwitterionic lipid systems, and that this binding does not correlate with membrane activity. Surface plasmon resonance tells a similar story, where the increase in binding due to the presence of anionic lipid is far smaller than that due to added polymer hydrophobicity.

From this data, then, a clearer picture of how these polymers are able to translocate phospholipid membranes begins to appear. The first step is a membrane association driven by hydrophobic interaction. Once on the lipid surface, anionic content on the surface will “pin” the polymer on that outer leaflet and prevent further penetration. As polymer hydrophobicity is increased, however, the polymer is able to overcome that electrostatic interaction, reducing the gap in activity between purely zwitterionic and anion-containing lipid systems. This concept of a membrane feature acting as a barrier to activity, but one that can be overcome by added hydrophobicity was previously explored with regards to membrane phase in chapter 2. It is possible that a similar experimental model could be applied to other membrane components, such as protein content. The result is a system where a “generic” zwitterionic, fluid-phase lipid



system may be easy for a hydrophilic polymer to penetrate, but that additional membrane components will increase the hydrophobicity threshold for activity.

It is important to remark that the implications of this study are limited to this particular PTDM design. As mentioned in the introduction, similar studies of the effect of anionic lipid on the activity of oligo- and polyarginine have produced very different results. While the exact reason for this discrepancy is still unclear, it is possible that the ROMP-based PTDM activity is more dominated by polymer hydrophobicity than polyarginine, which has substantially less hydrophobic content. Thus, while the difference in membrane association between anionic and zwitterionic lipid systems and ROMP PTDMs is small, it may be much larger for polyarginine. Additionally, as was shown in chapter 2 (Figures 2.5 and 2.7), R9 does not induce dye release in EYPC vesicles, so it is perhaps no surprise that this polymer system produces mechanistically different results. The results are nonetheless important, though, as they provide guidelines for the design of new and superior polymers for cellular uptake, as well as insight into the physics of this apparently unique membrane transporting molecules.

### 3.5 References

1. Wender, P.A., et al., *The design of guanidinium-rich transporters and their internalization mechanisms*. *Advanced Drug Delivery Reviews*, 2008. **60**(4-5): p. 452-472.
2. Richard, J.P., et al., *Cell-penetrating Peptides*. *Journal of Biological Chemistry*, 2003. **278**(1): p. 585-590.
3. Nakase, I., et al., *Cellular Uptake of Arginine-Rich Peptides: Roles for Macropinocytosis and Actin Rearrangement*. *Molecular Therapy*, 2004. **10**(6): p. 1011-1022.
4. Takeuchi, T., et al., *Direct and Rapid Cytosolic Delivery Using Cell-Penetrating Peptides Mediated by Pyrenebutyrate*. *ACS Chemical Biology*, 2006. **1**(5): p. 299-303.
5. Al-Taei, S., et al., *Intracellular Traffic and Fate of Protein Transduction Domains HIV-1 TAT Peptide and Octaarginine. Implications for Their Utilization as Drug Delivery Vectors*. *Bioconjugate Chemistry*, 2006. **17**(1): p. 90-100.
6. Futaki, S., *Membrane-permeable arginine-rich peptides and the translocation mechanisms*. *Advanced Drug Delivery Reviews*, 2005. **57**(4): p. 547-558.
7. Tezgel, A.Ö., et al., *Novel Protein Transduction Domain Mimics as Nonviral Delivery Vectors for siRNA Targeting NOTCH1 in Primary Human T cells*. *Molecular Therapy*, 2013. **21**(1): p. 201-209.

8. Tezgel, A.O., *Protein Transduction Domain Mimics by ROMP and Their Bioactive Cargo Delivery*, in *Polymer Science and Engineering* 2013, University of Massachusetts--Amherst: Amherst, MA. p. 156.
9. Gait, M.J., *Peptide-mediated cellular delivery of antisense oligonucleotides and their analogues*. Cellular and molecular life sciences: CMLS, 2003. **60**(5): p. 844-853.
10. Moulton, H.M. and J.D. Moulton, *Arginine-rich cell-penetrating peptides with uncharged antisense oligomers*. Drug Discovery Today, 2004. **9**(20).
11. Nagahara, H., et al., *Transduction of full-length TAT fusion proteins into mammalian cells: TAT-p27Kip1 induces cell migration*. Nature medicine, 1998. **4**(12): p. 1449-1452.
12. Zatsepin, T., et al., *Conjugates of Oligonucleotides and Analogues with Cell Penetrating Peptides as Gene Silencing Agents*. Current Pharmaceutical Design, 2005. **11**(28): p. 3639-3654.
13. Sakai, N. and S. Matile, *Anion-Mediated Transfer of Polyarginine across Liquid and Bilayer Membranes*. Journal of the American Chemical Society, 2003. **125**(47): p. 14348-14356.
14. Nishihara, M., et al., *Arginine magic with new counterions up the sleeve*. Organic & Biomolecular Chemistry, 2005. **3**(9): p. 1659-1669.
15. Hennig, A., et al., *Stimuli-Responsive Polyguanidino-Oxanorbornene Membrane Transporters as Multicomponent Sensors in Complex Matrices*. Journal of the American Chemical Society, 2008. **130**(31): p. 10338-10344.
16. Som, A., A. Reuter, and G.N. Tew, *Protein Transduction Domain Mimics: The Role of Aromatic Functionality*. Angewandte Chemie International Edition, 2012. **51**(4): p. 980-983.
17. Som, A., et al., *Self-Activation in De Novo Designed Mimics of Cell-Penetrating Peptides*. Angewandte Chemie International Edition, 2011. **50**(27): p. 6147-6150.
18. Alves, I.D., et al., *Relationships between Membrane Binding, Affinity and Cell Internalization Efficacy of a Cell-Penetrating Peptide: Penetratin as a Case Study*. PLoS ONE, 2011. **6**(9).
19. Alves, I.D., et al., *Cell biology meets biophysics to unveil the different mechanisms of penetratin internalization in cells*. Biochimica et Biophysica Acta (BBA) - Biomembranes, 2010. **1798**(12): p. 2231-2239.
20. Jiao, C.-Y., et al., *Translocation and Endocytosis for Cell-penetrating Peptide Internalization*. Journal of Biological Chemistry, 2009. **284**(49): p. 33957-33965.
21. Walrant, A., et al., *Different membrane behaviour and cellular uptake of three basic arginine-rich peptides*. Biochimica et Biophysica Acta (BBA) - Biomembranes, 2011. **1808**(1): p. 382-393.
22. Mishra, A., et al., *Translocation of HIV TAT peptide and analogues induced by multiplexed membrane and cytoskeletal interactions*. Proceedings of the National Academy of Sciences of the United States of America, 2011. **108**(41): p. 16883-16888.
23. Schmidt, N.W., et al., *Molecular Basis for Nanoscopic Membrane Curvature Generation from Quantum Mechanical Models and Synthetic Transporter Sequences*. Journal of the American Chemical Society, 2012. **134**(46): p. 19207-19216.
24. Yandek, L.E., et al., *Mechanism of the Cell-Penetrating Peptide Transporter 10 Permeation of Lipid Bilayers*. Biophysical Journal, 2007. **92**(7): p. 2434-2444.
25. Kretschmann, E., *Die Bestimmung optischer Konstanten von Metallen durch Anregung von Oberflächenplasmaschwingungen*. Zeitschrift für Physik, 1971. **241**(4): p. 313-324.

26. Myszka, D.G., et al., *Extending the range of rate constants available from BIACORE: interpreting mass transport-influenced binding data*. Biophysical Journal, 1998. **75**(2): p. 583-594.
27. Segel, L. and M. Slemrod, *The Quasi-Steady-State Assumption: A Case Study in Perturbation*. SIAM Review, 1989. **31**(3): p. 446-477.
28. Zimmerberg, J. and M.M. Kozlov, *How proteins produce cellular membrane curvature*. Nature Reviews Molecular Cell Biology, 2006. **7**(1): p. 9-19.
29. Hierrezuelo, J., et al., *Electrostatic Stabilization of Charged Colloidal Particles with Adsorbed Polyelectrolytes of Opposite Charge*. Langmuir, 2010. **26**(19): p. 15109-15111.
30. Kleimann, J., et al., *Super-Stoichiometric Charge Neutralization in Particle–Polyelectrolyte Systems*. Langmuir, 2005. **21**(8): p. 3688-3698.
31. Gabriel, G.J., et al., *Interactions between Antimicrobial Polynorbornenes and Phospholipid Vesicles Monitored by Light Scattering and Microcalorimetry*. Langmuir, 2008. **24**(21): p. 12489-12495.
32. Beseničar, M., et al., *Surface plasmon resonance in protein–membrane interactions*. Chemistry and Physics of Lipids, 2006. **141**(1–2): p. 169-178.
33. Morton, T.A., D.G. Myszka, and I.M. Chaiken, *Interpreting complex binding kinetics from optical biosensors: a comparison of analysis by linearization, the integrated rate equation, and numerical integration*. Analytical Biochemistry, 1995. **227**(1): p. 176-185.
34. Mozsolits, H. and M.-I. Aguilar, *Surface plasmon resonance spectroscopy: An emerging tool for the study of peptide–membrane interactions*. Peptide Science, 2002. **66**(1): p. 3-18.
35. Fischer, D., et al., *In vitro cytotoxicity testing of polycations: influence of polymer structure on cell viability and hemolysis*. Biomaterials, 2003. **24**(7): p. 1121-1131.
36. Morgan, D.M., V.L. Larvin, and J.D. Pearson, *Biochemical characterisation of polycation-induced cytotoxicity to human vascular endothelial cells*. Journal of Cell Science, 1989. **94 ( Pt 3)**: p. 553-559.
37. Parhamifar, L., et al., *Polycation cytotoxicity: a delicate matter for nucleic acid therapy—focus on polyethylenimine*. Soft Matter, 2010. **6**(17): p. 4001-4009.

## CHAPTER 4

### GUANIDINIUM-RICH POLYMERS DISPLAY LENGTH- AND HYDROPHOBICITY-DEPENDENT NEGATIVE GAUSSIAN CURVATURE GENERATION

Note: This work has been previously published as:

Schmidt N., M. Lis, K. Zhao, G. Lai, A. Anastassia, G. Tew, G. Wong. (2012) *Molecular basis for nanoscopic membrane curvature generation from quantum mechanical models and synthetic transporter sequences*. Journal of the American Chemical Society, 134, 19207

The computational modelling sections of this publication are not featured below, as the author did not contribute to that work.

#### 4.1 Introduction

Membrane-active peptides and proteins often use arginine to confer strong interactions with cell membranes. For example, hydrophilic arginine-rich cell penetrating peptides (CPP) such as the TAT peptide can efficiently translocate across cellular membranes.[1-6] Many types of antimicrobial peptides (AMP) like amphipathic  $\alpha$ - and  $\theta$ -defensins from mammals, which display potent in vitro activity against bacteria via membrane permeabilization, use arginine over lysine.[7-9] Due to their biological significance and complex interactions with cell membranes, much scientific effort has gone into understanding the observed structure–function relationships between arginine-rich peptides and biomembranes.

There is substantial evidence that the guanidine side chain of arginine is responsible for its unique membrane interactions. For CPPs, the first indication of its importance was demonstrated when Vives[1] showed that an arginine-rich, 11AA sequence from the transactivator of transcription (TAT) protein of HIV, YGRKKRRQRRR, now referred to as the TAT

peptide, is sufficient for cellular uptake. It was soon realized by Wender[10] and Mitchell[11] that the uptake ability of the TAT peptide was due to its guanidinium ions as exemplified by their demonstrations that l- and d-arginine oligomers were more efficient than the TAT peptide, and homopeptides consisting of other cationic residues including histidine, lysine, and ornithine were less effective. They also showed that cellular uptake was a nonmonotonic function of poly arginine length[11] and depended on residue spacing.[12] As uptake is sensitive to the arrangement of arginine side chains a number of groups have designed synthetic guanidinium-rich cell penetrating molecules, or molecular transporters, using oligoarginine peptoids,[10] and nonpeptidic versions including synthetic polymers,[13-18] oligocarbamates,[19] polyguanidino dendrimers based on diamino acid monomeric units,[20] and carbohydrate-based molecules like guanidinylated neomycin.[21] Many of these molecules displayed similar or better uptake than poly arginine and the TAT peptide, suggesting that synthetic guanidinium-rich molecular transporters have a rich potential for applications such as drug delivery and antibiotics.

How CPP-membrane interactions promote uptake is not well understood at a fundamental molecular level. To explain the central role of the guanidinium group, Mitchell[11] originally cited its ability to form stable bidentate hydrogen bonds with anions such as phosphate or sulfate, which was believed to distinguish arginine from lysine and histidine. This was an interesting and conceptually powerful proposal. It implied that Arg-rich CPPs could in principle form strong complexes with anionic membrane components like phospholipid headgroups and enable uptake.[22] Conversely, the monodentate H-bonding abilities of Lys might be incapable of stabilizing strong complexes so Lys-rich peptides exhibit poor uptake.[22, 23] As the CPP discourse has primarily focused on whether they enter cells by direct translocation[24-29] or endocytosis,[30-34] the prevailing explanation for why Arg-rich peptides have better uptake than Lys-rich peptides has remained in terms of qualitative H-bonding

descriptions.[29, 35-38] Despite the widespread description of Arg vs Lys in terms of bidentate vs monodentate H-bonding for cationic, membrane-active transporters, there is no molecular understanding of how the interactions of guanidinium groups with anionic membrane components lead to translocation, while the interactions of amine groups with these components do not.

Recent work by the Wong group proposed a qualitative nanoscale model for understanding membrane curvature generation by CPPs[39] and AMPs.[40] Cationic polymers such as poly-Arg and poly-Lys can generate negative curvature via electrostatic interactions with anionic membranes.[41] For guanidinium groups, bidentate H-bonding[42] can in principle lead to enhanced steric effects that generate positive membrane curvature along a poly-Arg chain. Therefore, poly-Arg can generate negative Gaussian curvature, positive and negative curvature in orthogonal directions, which is necessary for active membrane permeation processes like pore formation and the membrane protrusions and invaginations present in endocytic processes.[41, 43, 44] This stands in contrast to presumed monodentate H-bonding of primary amine groups, the side chain of Lys, which cannot translocate across membranes. In this proposed qualitative model, the propensity for monodentate and bidentate H-bonding for lysine and arginine is assumed for simplicity. However, such propensity is likely complex because these interactions depend on the molecular details of the surrounding environment. Previous theoretical works[34, 35, 45, 46] on Arg-Arg and Lys-Lys associations in bulk water have shown that like-charge pairing is more stable between guanidinium groups than ammonium groups, and that interactions of guanidinium pairs are optimal when the side chains are in a stacking arrangement. Similar trends were observed at the level of potential of mean force from MD studies of guanidinium groups at the lipid bilayer-water interface.[47] What is not known is how these structural tendencies are expressed when Arg and Lys interact with phospholipid

headgroups, and how such tendencies are dependent on the effective spacing of the amino acid side chains. There is a significant need for a deeper understanding for how ensembles of side chains hydrogen bond to lipid headgroups.

In concurrently presented research, we investigated the physical origin of peptide-induced membrane curvature by contrasting differences between H-bonding interactions of Arg and Lys with phosphate groups using quantum mechanical (QM) calculations.[48] This chapter presents a test of those results via engineered molecular transporters without the geometric constraints imposed by polypeptide backbones. Surprisingly, QM calculations suggested that individual Lys can coordinate two phosphates. However, they are not able to do so at small inter-Lys distances without drastic energetic penalties. In contrast, Arg are able to coordinate two phosphates stably down to interguanidinium distances of less than 5 Å, where guanidinium groups stack “face to face”. We hypothesize that the persistence of this stacking arrangement in poly-Arg allows it to “cross-link” lipid headgroups into composite objects with a large effective head area and generate positive intrinsic curvature via excluded volume interactions in a manner that poly-Lys cannot duplicate. In agreement with this hypothesis, poly-Arg can generate the positive membrane curvature necessary for inducing negative Gaussian curvature, whereas poly-Lys cannot. Also consistent with QM calculations, polyguanidine-oxanorbornene homopolymers (PGONs), which have the same guanidinium side-chains as poly-Arg but are not constrained by distances characteristic of polypeptide chains, showed that curvature generation is exquisitely sensitive to the guanidinium group spacing when the phosphate groups are near close packing. An increase of guanidinium group spacing from 3.6 to 5.8 Å decreased the maximum induced negative Gaussian curvature by 22%. Our study provides a unified molecular description for how guanidinium groups contribute to the established membrane translocation abilities of molecular transporters.

Nanoscale positive curvature generation by lipid headgroup coordination is distinct from hydrophobic insertion, a complementary strategy of generating such curvature by peptides.[40, 49, 50] To examine how these two different mechanisms interact with one another, phenyl or butyl hydrophobic groups were added into guanidine-oxanorbornene polymers. In general, incorporation of hydrophobicity increased the amount of saddle-splay membrane curvature that was generated as well as broadened the range of lipid compositions where saddle-splay curvature was observed, showing that positive curvature generation by hydrophobicity can combine with lipid headgroup coordination by guanidinium to promote membrane permeation. Our results show that it is possible to design pore forming peptides with programmable membrane curvature generating abilities which influence their pore forming activities.

## 4.2 Materials and Methods

### 4.2.1 Synthetic Procedures

#### 4.2.1.1 Monomer Synthesis

The guanidine monomer was synthesized similar to previous reports,[14] with minor modifications. The hydrophobic monomers were synthesized as described previously[16, 17] with no modification, and therefore their syntheses are not reported here.

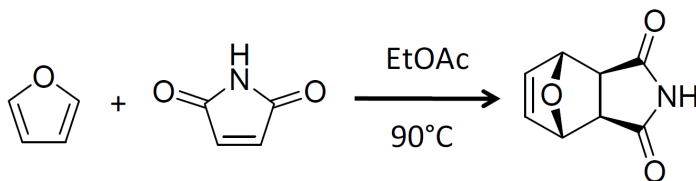


**Figure 4.1.** Diels-alder synthesis of oxanorbornene imide.

Oxanorbornene Imide. 10 g (103 mmol) of Maleimide and 10.0 g (10.6 mL, 146.8 mmol) furan were dissolved in 100 mL ethyl acetate. The Diels-Alder product was obtained by stirring at 90°C



for 3 h. The product precipitated upon cooling, and was filtered and dried under vacuum overnight. Yield=55%.

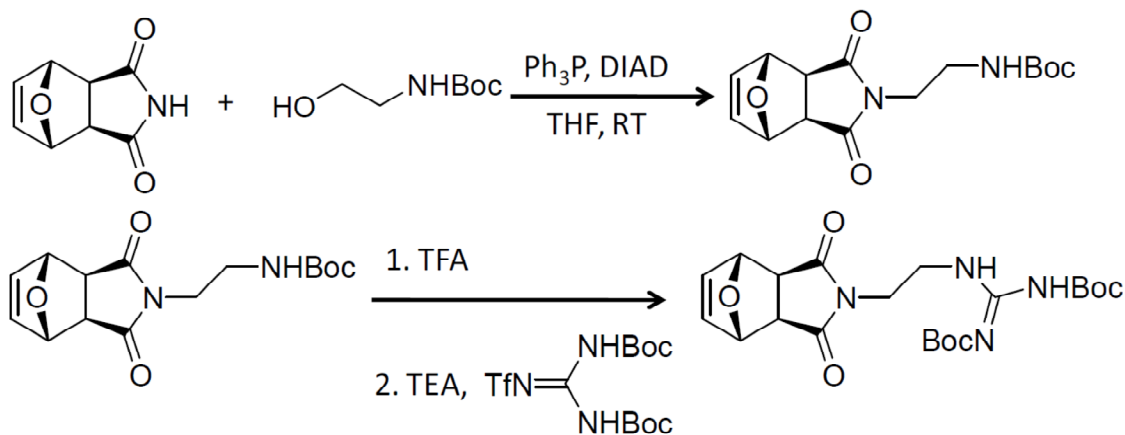


**Figure 4.2.** Synthesis of di-boc protected Guanidine monomer.

Di-Bioc Protected Guanidine Monomer. 5 g (30 mmol) oxanorbornene imide, 5.6 g (35 mmol) N-Boc-ethanolamine, and 8.0 g (30 mmol) triphenylphosphine were added to 100 mL dry THF and placed under nitrogen into an ice bath. 6.3 mL (30 mmol) diisopropyl azodicarboxylate (DIAD) is added dropwise, after which the solution is removed from the ice bath and the reaction is left for 24 hours. The solvent is reduced by rotary evaporator, and the concentrated solution is precipitated twice in diethyl ether. The yield is 5.2 g (17 mmol, 56%). The product is then deprotected in neat trifluoroacetic acid (TFA) and precipitated again in diethyl ether. The protonated salt and 5 mL triethylamine were added to 100 mL of dichloromethane. To the solution was added 9.8 g (25 mmol) 1,3-Di-Boc-2-(trifluoromethylsulfonyl)guanidine, and was allowed to stir 12 h. The solution was concentrated, washed with 10% potassium hydrogen sulfate, then saturated sodium bicarbonate, and purified by column chromatography. The final yield was 6.5 g (14 mmol).

$^1\text{H}$  NMR (300 MHz,  $\text{CDCl}_3$ ):  $\delta$  = 11.42 (1H, s), 8.41 (1H, t), 6.51 (2H, s), 5.26 (2H, s), 3.70 (2H, m), 3.60 (2H, m), 2.86 (2H, s), 1.47 (9H, s), 1.39 (9H, s).

$^{13}\text{C}$ -NMR (75 MHz,  $\text{DMSO-d}_6$ ):  $\delta$  = 176.3, 156.6, 153.0, 136.5, 83.3, 80.9, 47.6, 39.0, 38.4, 28.3, 28.1.

HR-MS (FAB): calc. 451.49, found 451.22.

#### 4.2.1.2 Polymer Synthesis

Polymer synthesis was performed similarly to reported procedures.[14, 16, 17, 51] Monomers were polymerized/co-polymerized by ring-opening metathesis polymerization (ROMP) using a 3rd generation Grubbs' catalyst. The monomer (~200mg) and appropriate amount of catalyst were dissolved in dry dichloromethane in separate Schlenk flasks. The flasks were placed under nitrogen and degassed using a freeze-pump-thaw procedure. The monomer was transferred to the catalyst flask and the polymerization was allowed to proceed at 25°C for an hour, after which 1 mL ethyl vinyl ether was added to terminate the reaction. After an hour, the solution was concentrated and precipitated twice in 100 mL pentane.

The Boc-protected polymers were deprotected by stirring the polymer in 10 mL 1:1 TFA: $\text{CH}_2\text{Cl}_2$  for 12 hours. The TFA was then removed by repeatedly co-evaporating with methanol in a rotary evaporator, then by placing under a vacuum for 4 h. The solid polymer was then suspended in water and freeze-dried for 3 days.

**Boc-Protected PGON.**  $^1\text{H}$ -NMR (300 MHz,  $\text{CD}_2\text{Cl}_2$ ):  $\delta$  = 11.49 (1H, br), 8.45 (1H, br), 6.08 (trans) and 5.80 (cis) (2H total, br), 5.02 (cis) and 4.48 (trans) (2H total, br), 1.52 (9H, s), 1.47 (9H, br), cis:trans ratio = 48:52.

**PGON.** <sup>1</sup>H-NMR (300 MHz, DMSO-d<sub>6</sub>): δ=7.88 (1H, br), 7.36 (4H, br), 5.96 (1H, br), 5.74 (1H, br), 4.92 (1H, br), 4.43 (1H, br) 3.47 (4H, br).

**Boc-Protected Butyl-GON.** <sup>1</sup>H NMR (300 MHz, CD<sub>2</sub>Cl<sub>2</sub>): δ=11.49 (5H, br), 8.45 (5H, br), 6.08 (trans) and 5.81 (cis) (22H total, br), 4.99 (cis), 4.46 (trans) (22H, br), 1.52 (99H, br), 1.47 (99H, br), 1.32 (12H, br), 0.95 (18H, br); cis:trans ratio = 53:47.

**Butyl-GON.** <sup>1</sup>H NMR (300 MHz, DMSO-d<sub>6</sub>): δ = 7.67 (5H, br), 7.27 (20H, br), 5.96 (11H, br), 5.75 (11H, br), 4.88 (11H, br), 4.43 (11H, br), 1.45 (12H, br), 1.23 (12H, br), 0.83 (18H, br).

**Boc-Protected Phenyl-GON.** <sup>1</sup>H NMR (300 MHz, CD<sub>2</sub>Cl<sub>2</sub>): δ=11.46 (5H, br), 8.44 (5H, br), 7.21 (30H, br), 6.05 (trans), 5.76 (cis) (22H total, br), 4.99 (cis), 4.46 (trans) (22H, br), 4.08 (12H, br), 2.91 (12, br) 1.52 (99H, br), 1.47 (99H, br); cis:trans ratio = 44:56.

**Phenyl-G.** <sup>1</sup>H NMR (300 MHz, DMSO-d<sub>6</sub>): δ = 7.27 (5H, br), 5.96-5.72 (4H, br), 4.88 (1H, br), 4.43 (1H, br), 4.10 (2H, br), 2.85 (2H, br)

## 4.2.2 Dye Release Studies

### 4.2.2.1 Vesicle Preparation

A lipid film was created by evaporating a 2mL chloroform solution containing 25mg egg yolk phosphatidylcholine (EYPC) in a rotary evaporator the under high vacuum overnight. The lipid was then hydrated for 1 hr in a dye buffer (10mM Tris, 10mM NaCl, 50 mM calcein, pH 7.5)

accompanied by intermittent vortexing. The resulting vesicles were placed under 6 freeze-thaw cycles (liquid nitrogen to 25°C water bath) and then extruded nine times through a polycarbonate membrane (400nm pore size). Free dye outside the buffers was removed by size exclusion chromatography (Sephadex G-50 superfine, Sigma Aldrich) in Tris saline buffer (10 mM Tris, 107 mM NaCl, pH 7.5).

#### 4.2.2.2 Dye Release Experiments

Dye release experiments were performed with a Biotek Synergy Mx fluorescence plate reader. All fluorescence measurements were with an excitation frequency of 492nm and an emission of 517nm. 1960  $\mu$ L tris saline buffer was added to each well in a 12 well plate. 20  $\mu$ L vesicle solution (diluted to a post-triton fluorescence of 70,000 counts, or about 2.5  $\mu$ M, in the well) was added to the wells and the plates were shaken at 25°C for 3 minutes when a baseline measurement,  $F_0$ , was taken. 20  $\mu$ L polymer solutions of varying concentrations were then added to the wells while stirring. The plate was then allowed to shake for another 10 minutes and another reading,  $F_{10}$ . 20  $\mu$ L of 5% Triton X-100 in DMSO was then added to the wells to release all dye from the vesicles. After 3 minutes of shaking, a final measurement was taken,  $F_T$ . Results were normalized according to the baseline and Triton controls to yield fractional dye release:

$$Y = (F_{10} - F_0)/(F_T - F_0)$$

The fractional dye release Y was then fitted as a function of concentration, c, to the Hill equation by a least-squares method:

$$Y = Y_m \frac{(c/EC_{50})^n}{1 + (c/EC_{50})^n}$$

Where  $EC_{50}$  is the concentration of 50% of maximal dye release and  $n$  is a fitting parameter.

### **4.2.3 Antimicrobial and Hemolysis Testing**

Antimicrobial and hemolysis testing were done similar to previous procedures.[51] Bacterial strains of *E. coli* (D31) and *S. aureus* (ATCC 25923) were incubated in Mueller-Hinton Broth overnight at 37 °C. The culture was then diluted to 10<sup>6</sup> CFU/mL, as measured by OD600. Polymers were then dissolved in a stock solution of 40 mg/mL in DMSO. Serial dilutions were performed in phosphate-buffered saline (PBS). Antibacterial activity was expressed as the minimum inhibitory concentration (MIC<sub>90</sub>), the concentration at which bacterial growth was inhibited by at least 90% compared to growth in broth alone after 6 h at 37 °C, as measured by OD600. Hemolytic activity was measured using separated red blood cells. Thirty microliters of human blood was suspended in 10 mL PBS and centrifuged three times, resuspending in buffer each time. Polymers were dissolved in a stock solution of 40 mg/mL in DMSO. Serial dilutions are performed in PBS; 100 µL of these polymer solutions were added to 100 µL of the blood cell solutions. These suspensions were allowed to stir for 30 min, then centrifuged. The absorbance of the supernatant at 414 nm was used to measure the amount of hemoglobin release. The positive control (total hemolysis) was obtained by adding 10 µL 20% Triton X-100 solution to the red blood cells. The HC50 was reported as the concentration of polymer that causes 50% release of hemoglobin.

### **4.2.4 SAXS Studies**

#### **4.2.4.1 Liposome Preparation for X-Ray Measurements**

Liposomes were prepared as described previously.[40] Briefly, DOPC (1,2-dioleoyl-sn-glycero-3-phosphocholine), DOPE (1,2-dioleoyl-sn-glycero-3-phosphoethanolamine), and DOPS (1,2-dioleoyl-sn-glycero-3-phospho-l-serine (sodium salt)), lyophilized lipids from Avanti Polar lipids were used without further purification. SUVs were prepared by sonication. Individual stock

solutions of DOPS, DOPC, and DOPE were prepared in chloroform at 20 mg/mL. Ternary mixtures of these lipids were prepared at mass ratios, for example, DOPS/DOPE/DOPC = 20/60/20 corresponds to a 1:3:1 mass ratio. Chloroform was evaporated under N<sub>2</sub>, and the mixtures were further dried by overnight desiccation under vacuum. The dried lipids were resuspended the next day in 100 mM NaCl or in Millipore H<sub>2</sub>O. Solutions were incubated at 37 °C for 12–24 h and then sonicated until clear. Small unilamellar vesicles (SUV's) were obtained via extrusion (0.2 µm pore Nucleopore filter).

#### **4.2.4.2 SAXS Experiments**

All polymers were resuspended in either 100 mM NaCl or in Millipore H<sub>2</sub>O. Lipids were thoroughly mixed with polymers at specific peptide to lipid ratios (P/L) in 100 mM NaCl. The solutions were hermetically sealed in quartz capillaries (Hilgenberg GmbH, Mark-tubes, Code No: 4017515). SAXS experiments at synchrotron sources were conducted at the Stanford Synchrotron Radiation Laboratory (BL 4–2), and the Advanced Light Source (beamline 7.3.3). Monochromatic X-rays with energies 9–11 keV were used at SSRL and 10 keV at ALS. The scattered radiation was collected using a Rayonix MX225-HE detector (pixel size, 73.2 µm) at SSRL and a Pilatus 100k detector (pixel size, 172 µm). Samples were also measured at the California NanoSystems Institute (CNSI) at UCLA using an in house setup. A compact SAXS light source (Forvis Technologies, Inc.) was used in conjunction with a mar345 image plate detector (pixel size, 150 µm). Identical samples were prepared and measured at multiple sources to check for and ensure mutual consistency. The 2D SAXS powder patterns were integrated using the Nika 1.48 package[52] for Igor Pro 6.21 and FIT2D.[53]

#### 4.2.4.3 SAXS Data Fits

A similar approach to the one described previously[40] was used to determine cubic phase lattice parameters. The measured cubic Q peak positions were related to the Miller indices h, k, and l, for the observed reflections using the equation for a powder averaged Pn3m cubic phase,  $Q_{\text{meas}}^{\text{Cubic}} = 2\pi\sqrt{(h^2 + k^2 + l^2)}/a$ . The lattice parameter, a, was calculated from the slope of the trendline obtained from a linear fit of  $Q_{\text{meas}}^{\text{Cubic}}$  versus  $\sqrt{(h^2 + k^2 + l^2)}$ . For the plot of  $\langle K \rangle$  versus Degree of Polymerization for poly-Arg and PGON, the lines that guide the eye were constructed via fits of the data to exponentially modified Gaussian functions.

### 4.3 Results and Discussion

The QM calculations published alongside this work provided precise atomistic insight into the complex interactions between the phosphates of lipid headgroups and guanidinium and amine groups.[48] Small angle X-ray scattering can complement the computational data since these experiments directly measure the nanoscale membrane curvature generated by guanidinium polymers. The QM calculations suggest that guanidinium groups of poly-Arg stack “face to face” when interguanidinium group separations are  $<5 \text{ \AA}$ . In this regime, changes in the interguanidinium group spacing should lead to changes in induced curvature. We explore membrane curvature generation as a function of interguanidinium group spacing using CPPs based on nonpeptide polyguanidine-oxanorbornene homopolymers (PGONs), which are not constrained to have the same geometric interguanidinium spacing as those based on polypeptide backbones. We present a systematic comparison between PGON and poly-Arg in the context of their membrane interactions.

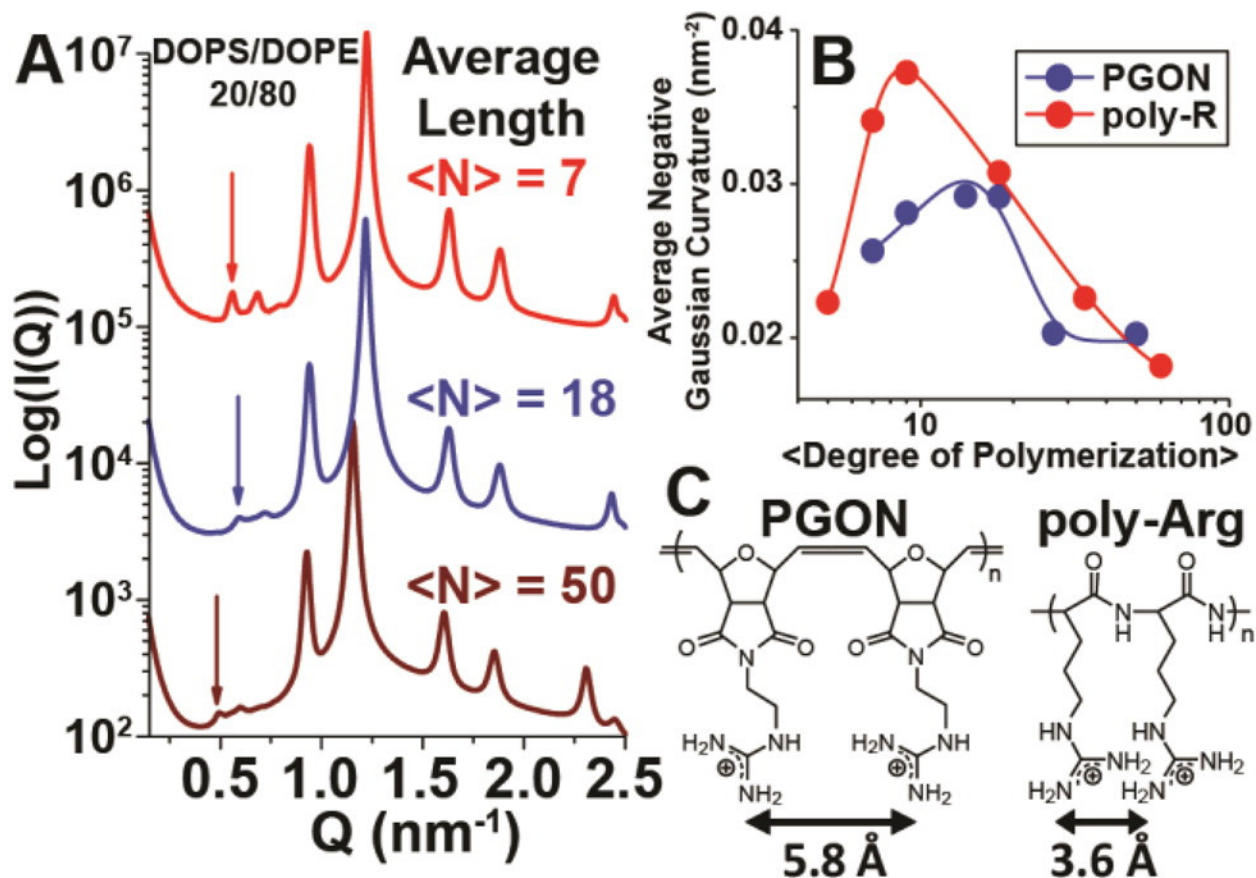


**Figure 4.3.** Generation of negative Gaussian curvature by guanidinium-rich polymers depends on average polymer length and average spacing between monomers. (A) Representative scattering spectra of PGONs with degree of polymerization 7, 18, and 50 (top to bottom) with DOPS/DOPE = 20/80 membranes at the polymer to lipid isoelectric point. Arrows indicate the first order reflection of the Pn3m cubic phase. A first order reflection at higher Q indicates the generation of greater negative Gaussian curvature. (B) Plots of polymer-induced average negative Gaussian curvature generation,  $|\langle K \rangle|$ , versus polymer length for both PGON and poly arginine. The maximum amount of  $|\langle K \rangle|$  occurs around  $\text{Arg}_9$  for poly arginine, while for PGON it is around an average degree of polymerization of 14. The lines are to guide the eye (see Experimental Section for details). (C) Schematic showing structural features of PGON and poly arginine, and effective spacing between guanidine groups.



#### 4.3.1 SAXS Study of PGON Polymers with Lipid Membranes

We use synchrotron small-angle X-ray scattering (SAXS) to characterize the interactions of model membranes with polyguanidine-oxanorbornene homopolymers (PGONs), which have been used as molecular transporters.[14, 16-18] PGON polymers substantially remodel small unilamellar vesicles (SUVs) into strongly scattering liquid crystalline structures as indicated by the appearance of sharp structure factor correlation peaks shown in representative spectra for PGON polymers with average degree of polymerization  $N = 7, 18, 50$  (Figure 4.3A). For each polymer the scattering spectra contains peaks with  $Q$  positions at ratio  $\sqrt{2} : \sqrt{3} : \sqrt{4}$ , evidence of the presence of  $Pn3m$  “double-diamond” cubic phases. The  $Pn3m$  is a bicontinuous cubic phase composed of two nonintersecting tetrahedral water channels separated by the lipid bilayer. The midpoint of the bilayer traces out a minimal surface which has zero mean curvature and negative Gaussian curvature at every point. Geometrically, minimal surfaces locally have the shape of a saddle; the surface curves maximally upward and downward in orthogonal directions. Negative Gaussian curvature is ubiquitous in membrane permeation. It is present in the interior of toroidal pores, as well as at the base of blebs and the “neck” of budding events which are topologically identical and morphologically similar to the membrane protrusions and invaginations observed in endocytic processes. For example, the surface of a lipid-lined toroidal pore has the same shape as the surface surrounding the hole in a donut. The surface curves toward the hole as the interior of the pore is traced, while moving out of the pore the surface curves away from the hole; opposite curvatures in orthogonal directions just like in a saddle (Figure 4.4). Because negative Gaussian curvature is necessary for all these membrane destabilization processes, the generation of saddle-splay curvature by molecular transporters is a potent way to circumvent the barrier function of cell membranes and enable uptake into cells. Interestingly, although negative Gaussian curvature on a monolayer leaflet (as in a

transmembrane pore) is distinct from negative Gaussian curvature in a bilayer (as in a bud or bleb), there is strong correlation between peptide-induced membrane permeation and peptide-induced formation of cubic phases,[39, 40, 54] which suggests that the root phenomenon of negative Gaussian membrane curvature generation by peptides can be expressed as different structural outcomes in isolated membranes under different conditions. By relating the peak Q positions to their Miller indices h, k, l, for each reflection using the equation for a powder averaged cubic phase,  $Q_{meas} = 2\pi\sqrt{(h^2 + k^2 + l^2)}/a$ , we calculate lattice parameters  $a_{N=7} = 16.0$  nm,  $a_{N=18} = 15.0$  nm, and  $a_{N=50} = 18.0$  nm. Cubic phases are observed in PE-rich membranes for PGONs with N = 7, 9, 14, 18, 27, and 50, implying that generation of negative Gaussian curvature is a general feature of PGON polymers with N = 7–50.

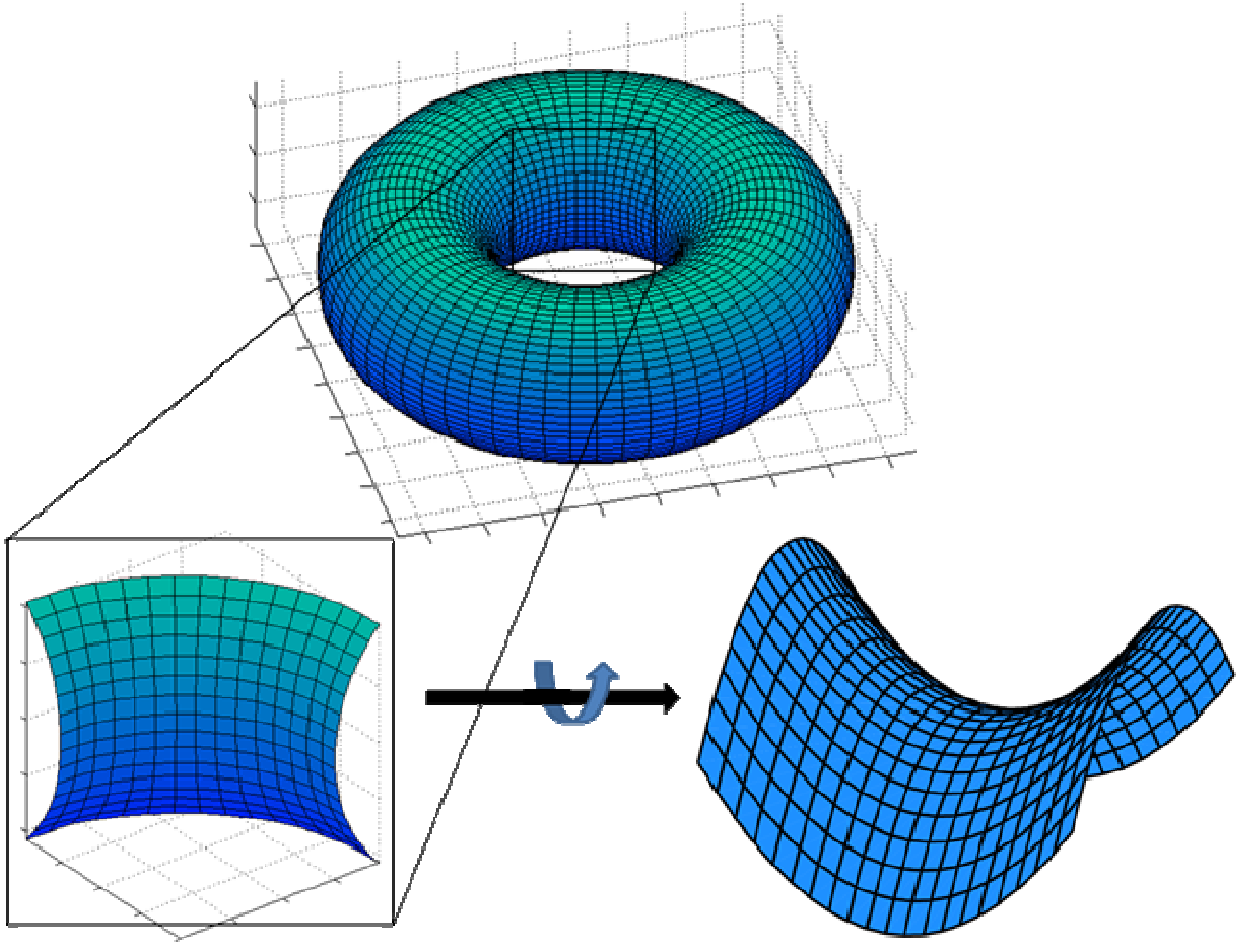


**Figure 4.4.** Illustration showing the connection between toroidal pores and saddle surfaces. The interior of a torus (top) has the same curvature as a ‘toroidal’ membrane pore. Close examination of the surface (bottom left) reveals that it bends in opposite directions at every point. This surface has saddle-splay curvature, positive curvature and negative curvature in orthogonal directions, as shown by rotating the surface (bottom right).

A nonmonotonic relationship between PGON length and cubic phase lattice parameter is observed (Figure 4.3A and B). This is strikingly similar to the trend found for poly-Arg.[39] Since the minimal surface of a cubic phase has average negative Gaussian curvature  $\langle K \rangle = 2\pi\chi/a^2A_0$ , where  $a$  is the measured cubic lattice parameter,  $\chi$  is the Euler characteristic, and  $A_0$  is the surface area per unit cell, the measured cubic lattice parameters can be used to extract the

$\langle K \rangle$  values for PGON polymers of different lengths.[55] Both PGON and poly-Arg generate maximum  $|\langle K \rangle|$  at intermediate polymer lengths (Figure 4.3B). The polymer length where maximum  $|\langle K \rangle|$  occurs for poly-Arg is around Arg<sub>9</sub>, whereas for PGON the maximum is shifted outward to an average degree of polymerization of about 14. The differences in  $|\langle K \rangle|$  versus polymer length must originate from the different structural properties of their backbones which necessarily influence how the guanidinium groups interact with membrane lipids.

The QM calculations presented previously[48] are consistent with the hypothesis that positive curvature generation by guanidinium group-directed lipid headgroup crowding can promote negative Gaussian curvature. This mechanism of generating positive curvature depends on a substantial degree of cooperativity, since both PGON and poly-Arg require a minimum number of guanidinium groups to induce such curvature. For example, the empirical observations that tetra-arginine, R<sub>4</sub>, induces an inverted hexagonal (H<sub>II</sub>) phase with negative mean curvature only and a minimum of 5 arginines is necessary before oligo-arginine can induce a Pn3m phase[39] implies that the structural tendency to form negative curvature is stronger than that to form positive curvature in short poly arginines. These results also suggest that two effects will progressively occur in the limit of dilute polymer to lipid molar ratios as the polymer chain length increases and thereby increases the amount of induced positive curvature. There will be a transition between inducing predominately negative membrane curvature to inducing a minimal surface with equal amounts of negative and positive curvature, or negative Gaussian curvature. The precise amount of induced negative Gaussian curvature depends on the relative amounts of positive and negative curvature generated, and achieves a maximum when the two are equal. Moreover, as the polymer length further increases, the excess induced positive curvature will interfere with generating the negative curvature component, and thereby ultimately limit the generation of negative Gaussian curvature. This is exactly what is observed

(Figure 4.3B) since the amount of negative Gaussian curvature initially increases, achieves a maximum as the curvatures are balanced, and eventually decreases. The precise polymer length that induces the maximum amount of negative Gaussian curvature depends on molecular details such as the effective guanidinium spacing, with closer spacings inducing more lipid head crowding and thereby more negative Gaussian curvature, which can also be seen in the comparison of polyarginine and PGON.

The spacing between guanidinium groups in oxanorbornene polymers is 5.8 Å, approximately 60% larger than the 3.6 Å spacing in poly arginine (Figure 4.3C). The larger spacing in PGON along with its stiffer backbone compared to poly-Arg indicate that the average distance between guanidine side chains is greater in PGON than poly-Arg.[14] Not only does PGON require more guanidinium units to generate maximal negative Gaussian curvature compared to poly-Arg, the maximum average negative Gaussian curvature generated by PGON is 22% less than that for poly-Arg (Figure 4.3B).(74) These two observations are mutually consistent. Increasing the average distance between guanidinium groups has the effect of relieving stress from molecular crowding interactions between bulky composite headgroups that generate positive membrane curvature. Since negative Gaussian curvature requires both positive and negative curvature, reducing the amount of positive curvature will impair generation of negative Gaussian curvature. Therefore, PGON polymers with larger average spacing between guanidinium groups will be less effective in generating negative Gaussian curvature compared with poly-Arg.

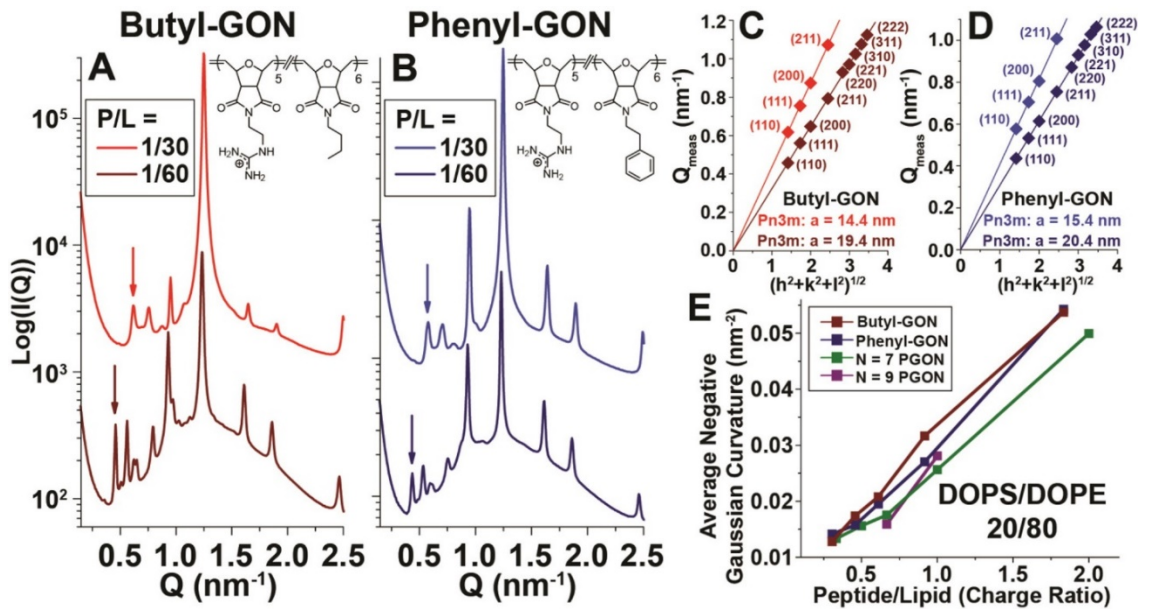


**Figure 4.5.** Hydrophobicity increases the amount of negative Gaussian curvature that guanidinium-rich polymers generate. (A) Butyl-GON polymer,  $N = 11$ , butyl/guanidine molar ratio =  $6/5$ , generates Pn3m cubic phases in DOPS/DOPE = 20/80 membranes at peptide/lipid =  $1/60$  and  $1/30$  molar ratios. The arrow points to the first (110) reflection of the Pn3m, which shifts to higher  $Q$  for greater P/L ratios. (B) A similar trend is observed for the phenyl-GON polymer,  $N = 11$ , phenyl/guanidine molar ratio =  $6/5$ . (C and D) Calculation of the Pn3m phase lattice parameters for butyl-GON (P/L =  $1/30$ , red, P/L =  $1/60$ , dark red) and phenyl-GON (P/L =  $1/30$ , blue, P/L =  $1/60$ , dark blue). Smaller lattices are seen for greater P/L ratios. (E) Average negative Gaussian curvature,  $|\langle K \rangle|$ , versus polymer/lipid charge ratios for polymers of similar charges and sizes. The hydrophobic butyl-GON and phenyl-GON induce greater  $|\langle K \rangle|$  than the hydrophilic PGONs.

#### 4.3.2 SAXS Study of Amphiphilic Butyl-GON and Phenyl-GON Polymers with Lipid Membranes

Many pore forming peptides such as mammalian defensins contain both arginine and hydrophobic groups.[7-9] Since hydrophobicity is known to generate positive curvature[49] this

trend suggests that hydrophobicity might complement the cooperative positive curvature generation by guanidinium groups, and promote negative Gaussian curvature formation and membrane permeation. To examine this specific hypothesis on the role of hydrophobicity without the potentially confounding factor of facial amphiphilicity, we added hydrophobic groups to these guanidinium-rich polymers by synthesizing random copolymers consisting of guanidinium groups with either hydrophobic butyl or phenyl side chains.[16, 17] SAXS experiments show that the strong induction of the Pn3m cubic phase is a general feature in the scattering spectra for both butyl-GON (Figure 4.5A) and phenyl-GON (Figure 4.5B). At peptide/lipid, P/L = 1/60 molar ratio, sharp correlation peaks at Q positions with ratios,  $\sqrt{2}:\sqrt{3}:\sqrt{4}:\sqrt{6}:\sqrt{8}:\sqrt{9}:\sqrt{10}:\sqrt{11}:\sqrt{12}$ , are seen for both butyl-GON and phenyl-GON. By fitting the peak Q positions to their respective reflections via linear trendlines (Figure 4.5C and D), we calculate Pn3m cubic lattice parameters of  $a = 19.4$  nm for butyl-GON and  $a = 20.4$  nm for phenyl-GON. Similar spectra are observed when the polymer concentration is doubled to P/L = 1/30 (Figure 4.5A and B). The cubic phase reflections shift to higher Q values, however, indicating that greater polymer concentrations induce smaller cubic lattices. At P/L = 1/30, the lattice parameters shrink to  $a = 14.4$  nm for butyl-GON (Figure 4.5C) and  $a = 15.4$  nm for phenyl-GON (Figure 4.5D). Since the cubic phase lattice parameter is inversely proportional to its average negative Gaussian curvature, increasing the polymer concentration increases the amount of negative Gaussian membrane curvature, as expected for polymers that generate such curvature.

We plot the average negative Gaussian curvature over a range of peptide to lipid ratios for polymers with similar lengths and net charge (Figure 4.5E), to directly compare their abilities to generate curvature. Interestingly,  $|\langle K \rangle|$  seems to increase linearly with polymer concentration over the range tested. Furthermore, while butyl-GON and phenyl-GON generate

roughly equivalent amounts of  $|\langle K \rangle|$ , both amphiphilic polymers consistently generate more  $|\langle K \rangle|$  than the  $N = 7, 9$  PGON polymers. Therefore, the net effect of adding hydrophobicity to guanidinium-rich polymers is to increase the amount of negative Gaussian membrane curvature they induce.

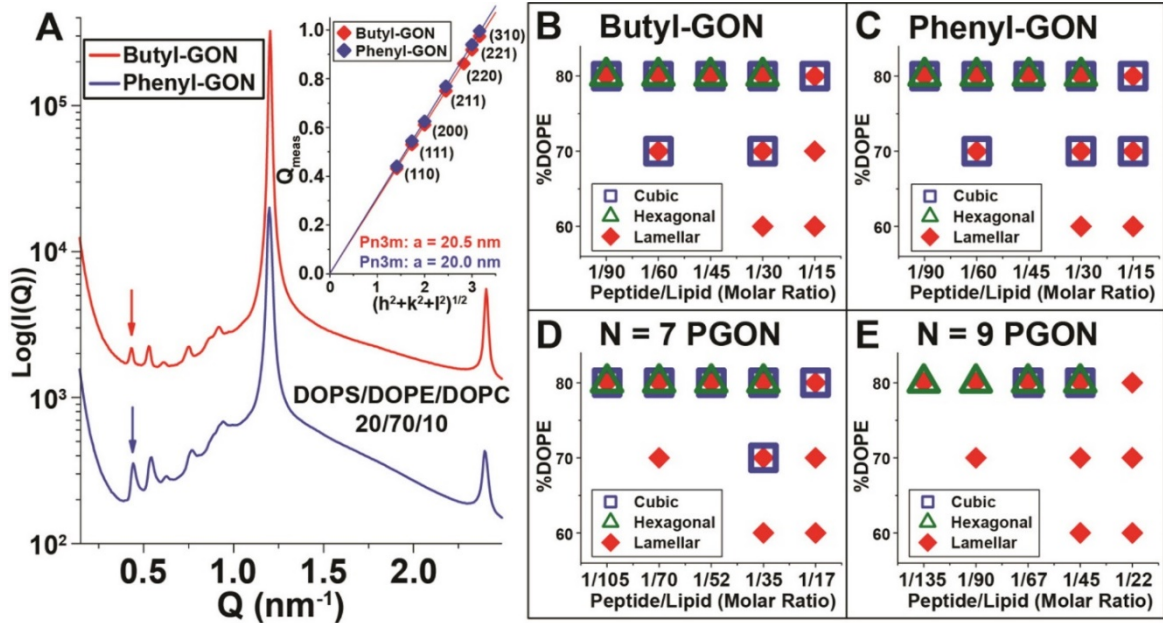


**Figure 4.6.** Hydrophobicity broadens the range of lipid compositions where guanidinium-rich polymers induce negative Gaussian curvature. (A) At P/L = 1/30, amphiphilic butyl-GON and phenyl-GON polymers both generate Pn3m cubic phases in membranes with reduced amounts of negative spontaneous curvature lipids, DOPS/DOPE/DOPC = 20/70/10. Inset shows indexation of the Pn3m cubic for both polymers. (B–E). Phase diagrams for guanidinium-rich polymers over a range of lipid compositions, DOPS/DOPE/DOPC = 20/x/(80 – x) where x = %DOPE, and peptide/lipid ratios. The amphiphilic butyl-GON and phenyl-GON polymers generate cubic phases over a larger region of the phase diagram compared with the hydrophilic PGON polymers.

Characterizing the effects of lipid composition on the curvature generating abilities of these guanidinium-rich polymers can elucidate their specific membrane permeating activities.



To do this, we use DOPS/DOPE/DOPC lipid compositions to perform a phase diagram study of polymer–lipid interactions. By changing the relative amounts of zwitterionic DOPC (spontaneous curvature,  $c_0 = 0$ ) and DOPE ( $c_0 < 0$ ) while holding constant the amount of anionic DOPS ( $c_0 = 0$ ) the amount of negative spontaneous curvature lipids in the membrane can be varied at constant membrane charge density. In DOPS/DOPE/DOPC = 20/70/10 membranes at P/L = 1/30, both butyl-GON and phenyl-GON generate Pn3m cubic phases with lattice parameters  $a = 20.5$  nm and  $a = 20.0$  nm, respectively (Figure 4.6A). These cubic lattices are larger than the ones for both polymers in 80% PE membranes, demonstrating that negative Gaussian curvature is more difficult to generate in membranes with lowered concentrations of DOPE lipids. Further reducing the amount of negative spontaneous curvature lipids to 60% DOPE suppresses cubic phase generation for both amphiphilic polymers (Figure 4.6B and C). Instead, pure lamellar phases are observed which consist of stacks of flat membranes with zero curvature. Comparing the phase diagrams for butyl-GON (Figure 4.6B) and phenyl-GON (Figure 4.6C) with the phase diagrams for N = 7 and 9, PGON (Figure 4.6D and E, and Figure 4.7) shows that, in general, the addition of hydrophobicity into guanidinium-rich polymers promotes saddle-splay curvature generation. Cubic phases are observed over a wider region of the phase diagram for the amphiphilic polymers, and the amphiphiles require less membrane PE content to generate negative Gaussian curvature.

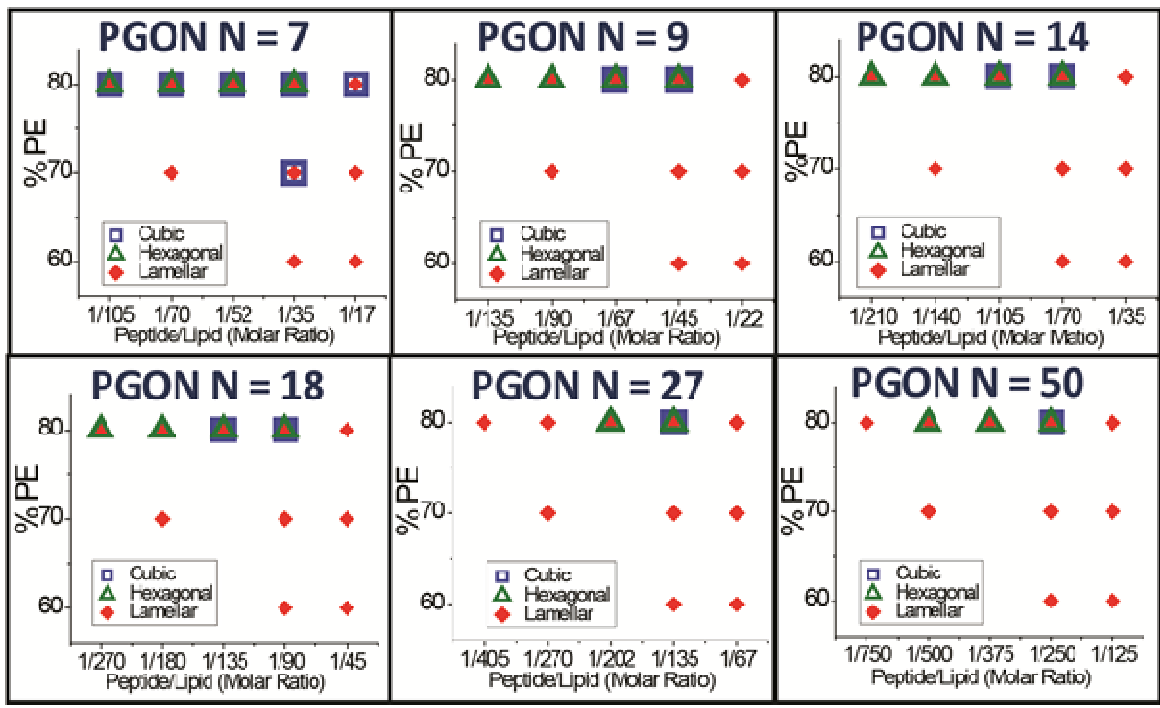


**Figure 4.7.** Phase diagrams of the PGON polymers used in this study.

Clearly, adding hydrophobicity to guanidinium-rich polymers can lead to a large enhancement of their negative Gaussian curvature generation abilities. While polymers with guanidinium decorated monomers generally induce both positive and negative curvature in the two principal directions, the relative amounts of each type of curvature is in general not equal. Since incorporating hydrophobicity into PGON polymers enhances their ability to generate negative Gaussian curvature, this implies that short PGON polymers tend to induce less positive curvature than negative curvature. Supplying additional positive curvature via hydrophobicity effectively makes up the difference resulting in an amphiphilic polymer with better membrane destabilizing activity. This is consistent with our previously reported saddle-splay curvature selection rules for cell-penetrating peptides[39] and antimicrobial peptides,[40] because in the extreme case of positive curvature starved polymers such as poly lysine which generate negative curvature only,[54] even greater amounts of hydrophobicity will be required to optimize saddle-splay curvature generation. Therefore, while lipid headgroup coordination by poly guanidinium

polymers can be a sufficient condition for generating positive curvature strain and therefore saddle-splay curvature, it can be enhanced by additional positive curvature strain from hydrophobicity. The addition of hydrophobicity, however, will in general make the membrane activity less specific in a broad range of peptides.[56-58] The curvature generating mechanism from hydrophobic insertion is inherently less specific than that from headgroup organization via cationic amino acids, since the latter interacts with headgroup chemistry, while the former interacts with the interior of the membrane.

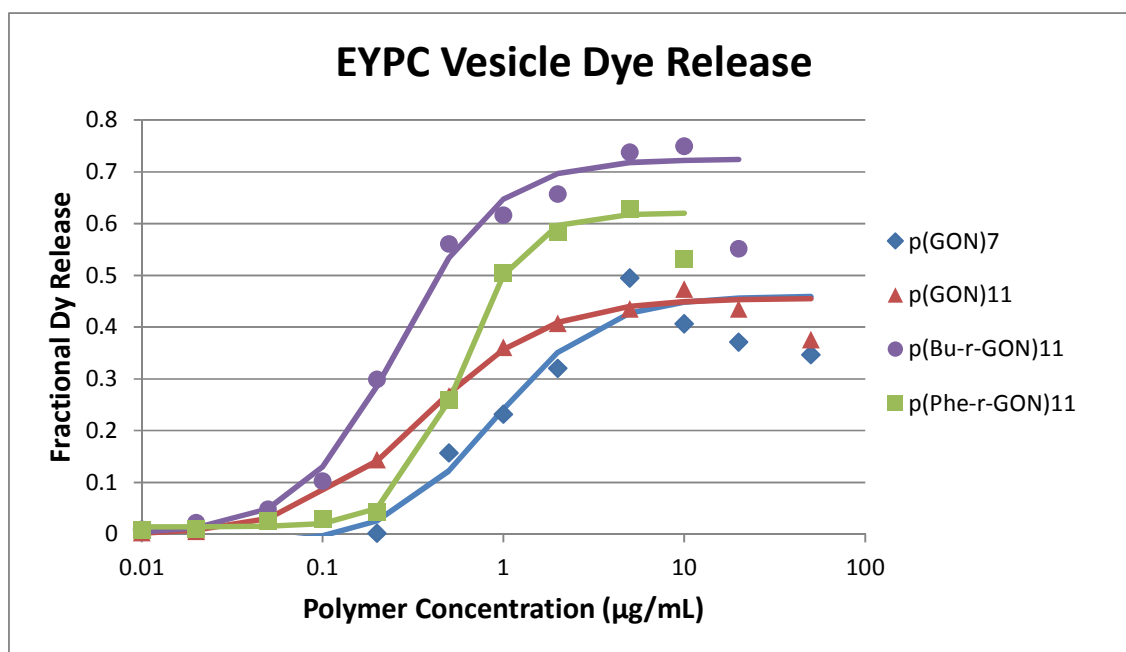


**Figure 4.8.** Fractional calcein release from EYPC 400 nm vesicles as a function of polymer concentration. The polymer with added hydrophobes induces more release than any of the PGON samples.

#### 4.3.3 Biological Activity of PGON, Butyl-GON, and Phenyl-GON Polymers

These design rules are evident in the biological activity of these polymers. Table 1 shows the hemolysis values for human red blood cells (RBC) along with the antibacterial activity against a gram-positive (*S. aureus*) and a gram-negative (*E. coli*) bacteria for a series of PGON-based

polymers. Comparing the  $HC_{50}$  values of the four polymers shows that the two PGON samples have higher values compared to the two samples designed with positive curvature generating components via hydrophobicity. Typically, the  $HC_{50}$  tracks most closely with membrane activity since the RBC is a nondividing cell type and the assay measures leakage of hemoglobin.[59] The antibacterial activity of the four polymer samples is similar and comparable to known antimicrobial peptides like Magainin. Understanding this activity is more complicated since the MIC is not a direct measure of membrane activity.[60] For example, it was shown previously that PGON is not strongly membrane active, yet displays MIC values in the range of 6–50  $\mu\text{g}/\text{mL}$ .[51] Using simple dye release assays (Figure 4.8), a similar trend is observed for these polymers in which the butyl-GON polymer induces more dye release than any of the PGON derivatives. Consistent with this we recently showed that incorporation of hydrophobic moieties into cell-penetrating peptides can change how they interact with membranes.[39] For example, while hydrophilic  $\text{Arg}_6$  ( $R_6$ ) crossed membranes via a rapid translocation mechanism, the addition of a single tryptophan into the peptide ( $R_6W$ ) was sufficient to induce slow dye leakage from intact vesicles. This change in behavior implies that incorporating hydrophobicity into hydrophilic peptides and polymers like poly-R and PGON can help to stabilize pore formation and increase membrane activity.

**Table 4.1.** Activity against Human Erythrocytes, *S. aureus*, and *E. coli*

Polymer	$HC_{50}$ ( $\mu\text{g}/\text{mL}$ )	MIC ( $\mu\text{g}/\text{mL}$ )	
		<i>S. aureus</i>	<i>E. coli</i>
P(GON) <sub>7</sub>	600	15	25
P(GON) <sub>11</sub>	>750	25	25
P(Ph-r-GON) <sub>11</sub>	30	15	25
P(Bu-r-GON) <sub>11</sub>	45	20	25

Our results raise the possibility of a mechanistic trade-off between activity from membrane disruption, and translocation across the membrane leading to activity from binding

intracellular targets. As shown above, hydrophobicity enhances saddle-splay curvature generation and therefore membrane activity, so association with cell membranes in the form of a stable pore inhibits an amphiphilic antimicrobial from reaching the cell interior. This implies that strong membrane activity may come at the expense of other forms of activity such as binding to intracellular targets. While hydrophilic guanidinium-rich polymers also generate sufficient saddle-splay curvature to permeate cell membranes, their membrane activity is reduced compared to their more hydrophobic counterparts. However, this decreases their likelihood of getting sequestered in the membrane, and upon crossing it, they are free to interact with intracellular targets and exact activity by inhibiting metabolic processes.

#### **4.4 Conclusion**

In summary we have shown that synthetic polyguanidine-oxanorbornene homopolymers, (PGONs), and amphiphilic phenyl-guanidine and butyl-guanidine random copolymers all generate saddle-splay curvature in membranes enriched with anionic lipids and negative spontaneous curvature lipids. QM calculations of the interactions of Arg with phosphate groups showed that guanidinium groups can coordinate two phosphates down to separations characteristic of poly-Arg via stacking adjacent diphosphated guanidinium complexes. Conversely, for Lys, two diphosphated amino groups cannot get closer than 7 Å without incurring a large energetic penalty. The stacking arrangement allows guanidinium-rich polymers to efficiently pack lipid headgroups, leading to steric crowding effects which generate positive curvature. This appears to be a key feature in its ability to organize lipid headgroups via H-bonding. Consistent with this result, poly-Arg and PGON generated saddle-splay curvature. The amount of curvature generated by PGON polymers was shown to be length dependent with maximal saddle-splay curvature generation occurring at intermediate polymer lengths, similar to

the trend observed for poly-Arg. However, in general, PGON generated less saddle-splay curvature than poly-Arg, and the polymer length that maximized saddle-splay curvature generation for PGON was longer than for poly-Arg. This occurs because the larger spacing between guanidine side chains in PGON and its stiffer backbone lessen the positive curvature strain due to guanidinium group-coordinated steric crowding effects, and supplying more guanidinium groups via longer PGON polymers only partially compensates.

Different positive curvature producing mechanisms can be combined to enhance negative Gaussian curvature, since incorporation of hydrophobic butyl and phenyl groups into guanidinium-rich polymers increased the amounts of saddle-splay curvature they generate as well as broadened the range of lipid compositions over which it was observed. This implies that adding hydrophobicity to guanidinium-rich polymers can enhance their saddle-splay curvature generating abilities by supplying additional positive curvature to help balance the unequal amounts of positive and negative curvature produced by certain guanidinium group spacings and polymer lengths. For 5:6 guanidine/hydrophobe polymers negligible differences between the curvature generating abilities of the hydrophobic butyl and phenyl moieties were observed. We believe that these results provide engineering guidelines for designing membrane-active molecules with specific curvature generating properties which control their pore forming activities.

#### 4.5 References

1. Vivès, E., P. Brodin, and B. Lebleu, *A truncated HIV-1 Tat protein basic domain rapidly translocates through the plasma membrane and accumulates in the cell nucleus*. The Journal of biological chemistry, 1997. **272**(25): p. 16010-16017.
2. Futaki, S., et al., *Arginine-rich Peptides AN ABUNDANT SOURCE OF MEMBRANE-PERMEABLE PEPTIDES HAVING POTENTIAL AS CARRIERS FOR INTRACELLULAR PROTEIN DELIVERY*. Journal of Biological Chemistry, 2001. **276**(8): p. 5836-5840.

3. El-Sayed, A., S. Futaki, and H. Harashima, *Delivery of Macromolecules Using Arginine-Rich Cell-Penetrating Peptides: Ways to Overcome Endosomal Entrapment*. The AAPS Journal, 2009. **11**(1): p. 13-22.
4. Wender, P.A., et al., *The design of guanidinium-rich transporters and their internalization mechanisms*. Advanced Drug Delivery Reviews, 2008. **60**(4-5): p. 452-472.
5. Torchilin, V.P., et al., *TAT peptide on the surface of liposomes affords their efficient intracellular delivery even at low temperature and in the presence of metabolic inhibitors*. Proceedings of the National Academy of Sciences, 2001. **98**(15): p. 8786-8791.
6. Lewin, M., et al., *Tat peptide-derivatized magnetic nanoparticles allow in vivo tracking and recovery of progenitor cells*. Nature Biotechnology, 2000. **18**(4): p. 410-414.
7. Ganz, T., *Defensins: antimicrobial peptides of innate immunity*. Nature Reviews Immunology, 2003. **3**(9): p. 710-720.
8. Lehrer, R.I., *Primate defensins*. Nature Reviews Microbiology, 2004. **2**(9): p. 727-738.
9. Selsted, M.E. and A.J. Ouellette, *Mammalian defensins in the antimicrobial immune response*. Nature Immunology, 2005. **6**(6): p. 551-557.
10. Wender, P.A., et al., *The design, synthesis, and evaluation of molecules that enable or enhance cellular uptake: Peptoid molecular transporters*. Proceedings of the National Academy of Sciences, 2000. **97**(24): p. 13003-13008.
11. Mitchell, D.j., et al., *Polyarginine enters cells more efficiently than other polycationic homopolymers*. The Journal of Peptide Research, 2000. **56**(5): p. 318-325.
12. Rothbard, J.B., et al., *Arginine-Rich Molecular Transporters for Drug Delivery: Role of Backbone Spacing in Cellular Uptake*. Journal of Medicinal Chemistry, 2002. **45**(17): p. 3612-3618.
13. Cooley, C.B., et al., *Oligocarbonate Molecular Transporters: Oligomerization-Based Syntheses and Cell-Penetrating Studies*. Journal of the American Chemical Society, 2009. **131**(45): p. 16401-16403.
14. Hennig, A., et al., *Stimuli-Responsive Polyguanidino-Oxanorbornene Membrane Transporters as Multicomponent Sensors in Complex Matrices*. Journal of the American Chemical Society, 2008. **130**(31): p. 10338-10344.
15. Kolonko, E.M. and L.L. Kiessling, *A Polymeric Domain That Promotes Cellular Internalization*. Journal of the American Chemical Society, 2008. **130**(17): p. 5626-5627.
16. Som, A., A. Reuter, and G.N. Tew, *Protein Transduction Domain Mimics: The Role of Aromatic Functionality*. Angewandte Chemie International Edition, 2012. **51**(4): p. 980-983.
17. Som, A., et al., *Self-Activation in De Novo Designed Mimics of Cell-Penetrating Peptides*. Angewandte Chemie International Edition, 2011. **50**(27): p. 6147-6150.
18. Tezgel, A.O.z.l., J.C. Telfer, and G.N. Tew, *De Novo Designed Protein Transduction Domain Mimics from Simple Synthetic Polymers*. Biomacromolecules, 2011. **12**(8): p. 3078-3083.
19. Wender, P.A., et al., *Oligocarbamate Molecular Transporters: Design, Synthesis, and Biological Evaluation of a New Class of Transporters for Drug Delivery*. Journal of the American Chemical Society, 2002. **124**(45): p. 13382-13383.
20. Wender, P.A., et al., *Dendrimeric Molecular Transporters: Synthesis and Evaluation of Tunable Polyguanidino Dendrimers That Facilitate Cellular Uptake*. Organic Letters, 2005. **7**(22): p. 4815-4818.
21. Elson-Schwab, L., et al., *Guanidinylated Neomycin Delivers Large, Bioactive Cargo into Cells through a Heparan Sulfate-dependent Pathway*. Journal of Biological Chemistry, 2007. **282**(18): p. 13585-13591.

22. Rothbard, J.B., T.C. Jessop, and P.A. Wender, *Adaptive translocation: the role of hydrogen bonding and membrane potential in the uptake of guanidinium-rich transporters into cells*. *Advanced Drug Delivery Reviews*, 2005. **57**(4): p. 495-504.
23. Rothbard, J.B., et al., *Role of membrane potential and hydrogen bonding in the mechanism of translocation of guanidinium-rich peptides into cells*. *Journal of the American Chemical Society*, 2004. **126**(31): p. 9506-9507.
24. Drin, G., et al., *Translocation of the pAntp Peptide and Its Amphipathic Analogue AP-2AL<sup>†</sup>*. *Biochemistry*, 2001. **40**(6): p. 1824-1834.
25. Iwasa, A., et al., *Cellular uptake and subsequent intracellular trafficking of R8-liposomes introduced at low temperature*. *Biochimica et Biophysica Acta (BBA) - Biomembranes*, 2006. **1758**(6): p. 713-720.
26. Maiolo, J.R., M. Ferrer, and E.A. Ottinger, *Effects of cargo molecules on the cellular uptake of arginine-rich cell-penetrating peptides*. *Biochimica et Biophysica Acta (BBA) - Biomembranes*, 2005. **1712**(2): p. 161-172.
27. Persson, D., et al., *Application of a Novel Analysis To Measure the Binding of the Membrane-Translocating Peptide Penetratin to Negatively Charged Liposomes<sup>†</sup>*. *Biochemistry*, 2003. **42**(2): p. 421-429.
28. Ter-Avetisyan, G., et al., *Cell Entry of Arginine-rich Peptides Is Independent of Endocytosis*. *Journal of Biological Chemistry*, 2009. **284**(6): p. 3370-3378.
29. Thorén, P.E.G., et al., *Membrane destabilizing properties of cell-penetrating peptides*. *Biophysical Chemistry*, 2005. **114**(2-3): p. 169-179.
30. Drin, G., et al., *Studies on the Internalization Mechanism of Cationic Cell-penetrating Peptides*. *Journal of Biological Chemistry*, 2003. **278**(33): p. 31192-31201.
31. Nakase, I., et al., *Cellular Uptake of Arginine-Rich Peptides: Roles for Macropinocytosis and Actin Rearrangement*. *Molecular Therapy*, 2004. **10**(6): p. 1011-1022.
32. Richard, J.P., et al., *Cellular Uptake of Unconjugated TAT Peptide Involves Clathrin-dependent Endocytosis and Heparan Sulfate Receptors*. *Journal of Biological Chemistry*, 2005. **280**(15): p. 15300-15306.
33. Richard, J.P., et al., *Cell-penetrating Peptides A REEVALUATION OF THE MECHANISM OF CELLULAR UPTAKE*. *Journal of Biological Chemistry*, 2003. **278**(1): p. 585-590.
34. Wadia, J.S., R.V. Stan, and S.F. Dowdy, *Transducible TAT-HA fusogenic peptide enhances escape of TAT-fusion proteins after lipid raft macropinocytosis*. *Nature Medicine*, 2004. **10**(3): p. 310-315.
35. Ziegler, A., *Thermodynamic studies and binding mechanisms of cell-penetrating peptides with lipids and glycosaminoglycans*. *Advanced Drug Delivery Reviews*, 2008. **60**(4-5): p. 580-597.
36. Gump, J.M. and S.F. Dowdy, *TAT transduction: the molecular mechanism and therapeutic prospects*. *Trends in Molecular Medicine*, 2007. **13**(10): p. 443-448.
37. Guterstam, P., et al., *Elucidating cell-penetrating peptide mechanisms of action for membrane interaction, cellular uptake, and translocation utilizing the hydrophobic counter-anion pyrenebutyrate*. *Biochimica et Biophysica Acta (BBA) - Biomembranes*, 2009. **1788**(12): p. 2509-2517.
38. Heitz, F., M.C. Morris, and G. Divita, *Twenty years of cell-penetrating peptides: from molecular mechanisms to therapeutics*. *British Journal of Pharmacology*, 2009. **157**(2): p. 195-206.
39. Mishra, A., et al., *Translocation of HIV TAT peptide and analogues induced by multiplexed membrane and cytoskeletal interactions*. *Proceedings of the National Academy of Sciences*, 2011. **108**(41): p. 16883-16888.



40. Schmidt, N.W., et al., *Criterion for amino acid composition of defensins and antimicrobial peptides based on geometry of membrane destabilization*. Journal of the American Chemical Society, 2011. **133**(17): p. 6720-6727.
41. Schmidt, N., et al., *Arginine-rich cell-penetrating peptides*. FEBS Letters, 2010. **584**(9): p. 1806-1813.
42. Schug, K.A. and W. Lindner, *Noncovalent Binding between Guanidinium and Anionic Groups: Focus on Biological- and Synthetic-Based Arginine/Guanidinium Interactions with Phosph[on]ate and Sulf[on]ate Residues*. Chemical Reviews, 2005. **105**(1): p. 67-114.
43. Conner, S.D. and S.L. Schmid, *Regulated portals of entry into the cell*. Nature, 2003. **422**(6927): p. 37-44.
44. Braun, A.R., et al.,  *$\alpha$ -Synuclein induces both positive mean curvature and negative Gaussian curvature in membranes*. Journal of the American Chemical Society, 2012. **134**(5): p. 2613-2620.
45. Pednekar, D., A. Tendulkar, and S. Durani, *Electrostatics-defying interaction between arginine termini as a thermodynamic driving force in protein-protein interaction*. Proteins: Structure, Function, and Bioinformatics, 2009. **74**(1): p. 155-163.
46. Papoian, G.A., et al., *Water in protein structure prediction*. Proceedings of the National Academy of Sciences of the United States of America, 2004. **101**(10): p. 3352-3357.
47. Yuzlenko, O. and T. Lazaridis, *Interactions between Ionizable Amino Acid Side Chains at a Lipid Bilayer-Water Interface*. The Journal of Physical Chemistry B, 2011. **115**(46): p. 13674-13684.
48. Schmidt, N.W., et al., *Molecular Basis for Nanoscopic Membrane Curvature Generation from Quantum Mechanical Models and Synthetic Transporter Sequences*. Journal of the American Chemical Society, 2012. **134**(46): p. 19207-19216.
49. McMahon, H.T. and J.L. Gallop, *Membrane curvature and mechanisms of dynamic cell membrane remodelling*. Nature, 2005. **438**(7068): p. 590-596.
50. Matsuzaki, K., et al., *Relationship of Membrane Curvature to the Formation of Pores by Magainin 2<sup>†</sup>*. Biochemistry, 1998. **37**(34): p. 11856-11863.
51. Gabriel, G.J., et al., *Synthetic Mimic of Antimicrobial Peptide with Nonmembrane-Disrupting Antibacterial Properties*. Biomacromolecules, 2008. **9**(11): p. 2980-2983.
52. Ilavsky, J., *<i>Nika</i>: software for two-dimensional data reduction*. Journal of Applied Crystallography, 2012. **45**(2): p. 324-328.
53. Hammersley, A. *THE FIT2D HOME PAGE*. 2014/04/20/13:41:53; Available from: <http://www.esrf.eu/computing/scientific/FIT2D/>.
54. Mishra, A., et al., *HIV TAT Forms Pores in Membranes by Inducing Saddle-Splay Curvature: Potential Role of Bidentate Hydrogen Bonding*. Angewandte Chemie International Edition, 2008. **47**(16): p. 2986-2989.
55. Harper, P.E. and S.M. Gruner, *Electron density modeling and reconstruction of infinite periodic minimal surfaces (IPMS) based phases in lipid-water systems. I. Modeling IPMS-based phases*. The European Physical Journal E, 2000. **2**(3): p. 217-228.
56. Yeaman, M.R. and N.Y. Yount, *Mechanisms of Antimicrobial Peptide Action and Resistance*. Pharmacological Reviews, 2003. **55**(1): p. 27-55.
57. Tew, G.N., et al., *De Novo Design of Antimicrobial Polymers, Foldamers, and Small Molecules: From Discovery to Practical Applications*. Accounts of Chemical Research, 2010. **43**(1): p. 30-39.
58. Tossi, A., L. Sandri, and A. Giangaspero, *Amphipathic,  $\alpha$ -helical antimicrobial peptides*. Peptide Science, 2000. **55**(1): p. 4-30.

59. Fischer, D., et al., *In vitro cytotoxicity testing of polycations: influence of polymer structure on cell viability and hemolysis*. *Biomaterials*, 2003. **24**(7): p. 1121-1131.
60. Epan, R.F., et al., *Dual Mechanism of Bacterial Lethality for a Cationic Sequence-Random Copolymer that Mimics Host-Defense Antimicrobial Peptides*. *Journal of Molecular Biology*, 2008. **379**(1): p. 38-50.

## CHAPTER 5

### PTDM LENGTH, AROMATICITY AND ARCHITECTURE: SEARCHING FOR IDEAL PARAMETERS FOR NEGATIVE GAUSSIAN CURVATURE GENERATION

#### 5.1 Introduction

In the previous chapter, the effects of both length and polymer hydrophobicity were examined with regard to their ability to generate negative Gaussian curvature in bulk lipid systems. Length was found to play a key role, as a the guanidinium-containing homopolymer was less active at low and high molecular weights, displaying peak curvature generation in the 14-18 unit length range. Hydrophobicity was also tremendously important in generating membrane curvature. Not only did more hydrophobic copolymers generate more curvature, but they also were able to generate curvature in lipid systems containing only 70% negative intrinsic curvature phosphatidylethanolamine. These hydrophobic copolymers, however, were also far more hemolytic than their homopolymer counterparts. Between this bounding of effectiveness and toxicity, along with optimal length, it appeared possible to achieve an “ideal” structure with the right intermediate combination of polymer length and hydrophobicity.

Aromaticity has also been explored as an important parameter for membrane interactions. Trans membrane proteins generally have unusually high quantities of aromatic residues, especially concentrated in so-called “aromatic belts” at either end of the transmembrane region.[1-3] Additionally, aromatic peptide residues interact more strongly with phospholipid bilayers than would be expected based purely upon their hydrophobicity. A comparison of octanol-water to phospholipid-water partitioning demonstrated that aromatic residues associate unusually strongly with phospholipids.[4] This suggests that there is some important interaction between the aromatic residues and the polar regions of the phospholipid

membrane. The exact cause of this favorability is uncertain, although NMR studies[3] suggested that it may be due to a combination of the flat geometry of the aromatic ring as well as the shared electronic structure and its various interactions with charged and polar molecules. Preliminary work using ROMP-based PTDMs suggested that incorporation of aliphatic moieties may enhance the activity of these polymers over similar ones with aliphatic hydrophobic groups.[5]

Perhaps most important yet least explored parameter in terms of biophysical experiments is the effect of polymer architecture. While previous studies examining PTD(M)s and negative Gaussian curvature generation have focused on peptides,[6] homopolymers, and random copolymers (Chapter 4),[7] tremendous success has been had in the use of block copolymer PTDMs for non-covalent delivery of macromolecular cargo to cells.[8-10] This polymer design combines the best aspects of two important classes of molecules. The guanidinium-rich block closely resembles the Tat-inspired PTDMs that have been studied in these preceding chapters, while the addition of the hydrophobic block gives it a structure resembling Pep-1, a chimeric peptide that has been widely used for delivery and is known commercially as Chariot<sup>TM</sup>. [11] The polymers have only just begun to be investigated, and few studies compare their interaction with cells to polymers with similar hydrophobicities and different polymer architectures.[10, 12]

To this end, the following study examines the importance of length, aromaticity, and polymer architecture regarding their interaction with phospholipids. Using our imide-based ROMP copolymer system, we are able to make guanidinium-rich polymers with an intermediate hydrophobicity, but varying length, aromaticity, and polymer architecture. As standards for membrane activity, we look at the ability of these polymers to induce negative Gaussian curvature in bulk lipid systems using small-angle X-ray scattering (SAXS) as well as dye release

from egg yolk phosphatidylcholine (EYPC) vesicles. The formation of negative Gaussian curvature, while not a direct measure of membrane transport, is necessary to create the kind of toroidal structure associated with pore formation or the insertion of a hydrophilic molecule into a lipid membrane.[6] Dye release, rather than looking for a specific mechanistic component, strictly measures membrane permeation, regardless of how it occurs.[5, 13-17] Thus, between these two measures, we are able to understand the effect of these changes in polymer structure on a specific mechanism suspected to be important in membrane activity, and then in turn measure how a change in that aspect alters overall dye release.

## **5.2 Experimental Methods**

### **5.2.1 Monomer Synthesis**

Monomer syntheses were performed as by previous reports and Chapter 4.[5, 7, 16, 18]

### **5.2.2 Polymer Synthesis**

Polymer synthesis was performed similarly to reported procedures.[5, 15, 16, 19]

Monomers were co-polymerized by ring-opening metathesis polymerization (ROMP) using a 3rd generation Grubbs' catalyst. The monomer (~200mg) and appropriate amount of catalyst were dissolved in dry dichloromethane in separate Schlenk flasks. The flasks were placed under nitrogen and degassed using a freeze-pump-thaw procedure. The monomer was transferred to the catalyst flask and the polymerization was allowed to proceed at 25°C for an hour, after which 1 mL ethyl vinyl ether was added to terminate the reaction. After an hour, the solution was concentrated and precipitated twice in 100 mL pentane.

The Boc-protected polymers were deprotected by stirring the polymer in 10 mL 1:1 TFA:CH<sub>2</sub>Cl<sub>2</sub> for 12 hours. The TFA was then removed by repeatedly co-evaporating with

methanol in a rotary evaporator, then by placing under a vacuum for 4 h. The solid polymer was then suspended in water and freeze-dried for 3 days.

**Boc-Protected G<sub>4n</sub>-r-Ph<sub>n</sub>**: <sup>1</sup>H NMR (300 MHz, CD<sub>2</sub>Cl<sub>2</sub>): δ=11.46 (4H, br), 8.44 (4H, br), 7.21 (5H, br), 6.05 (trans), 5.76 (cis) (10H total, br), 4.99 (10H, br), 4.46 (8H, br), 4.08 (2H, br), 3.73 (12H, br), 3.38 (10H, br) 2.91 (2, br) 1.52 (36H, br), 1.47 (36H, br)

**G<sub>4n</sub>-r-Ph<sub>n</sub>**: <sup>1</sup>H NMR (300 MHz, DMSO-*d*<sub>6</sub>): δ = 7.27 (5H, br), 5.96-5.72 (10H, br), 4.88 (8H, br), 4.43 (2H, br), 4.10 (2H, br), 2.85 (2H, br)

**Boc-Protected G<sub>4n</sub>-b-Ph<sub>n</sub>**: <sup>1</sup>H NMR (300 MHz, CD<sub>2</sub>Cl<sub>2</sub>): δ=11.46 (4H, br), 8.44 (4H, br), 7.21 (5H, br), 6.05 (trans), 5.76 (cis) (10H total, br), 4.99 (10H, br), 4.46 (4H, br), 4.08 (1H, br), 3.73 (12H, br), 3.38 (8H, br) 2.91 (2, br) 1.52 (36H, br), 1.47 (36H, br)

**G<sub>4n</sub>-b-Ph<sub>n</sub>**: <sup>1</sup>H NMR (300 MHz, DMSO-*d*<sub>6</sub>): δ = 7.27 (5H, br), 5.96-5.72 (10H, br), 4.88 (8H, br), 4.43 (2H, br), 4.10 (2H, br), 2.85 (2H, br)

**Boc-Protected G<sub>4n</sub>-r-Cy<sub>n</sub>**: <sup>1</sup>H NMR (300 MHz, CD<sub>2</sub>Cl<sub>2</sub>): δ=11.46 (4H, br), 8.44 (4H, br), 6.05 (trans), 5.76 (cis) (10H total, br), 4.99 (10H, br), 4.46 (8H, br), 3.73 (10H, br), 3.38 (10H, br), 1.68 (3H, br), 1.52 (36H, br), 1.47 (36H, br), 1.18 (6H), 0.9 (4H)

**G<sub>4n</sub>-r-Cy<sub>n</sub>**: <sup>1</sup>H NMR (300 MHz, CD<sub>3</sub>OD): δ = 6.08 (5H, br), 5.84 (5H, br), 5.02 (5H, br), 4.52 (5H, br), 3.69 (8H, br), 3.46 (20H, br), 1.76 (2H, br), 1.45 (1H, br), 1.25 (6H, br), 0.96 (4H, br)

**Boc-Protected G<sub>16</sub>-r-Oct<sub>4</sub>** <sup>1</sup>H NMR (300 MHz, CD<sub>2</sub>Cl<sub>2</sub>): δ=11.53 (4H, br), 8.49 (4H, br), 6.12 (trans), 5.84 (cis) (10H total, br), 5.05(cis), 4.51 (cis) (10H total, br), 3.73 (18H, br), 3.42 (10H, br), 1.47 (72H, br), 1.25 (12H, br), 0.9 (3H)

**G<sub>4n</sub>-r-Oct<sub>n</sub>**: <sup>1</sup>H NMR (300 MHz, CD<sub>3</sub>OD): δ = 5.94 (5H, br), 5.72 (5H, br), 4.86 (5H, br), 4.41 (5H, br), 1.44 (2H, br), 1.21 (10H, br), 0.82 (3H, br)

### 5.2.3 SAXS Studies

#### 5.2.3.1 Liposome Preparation for X-Ray Measurements

Liposomes were prepared as described previously.[20] Briefly, DOPC (1,2-dioleoyl-sn-glycero-3-phosphocholine), DOPE (1,2-dioleoyl-sn-glycero-3-phosphoethanolamine), and DOPS (1,2-dioleoyl-sn-glycero-3-phospho-l-serine (sodium salt)), lyophilized lipids from Avanti Polar lipids were used without further purification. SUVs were prepared by sonication. Individual stock solutions of DOPS, DOPC, and DOPE were prepared in chloroform at 20 mg/mL. Ternary mixtures of these lipids were prepared at mass ratios, for example, DOPS/DOPE/DOPC = 20/60/20 corresponds to a 1:3:1 mass ratio. Chloroform was evaporated under N<sub>2</sub>, and the mixtures were further dried by overnight desiccation under vacuum. The dried lipids were resuspended the next day in 100 mM NaCl or in Millipore H<sub>2</sub>O. Solutions were incubated at 37 °C for 12–24 h and then sonicated until clear. Small unilamellar vesicles (SUV's) were obtained via extrusion (0.2 μm pore Nucleopore filter).

### 5.2.3.2 SAXS Experiments

All polymers were resuspended in either 100 mM NaCl or in Millipore H<sub>2</sub>O. Lipids were thoroughly mixed with polymers at specific peptide to lipid ratios (P/L) in 100 mM NaCl. The solutions were hermetically sealed in quartz capillaries (Hilgenberg GmbH, Mark-tubes, Code No: 4017515). SAXS experiments at synchrotron sources were conducted at the Stanford Synchrotron Radiation Laboratory (BL 4–2), and the Advanced Light Source (beamline 7.3.3). Monochromatic X-rays with energies 9–11 keV were used at SSRL and 10 keV at ALS. The scattered radiation was collected using a Rayonix MX225-HE detector (pixel size, 73.2 μm) at SSRL and a Pilatus 100k detector (pixel size, 172 μm). Samples were also measured at the California NanoSystems Institute (CNSI) at UCLA using an in house setup. A compact SAXS light source (Forvis Technologies, Inc.) was used in conjunction with a mar345 image plate detector (pixel size, 150 μm). Identical samples were prepared and measured at multiple sources to check for and ensure mutual consistency. The 2D SAXS powder patterns were integrated using the Nika 1.48 package[21] for Igor Pro 6.21 and FIT2D.[22]

#### SAXS Data Fits

A similar approach to the one described previously[20] was used to determine cubic phase lattice parameters. The measured cubic Q peak positions were related to the Miller indices h, k, and l, for the observed reflections using the equation for a powder averaged Pn3m cubic phase,  $Q_{\text{meas}}^{\text{Cubic}} = 2\pi\sqrt{(h^2 + k^2 + l^2)}/a$ . The lattice parameter, a, was calculated from the slope of the trendline obtained from a linear fit of  $Q_{\text{meas}}^{\text{Cubic}}$  versus  $\sqrt{(h^2 + k^2 + l^2)}$ . The minimal surface of a Pn3m cubic phase has the average negative Gaussian curvature:

$$\langle K \rangle = \frac{2\pi\chi}{a^2 A_0}$$



where  $a$  is the measured cubic lattice parameter,  $\chi$  is the Euler characteristic, and  $A_0$  is the surface area per unit cell.

## **5.2.4 Dye Release Studies**

### **5.2.4.1 Vesicle Preparation**

25mg egg yolk phosphatidylcholine (EYPC) in 3 mL of chloroform was evaporated onto the wall of a 10 mL flask using a rotary evaporator, then placed under vacuum overnight. The lipid film was resuspended in buffer containing 10 mM Tris and 50 mM carboxyfluorescein dye, titrated to pH 7.5. The buffer was allowed to sit for an hour, vortexing every 15 minutes. The DPPC vesicles were swelled in a water bath set to 50°C during this time. The vesicle solution was then put through six freeze-thaw cycles. The solution was then extruded nine times through a 100 nm pore membrane. The DPPC vesicles were warmed with a heat gun during the extrusion process. Dye-loaded vesicles were separated from free dye by size exclusion chromatography (Sephadex G-50 superfine, Sigma Aldrich) in Tris saline buffer (10 mM Tris, 107 mM NaCl, pH 7.5).

### **5.2.4.2 EYPC Dye Release**

Experiments similar to those published previously[7] were performed using a Biotek Synergy Mx fluorescence plate reader. All Fluorescence measurements were taken at an excitation wavelength of 492 nm and emission wavelength of 517 nm. 1,960  $\mu$ L Tris buffer (10 mM Tris, 107 mM NaCl, pH 7.5) was added to the wells of a 12-well plate. 20  $\mu$ L of 250  $\mu$ M vesicle solution (as defined above) was added to each well, creating an in-well concentration of 2.5  $\mu$ M. The plate reader was heated to 25°C before continuing. The plates were shaken at

25°C and after three minutes a baseline fluorescence measurement,  $F_0$ , was taken. 20  $\mu\text{L}$  polymer/DMSO solutions containing varying concentrations (0.01-1000  $\mu\text{L}$ ) of polymer were added to wells with stirrers, and the plate was returned to the reader for 10 minutes of shaking. After 10 minutes, another reading,  $F_{10}$ , was taken. 20  $\mu\text{L}$  5% Triton X-100 in DMSO was added to the wells and after three minutes a final measurement,  $F_T$ , was taken.  $F_T$  and  $F_0$  allowed use to normalize fluorescence to measure the fractional dye release:

$$Y = (F_{10} - F_0)/(F_T - F_0)$$

The fractional dye release  $Y$  was then fitted as a function of concentration,  $c$ , to the Hill equation by a least-squares method:

$$Y = Y_m \frac{(c/EC_{50})^n}{1 + (c/EC_{50})^n}$$

Where  $EC_{50}$  is the concentration of 50% of maximal dye release and  $n$  is a fitting parameter.

### 5.3 Results and Discussion

#### 5.3.1 Polymer Design

The polymer library used in this study (Figure 5.1, Table 5.1) presents range of polymer architectures, lengths, and types of hydrophobic moieties. In all cases, these polymers have a fixed hydrophobic residue content of 20%. To examine the effect of different types of hydrophobic residues, polymers containing phenyl, cyclohexyl, and octyl moieties were used. To examine the effect of aromaticity on negative Gaussian curvature generation, phenyl, cyclohexyl, and octyl random copolymers were created. Each hydrophobic moiety contains the same carbon content, but the phenyl monomer is aromatic while the cyclohexyl and octyl are not. Previous studies of homopolymers[7] demonstrated that length played an important role in the amount of curvature these polymers are able to create in bulk systems. The phenyl

random, phenyl block, and cyclohexyl series each have polymers of total average length 10, 20, and 40 to determine the effect of length for this series. Lastly, there is a random phenyl and a block series to distinguish between the two different architectures.

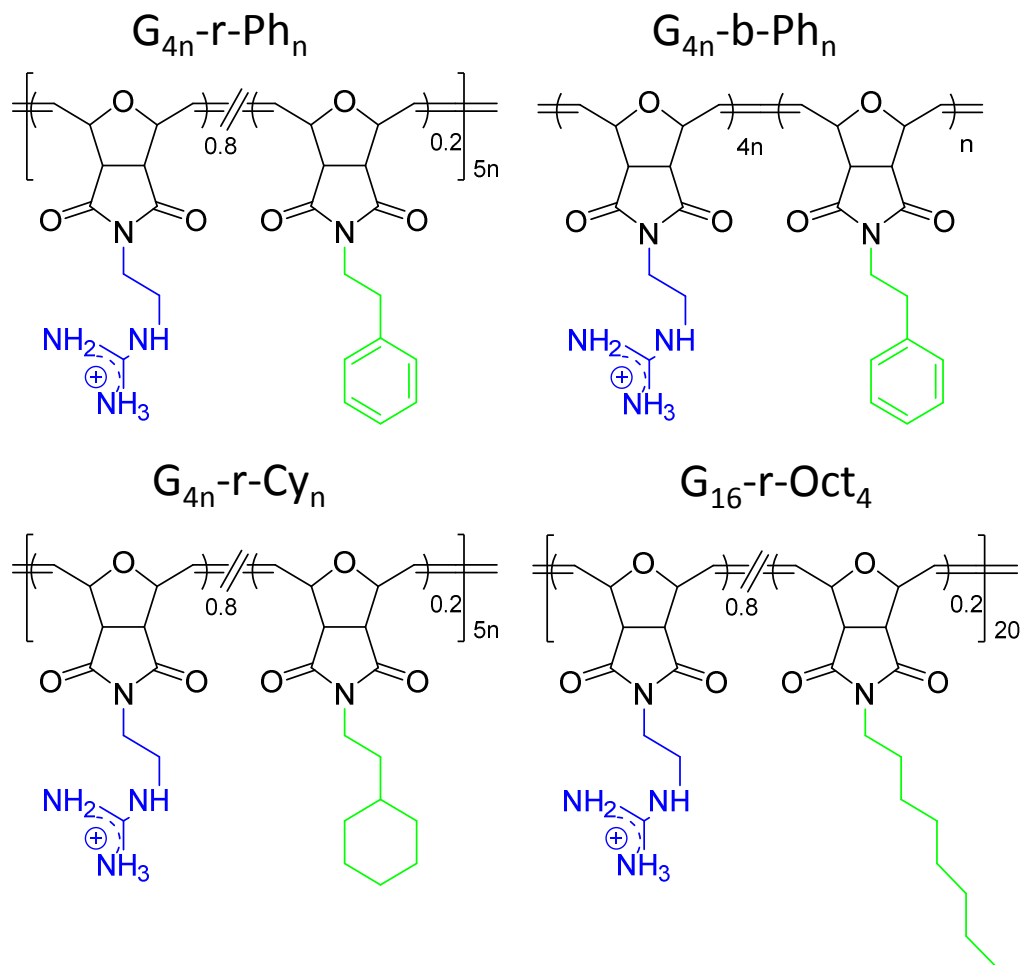


**Figure 5.1.** Polymers used for this study. Polymers were synthesized with n values of 2, 4, and 8.

**Table 5.1.** Polymers used in this study.

Name	DP	Hydrophobe	Guanidine	Expected MW
G <sub>8</sub> -r-Ph <sub>2</sub>	10	2	8	4100
G <sub>16</sub> -r-Ph <sub>4</sub>	20	4	16	8300
G <sub>32</sub> -r-Ph <sub>8</sub>	40	8	32	16500
G <sub>8</sub> -b-Ph <sub>2</sub>	10	2	8	4100
G <sub>16</sub> -b-Ph <sub>4</sub>	20	4	16	8300
G <sub>32</sub> -b-Ph <sub>8</sub>	40	8	32	16500

$G_8-r-Cy_2$	10	2	8	4100
$G_{16}-r-Cy_4$	20	4	16	8300
$G_{32}-r-Cy_8$	40	8	32	16600
$G_{16}-r-Oct_4$	20	4	16	8300

### 5.3.2 Random Copolymer Series

All polymers were shown to be capable of generating the negative Gaussian curvature-containing Pn3m phase in 20:80 DOPS:DOPE by small angle X-ray scattering (SAXS). The X-diffraction plots for the phenyl and cyclohexyl random copolymer series are shown in Figure 5.2. All Pn3m lattice parameters and derived curvature values are listed in Table 5.2. The random phenyl series (Figure 5.2a) was shown to have Pn3m lattice parameters of  $a=17.0, 16.9,$  and  $16.5$  for  $G_8-r-Ph_2, G_{16}-r-Ph_4,$  and  $G_{32}-r-Ph_8,$  respectively. While these values are commensurate with those found for optimal-length homopolymer and more hydrophobic copolymers from Chapter 4,[7] they show no meaningful variation with length. Similarly, the cyclohexyl series (Figure 5.2b) shows lattice parameters of  $a=16.2, 16.1,$  and  $16.25$  for  $G_8-r-Cy_2, G_{16}-r-Cy_4,$  and  $G_{32}-r-Cy_8,$  respectively. This is slightly more curvature than generated for the random phenyl series, but the significance of this result is unknown. The variation between the two series is much smaller than between the guanidine homopolymer and polyarginine, for example.[7] Furthermore, the cyclohexyl series also shows no length dependence for Gaussian curvature generation. Thus, it does not appear as if either aromaticity or polymer length measurably alters negative Gaussian curvature generation of these random, 20% hydrophobic residue polymers.

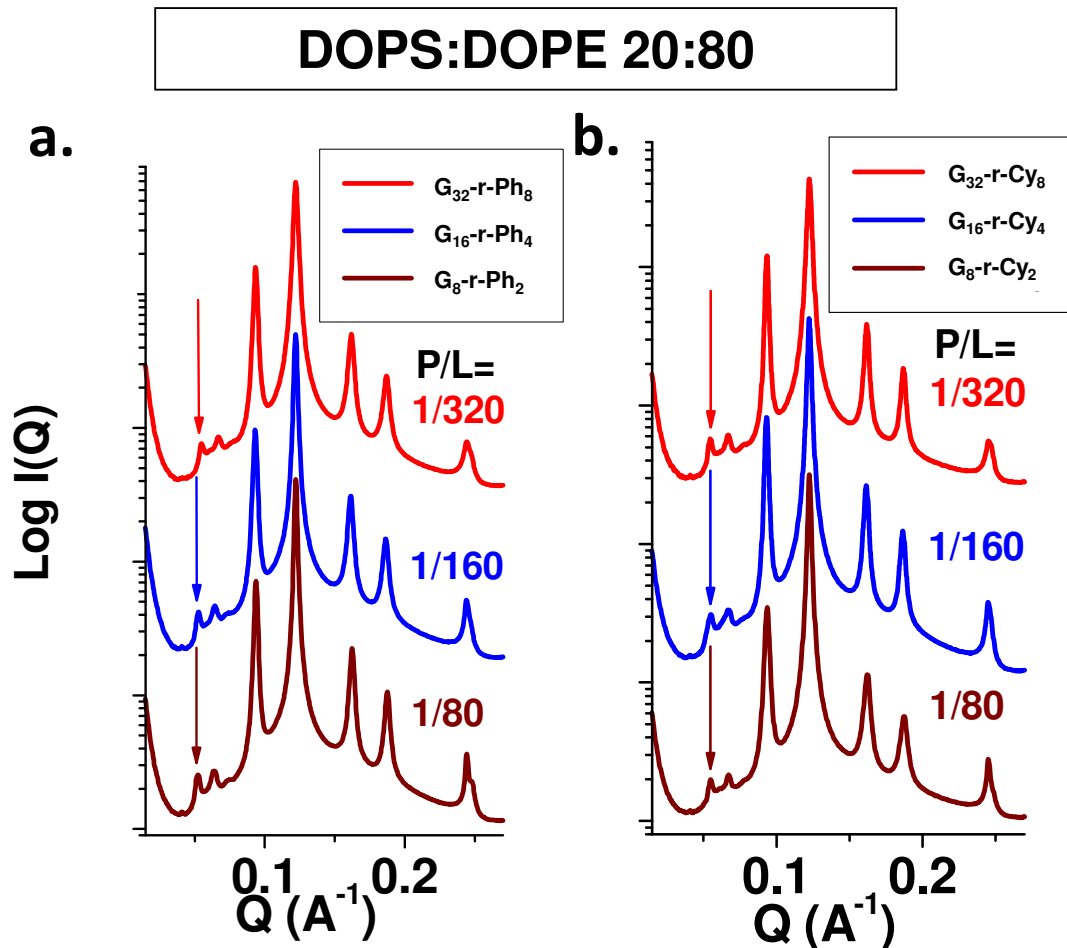


**Figure 5.2.** Small-angle X-ray scattering plots for 20:80 DOPS:DOPE lipid systems combined with a) the random phenyl copolymer series and b) the random cyclohexyl copolymer series. Arrows indicate the (110) peak of the Pn3m phase. The series show similar ability to generate negative Gaussian curvature, and no length dependence.

This data is perhaps most interesting when compared to the data from Chapter 4. There, the guanidine containing polymer had a strong length dependence, with the strongest curvature occurring for polymers 14-18 units long. The curvature values obtained for these polymers are never quite as high as the curvature obtained for those polymers, but curvature also does not decrease for either shorter or longer polymers. In chapter 4, this relationship was speculated as due to a shift between the polymer inducing a predominantly negative curvature

at shorter lengths and a predominantly positive curvature at longer lengths. At a sweet spot in the middle of these two trends, the balance is ideal for maximum negative Gaussian curvature generation. If that were the case for these homopolymers, then the additional positive curvature contributed by the addition of hydrophobic groups should mean that the maximum curvature occurs at a lower molecular weight. This is not the case, however. There are two potential factors at play here. The first is that the introduction of hydrophobic groups, while adding positive curvature, also add spacing between guanidinium units. As was shown in the comparison of the homopolymer to polyarginine (Figure 4.3), the increased guanidinium spacing both decreases the maximum curvature generation as well as pushes the optimum length upwards. The second component is that the claim that curvature is predominantly negative at low molecular weight and predominantly positive at high molecular weight was somewhat arbitrary, and it is entirely possible that negative curvature dominates for both short and long polymers. In such a case, then, the added hydrophobicity significantly broadens the ideal length range for negative Gaussian curvature generation.

**Table 5.2.** Collected SAXS data. Cells designated “-“ were tested but displayed no Pn3m phase peaks.

Name	20:80 DOPS:DOPE		20:70:10 DOPS:DOPE:DOPC	
	a (nm)	<K>  (nm <sup>-2</sup> )	a (nm)	<K>  (nm <sup>-2</sup> )
G <sub>8</sub> -r-Ph <sub>2</sub>	17	0.226	-	-
G <sub>16</sub> -r-Ph <sub>4</sub>	16.9	0.228	-	-
G <sub>32</sub> -r-Ph <sub>8</sub>	16.5	0.240	-	-
G <sub>8</sub> -b-Ph <sub>2</sub>	18	0.201	-	-
G <sub>16</sub> -b-Ph <sub>4</sub>	15.6	0.268	-	-
G <sub>32</sub> -b-Ph <sub>8</sub>	14.8	0.298	18.4	0.193
G <sub>8</sub> -r-Cy <sub>2</sub>	16.2	0.248	-	-
G <sub>16</sub> -r-Cy <sub>4</sub>	16.1	0.251	-	-
G <sub>32</sub> -r-Cy <sub>8</sub>	16.25	0.247	-	-

As a complement to these studies, dye release from EYPC vesicles was also measured for each polymer of total length 20 (Figure 5.3). Rather than looking for a specific mechanistic feature regarding pore formation as is the case with the SAXS experiments above, dye release simply measures a change in the permeability of the phospholipid membrane to the dye, regardless of mechanism. As has been shown in many studies[5, 13, 14, 16-18] and earlier chapters of this work, this approach is often very sensitive to changes in polymer structure, membrane composition, and overall hydrophobicity. In this case, however, there does not appear to be any meaningful difference in the dye release profiles of the polymers involved. All four polymers measured had  $EC_{50}$  values ranging from 5.3nM (**G<sub>16</sub>-r-Ph<sub>4</sub>**) to 6.8 nM (**G<sub>16</sub>-r-Cy<sub>4</sub>**) and Hill curve maxima ranging from 0.56 (**G<sub>16</sub>-r-Oct<sub>4</sub>**) to 0.65 (**G<sub>16</sub>-r-Ph<sub>4</sub>**). Similar to the small-angle X-ray scattering data above, aromaticity of the hydrophobic moieties does not appear to be a factor for the random copolymer series.

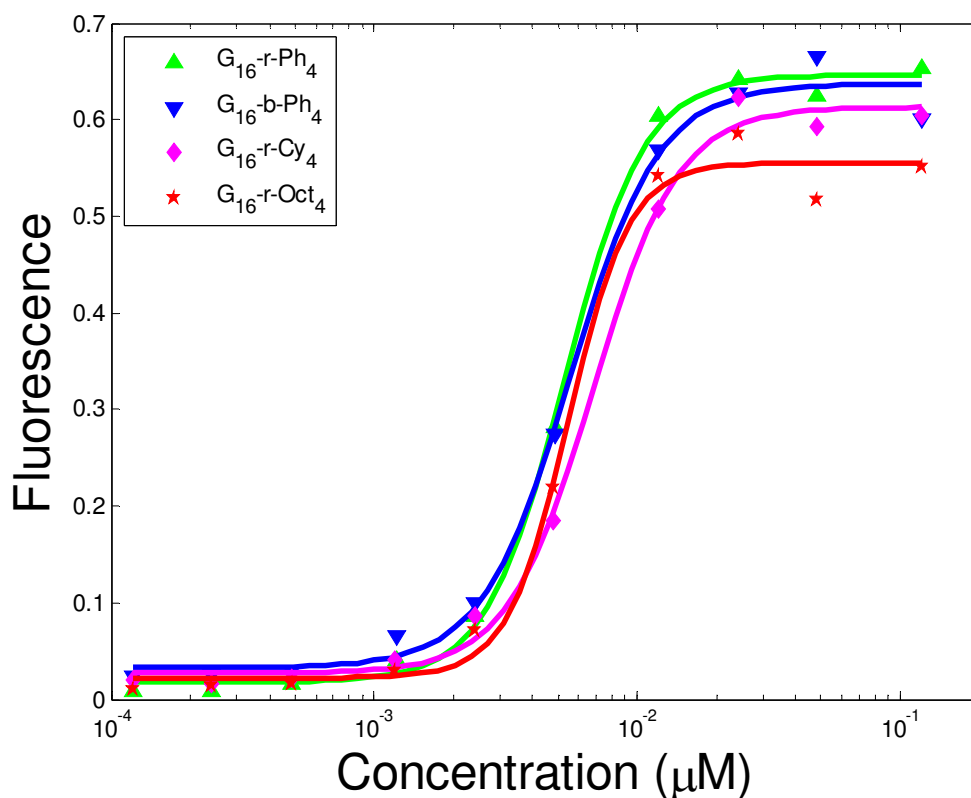


**Figure 5.3.** Dye release of all four polymers of length 20 with EYPC large unilamellar vesicles.

Very little variation is shown between samples.

### 5.3.3 Block Copolymer Series

The SAXS data for the block copolymer series (Figure 5.4), however, yields far more interesting results. The diffraction shows a steadily increasing curvature with polymer length, with lattice parameters  $a=18.0$ ,  $15.6$ , and  $14.8$  for **G<sub>8</sub>-b-Ph<sub>2</sub>**, **G<sub>16</sub>-b-Ph<sub>4</sub>**, and **G<sub>32</sub>-b-Ph<sub>8</sub>**, respectively. While the curvature obtained for **G<sub>16</sub>-b-Ph<sub>4</sub>** is similar to that of **G<sub>16</sub>-r-Ph<sub>4</sub>** and **G<sub>16</sub>-r-Cy<sub>4</sub>**, the shorter polymer generates far less curvature and the longer polymer generates far more curvature. This can best be seen in the plot of the mean curvature for all three polymer series shown in Figure 5.5. While the two random copolymer series show relatively little variance amongst themselves, the block copolymer series show both a strong length



dependence and a strong differentiation from the random series. Also of importance, **G<sub>32</sub>-b-Ph<sub>8</sub>** is the only polymer of any series able to induce negative Gaussian curvature with only 70% PE content (Figure 5.4b). This clearly indicates that, while there may not be a huge difference in the curvature values for **G<sub>16</sub>-b-Ph<sub>4</sub>** and **G<sub>32</sub>-b-Ph<sub>8</sub>** at 80% PE, the latter polymer is clearly more capable of inducing the Pn3m phase.

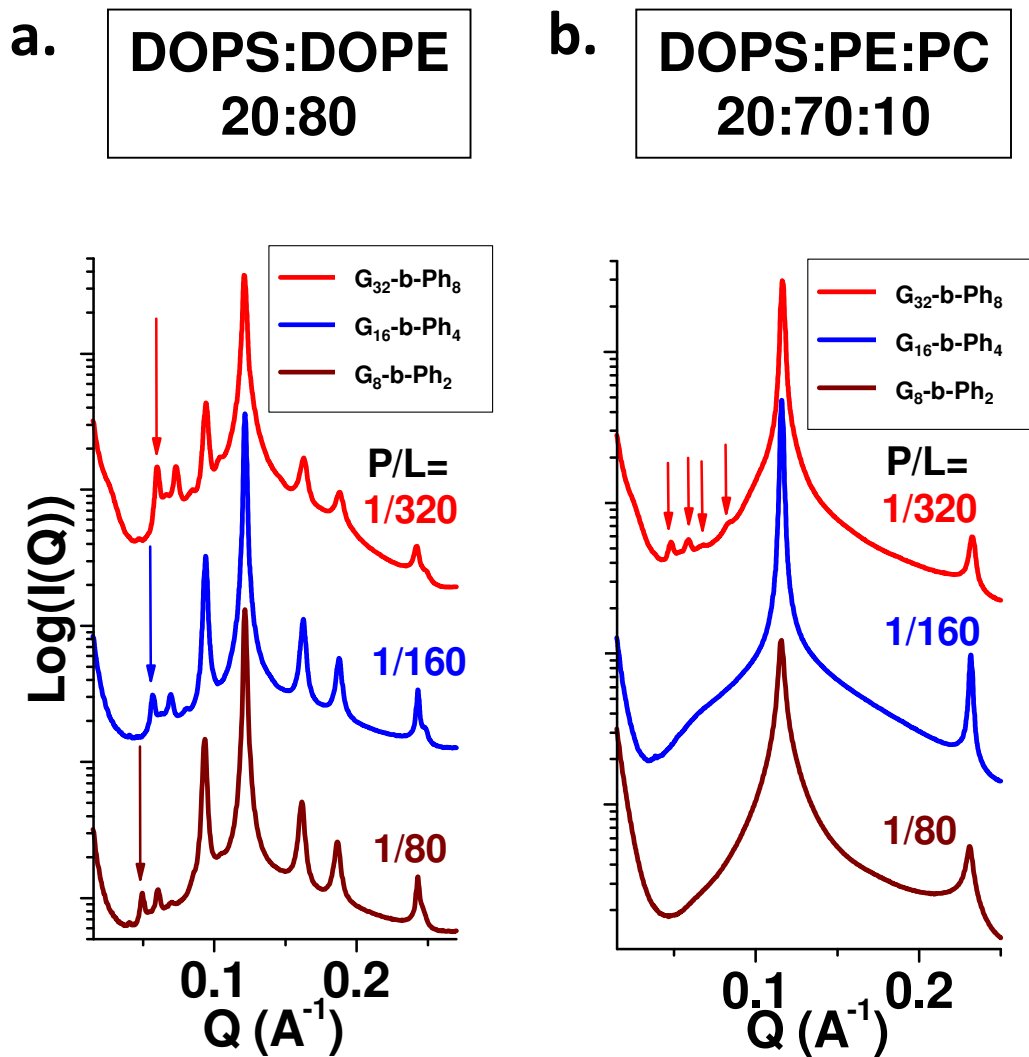


**Figure 5.4.** Small-angle X-ray scattering plots for the block phenyl series with a) 20:80 DOPS:DOPE and b) 20:70:10 DOPS:DOPE:DOPC lipid systems. Arrows in a) indicate the (110) peak of the Pn3m phase. Arrows and b) indicate the (110), (111), (200), and (211) phases. The polymer series shows a strong length dependence on curvature generation in a) and only  $G_{32}$ - $b$ - $Ph_8$  shows and Pn3m phase generation in b).

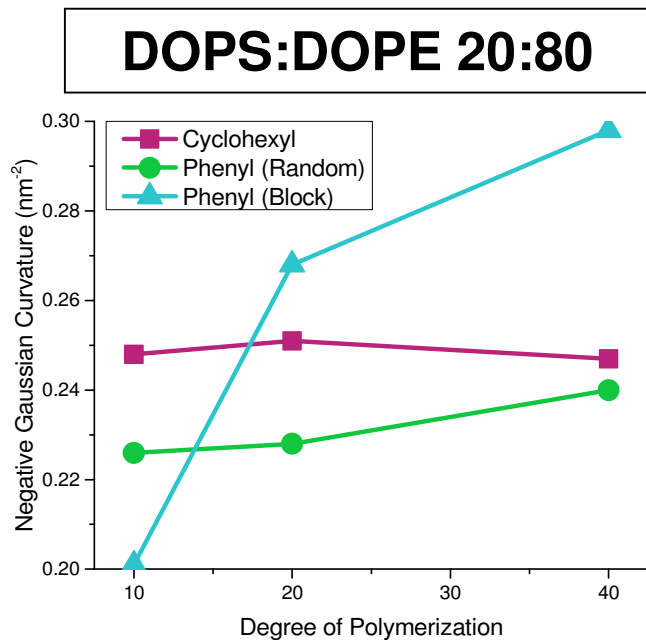


**Figure 5.5.** Compiled curvature generation as a function of polymer length for all three series. The two random series show little separation and little length dependence, while the block copolymer series shows a strong length dependence.

While the random copolymer might be seen as a single chain that is more hydrophobic than the guanidinium-containing homopolymer, the block copolymer can perhaps be seen as consisting of two different components fused together, one resembling the homopolymer and one resembling a purely hydrophobic group. We then have guanidinium-rich chains of average lengths 8, 16, and 32 fused to hydrophobic groups of 2, 4, and 8 units in length. Chapter 4 clearly showed a relationship between homopolymer length and curvature generation (Figure 4.3), and the difference between polymers of length 7-9 and length 14-18 is similar to the difference between  $\mathbf{G}_8\text{-}b\text{-Ph}_2$  and  $\mathbf{G}_{16}\text{-}b\text{-Ph}_4$ . However, that relationship also entails a large drop in curvature generation between unit lengths 18 and 27, whereas  $\mathbf{G}_{32}\text{-}b\text{-Ph}_8$  actually has higher curvature than  $\mathbf{G}_{16}\text{-}b\text{-Ph}_4$ . This suggests, then, that the longer hydrophobic block is able to

maintain high degrees of curvature for longer polymers. It is uncertain if this is achieved by the hydrophobic region inserting into the membrane, or if the polymer forms a micelle before interacting with the membrane. In either case, though, it does not appear as if the series has reached a maximum membrane curvature generation, and longer block copolymers may still generate more curvature.

To see if this effect carries over to membrane activity, dye release experiments were performed for the block copolymer series (Figure 5.6). The curves are shown on a mass concentration plot, rather than a molar concentration one, so that each point on the x-axis represents a similar ratio between polymer cations and lipid anions. This is the same standard of comparison that is used in the SAXS experiments above, which are all performed at constant charge ratio. These polymers show  $EC_{50}$  values of 89, 46, and 71 ng/mL for polymers **G<sub>8</sub>-b-Ph<sub>2</sub>**, **G<sub>16</sub>-b-Ph<sub>4</sub>**, and **G<sub>32</sub>-b-Ph<sub>8</sub>**, respectively. While these are not large differences (especially when compared to the ratios of an order of magnitude or more seen in Chapters 2 and 3), they seem more reflective of an optimum length at around DP=20, more like what is seen with the homopolymer in Chapter 4. It is likelier, though, that these differences in  $EC_{50}$  values are not particularly meaningful, and that whatever causes the increase in curvature with polymer length in the SAXS studies does not carry over to the dye release studies. This can be due to multiple factors. First and foremost, the lipid systems are very different. The SAXS studies are dominated by negative intrinsic curvature PE lipid, while the dye release studies are performed with near-zero curvature EYPC.[23] PE content is relatively low in mammalian cells, and this difference in membrane composition has been demonstrated to be responsible for differences in membrane activity in antimicrobial compounds.[24-26] That relationship between PE lipid content and activity of PTD(M)s is far less well established, however. Unlike antimicrobials, PTD(M)s are able to induce dye release in PC vesicles, but at the same time cannot induce

negative Gaussian curvature in low PE systems. Whether trends in negative Gaussian curvature generation by PTD(M)s can more generally be applied to overall membrane activity still remains to be seen. While these two tests (SAXS and dye release studies) measured the same effects for antimicrobials, it is possible that SAXS and dye release studies measure two different mechanisms of action for PTD(M)s.

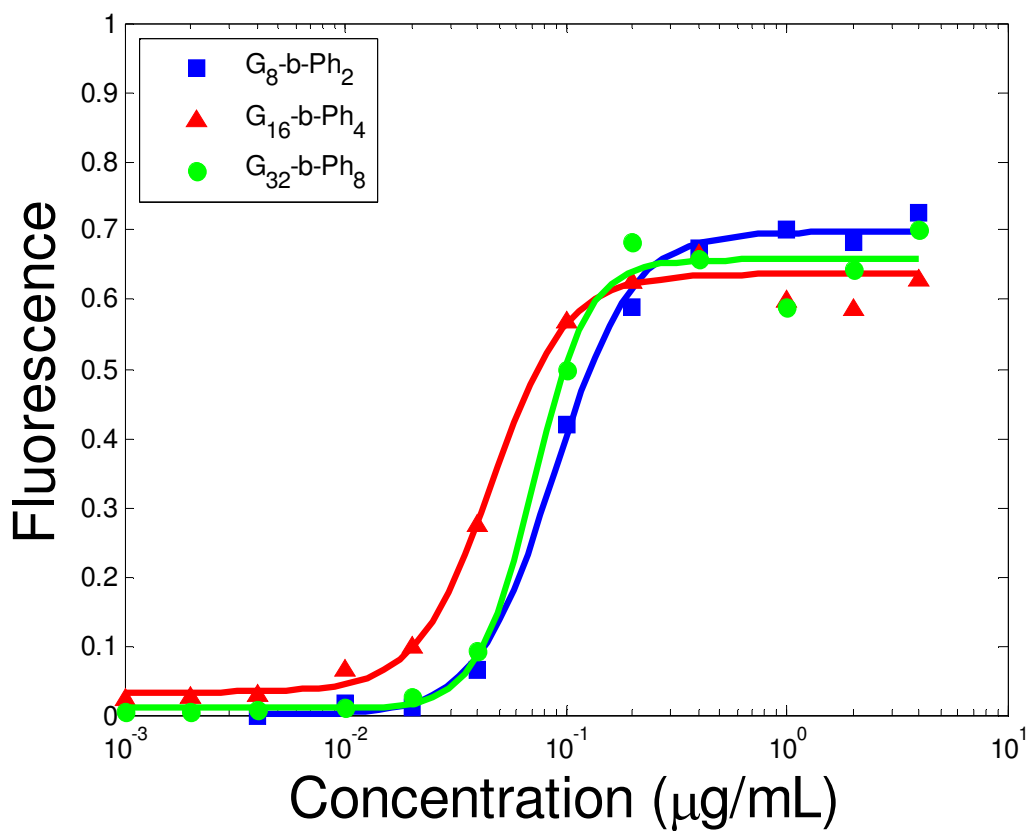


**Figure 5.6.** Dye release for the block copolymer series with large unilamellar vesicles. x-axis is given in units of  $\mu\text{g/mL}$  instead of  $\mu\text{M}$  to maintain a fixed polymer cation to lipid anion ratio, as was done with the SAXS experiments.

## 5.4 Conclusions

A diverse series of guanidinium-rich PTDMs was created, with similar hydrophobic contents but differing degrees of aromaticity and varying polymer architecture. It was shown that both cyclohexyl- and phenyl-containing random copolymers were able to induce negative Gaussian curvature in 80% PE bulk lipid systems, but that there was no variation between the series or along polymer length. The block-phenyl copolymer system  $G_{4n}$ - $b$ - $Ph_n$ , however, differed from the random copolymer system and furthermore showed a substantial increase in curvature generation with polymer length. Dye release experiments showed all polymers as having similar dye release profiles. While both experiments have in various experiments been shown to correlate with actual cellular activity, it is possible that they are measuring aspects, and we should not assume a uniform relationship. What is clearer from this study is that the difference in activity between block and random copolymers deserves far more study. While such structures have not been heavily studied in the biophysical realm, polymers with this design have been some of the most effective at carrying cargo into cells.[8-10] It is quite likely that there is far more to understand about the nuances of what block copolymer architecture does to membrane activity, and this region remains largely unexplored.

## 5.5 References

1. Killian, J.A. and G. von Heijne, *How proteins adapt to a membrane–water interface*. Trends in Biochemical Sciences, 2000. **25**(9): p. 429-434.
2. White, S.H. and W.C. Wimley, *MEMBRANE PROTEIN FOLDING AND STABILITY: Physical Principles*. Annual Review of Biophysics and Biomolecular Structure, 1999. **28**(1): p. 319-365.
3. Yau, W.-M., et al., *The Preference of Tryptophan for Membrane Interfaces†*. Biochemistry, 1998. **37**(42): p. 14713-14718.

4. Wimley, W.C. and S.H. White, *Experimentally determined hydrophobicity scale for proteins at membrane interfaces*. Nature Structural & Molecular Biology, 1996. **3**(10): p. 842-848.
5. Som, A., A. Reuter, and G.N. Tew, *Protein Transduction Domain Mimics: The Role of Aromatic Functionality*. Angewandte Chemie International Edition, 2012. **51**(4): p. 980-983.
6. Mishra, A., et al., *Translocation of HIV TAT peptide and analogues induced by multiplexed membrane and cytoskeletal interactions*. Proceedings of the National Academy of Sciences of the United States of America, 2011. **108**(41): p. 16883-16888.
7. Schmidt, N.W., et al., *Molecular Basis for Nanoscopic Membrane Curvature Generation from Quantum Mechanical Models and Synthetic Transporter Sequences*. Journal of the American Chemical Society, 2012. **134**(46): p. 19207-19216.
8. Tezgel, A.O., *Protein Transduction Domain Mimics by ROMP and Their Bioactive Cargo Delivery*, in *Polymer Science and Engineering 2013*, University of Massachusetts--Amherst: Amherst, MA. p. 156.
9. Tezgel, A.Ö., et al., *Novel Protein Transduction Domain Mimics as Nonviral Delivery Vectors for siRNA Targeting NOTCH1 in Primary Human T cells*. Molecular Therapy, 2013. **21**(1): p. 201-209.
10. Sgolastra, F., et al., *Sequence Segregation Improves Non-covalent Protein Delivery*, 2014, University of Massachusetts--Amherst: Amherst, MA.
11. Deshayes, S., et al., *Delivery of proteins and nucleic acids using a non-covalent peptide-based strategy*. Advanced Drug Delivery Reviews, 2008. **60**(4-5): p. 537-547.
12. Sgolastra, F., et al., *The Importance of Sequence Specific Hydrophobicity in Synthetic Protein Transduction Domain Mimics*. Biomacromolecules, 2014. **15**(3): p. 812-820.
13. Almeida, P.F. and A. Pokorny, *Mechanisms of Antimicrobial, Cytolytic, and Cell-Penetrating Peptides: From Kinetics to Thermodynamics*. Biochemistry, 2009. **48**(34): p. 8083-8093.
14. Yandek, L.E., et al., *Mechanism of the Cell-Penetrating Peptide Transporter 10 Permeation of Lipid Bilayers*. Biophysical Journal, 2007. **92**(7): p. 2434-2444.
15. Som, A., et al., *Self-Activation in De Novo Designed Mimics of Cell-Penetrating Peptides*. Angewandte Chemie International Edition, 2011. **50**(27): p. 6147-6150.
16. Hennig, A., et al., *Stimuli-Responsive Polyguanidino-Oxanorbornene Membrane Transporters as Multicomponent Sensors in Complex Matrices*. Journal of the American Chemical Society, 2008. **130**(31): p. 10338-10344.
17. Sakai, N. and S. Matile, *Anion-Mediated Transfer of Polyarginine across Liquid and Bilayer Membranes*. Journal of the American Chemical Society, 2003. **125**(47): p. 14348-14356.
18. Som, A., et al., *Self-Activation in De Novo Designed Mimics of Cell-Penetrating Peptides*. Angewandte Chemie International Edition, 2011. **50**(27): p. 6147-6150.
19. Gabriel, G.J., et al., *Synthetic Mimic of Antimicrobial Peptide with Nonmembrane-Disrupting Antibacterial Properties*. Biomacromolecules, 2008. **9**(11): p. 2980-2983.
20. Schmidt, N.W., et al., *Criterion for amino acid composition of defensins and antimicrobial peptides based on geometry of membrane destabilization*. Journal of the American Chemical Society, 2011. **133**(17): p. 6720-6727.
21. Ilavsky, J., *Nika*: software for two-dimensional data reduction. Journal of Applied Crystallography, 2012. **45**(2): p. 324-328.
22. Hammersley, A. *THE FIT2D HOME PAGE*. 2014/04/20/13:41:53; Available from: <http://www.esrf.eu/computing/scientific/FIT2D/>.

23. Zimmerberg, J. and M.M. Kozlov, *How proteins produce cellular membrane curvature*. Nature Reviews Molecular Cell Biology, 2006. **7**(1): p. 9-19.
24. Som, A., et al., *Divalent Metal Ion Triggered Activity of a Synthetic Antimicrobial in Cardiolipin Membranes*. Journal of the American Chemical Society, 2009. **131**(42): p. 15102-15103.
25. Yang, L., et al., *Synthetic Antimicrobial Oligomers Induce a Composition-Dependent Topological Transition in Membranes*. Journal of the American Chemical Society, 2007. **129**(40): p. 12141-12147.
26. Yang, L., et al., *Mechanism of a prototypical synthetic membrane-active antimicrobial: Efficient hole-punching via interaction with negative intrinsic curvature lipids*. Proceedings of the National Academy of Sciences, 2008. **105**(52): p. 20595-20600.



## CHAPTER 6

### Summary and Future Work

#### 6.1 Conclusions

This thesis presents a step forward in our understanding of PTDM-membrane interactions. It has explored how guanidinium-rich polymers interact with phospholipid membrane phase, charge content, and negative Gaussian curvature induction. It has looked at these features across polymer length, charge density, hydrophobicity, aromaticity and architecture. The capability to so carefully compare the effects of different membrane and PTDM features is unique to this laboratory, and has resulted in mechanistic insight.

Chapter 2 presented the relationship between membrane phase and polymer activity. Cooling phospholipid membranes below their phase transition temperature was found to inhibit dye release from vesicles as well as uptake in cells. This is important because cooling cells to refrigerator temperatures is a common practice to inhibit endocytosis and to distinguish energy-dependent from energy-independent uptake. Additional polymer hydrophobicity, however, was found to overcome this barrier.

Chapter 3 demonstrated that for this class of polymers, anionic lipid content inhibited the ability of these polymers to insert with phospholipid membranes. This is in direct conflict with the generally accepted “adaptive translocation” model of PTDM activity. It was also shown that while anionic lipid content is usually assumed as a necessary feature for surface association of the polymer on the lipid membrane, for this class polymer association is driven by hydrophobic interactions and the anionic content serves only to “pin” the PTMD to the surface of the membrane, and thus acts as a barrier to activity. Much like the gel phase, however, this barrier can be overcome by additional polymer hydrophobicity. These results call into question

the necessity of the cationic nature of the polymer, and suggest that charge-neutral varieties may be equally or more effective.

Chapters 4 and 5 examine the relationship between PTDM structure and negative Gaussian curvature formation in high PE-content lipid systems. Polymer length, charge density, hydrophobicity, and architecture are all found to be important determining factors in the effectiveness of these polymers to generate curvature. While said relationship between polymer structure and phase generation in bulk systems is well established, it is still unclear how well these results correlate to actual membrane activity.

From the sum of these, we find that the energy-independent interactions of PTDMs are largely driven by phase and solubility interactions. Active polymers are soluble enough in solution to reach the membrane, but hydrophobic enough to insert into it. Barriers to activity such as anionic lipid content and gel lipid phase can be overcome by additional hydrophobicity, or by addressing the barriers more directly. This research leads us to a better understanding of PTDM interaction with membranes as a whole, as well as specific design constraints to consider when making polymers for delivery purposes.

## **6.2 Future Work**

While meaningful progress was made in this work, there is an enormous wealth of topics still remaining to be explored. Some of the more immediately pressing and achievable targets are listed below, areas that each could spawn extensive additional research themselves.

### **6.2.1 More complex membrane systems**

The work presented in this thesis has highlighted the important impact of membrane phase and anionic lipid content, but cell membranes contain many other variables to consider.

Sphingolipids, cholesterol, glycolipids and membrane proteins can all be integrated into vesicle structures, but none of which are accounted for in most model systems. While true parity with the organization present in a living cell can never be achieved, systematic understanding of the role of each of these components can give us a much better understanding of the relationship between membrane components and cellular uptake of PTDMs.

### **6.2.2 Membrane activity and osmotic pressure**

Biophysical studies of PTD(M)s have largely focused varying compositional, rather than mechanical, aspects of the membrane. There is, however, a great wealth of literature examining the relationship between polymer/peptide adhesion onto and insertion into membranes under varying physical constraints.[1-5] While much of that literature is dedicated to sophisticated apparatus such as Langmuir troughs and pipette aspiration, a far simpler approach can be used with dye release experiments. In dye release experiments, the vesicles are removed from their normal medium by size-exclusion chromatography and replaced with a buffer of similar osmolarity. Changing the osmolarity of the external buffer through varying concentrations of glucose, on the other hand, would provide insight into the relationship between membrane tension and PTDM activity.

### **6.2.3 Biophysical studies of polymer-cargo complexes**

The studies presented in this thesis have focused on the interaction of individual polymers with lipid membranes. The intended application of this class of molecules, however, is the delivery of macromolecular cargo to cells. This consists of either direct conjugation of the PTDM to the cargo, or the formation of a self-assembled complex of PTDM and cargo. It is likely that the interactions of such aggregates with phospholipid membranes is fundamentally

different than the interaction pure polymer in solution. While dye release and surface plasmon resonance will give some insight into how the complex interacts with the membranes, FRET pairing between PTDMs and cargo will make it possible to monitor the interaction between the two components after introduction into the membrane.[6]

#### 6.2.4 Zwitterionic PTDMs

Chapter 3 demonstrated that surface association of ROMP-based PTDMs was largely driven by hydrophobicity, and that electrostatic interactions between the cationic polymer and anionic lipid actually reduced membrane activity. It then follows that even if there is some importance to the hydrogen bonding behavior of the guanidinium group, cationic nature *in itself* may not be particularly useful for membrane activity. A zwitterionic molecule, then, with the right balance of water and membrane solubility may make for a superior drug delivery agent. To the author's knowledge, such a system has only been attempted once, with a micelle-forming polymer.[7] While the results are promising, they are extremely preliminary and far more work needs to be done to investigate the effects of changing the charge content of the polymer. This research group is uniquely positioned to advance this field however, due to our experience both with PTDMs and in designing zwitterionic polymer systems.

### 6.3 References

1. Frey, S.L. and K.Y.C. Lee, *Temperature Dependence of Poloxamer Insertion Into and Squeeze-Out from Lipid Monolayers*. *Langmuir*, 2007. **23**(5): p. 2631-2637.
2. Frey, S.L., et al., *Effects of block copolymer's architecture on its association with lipid membranes: Experiments and simulations*. *The Journal of Chemical Physics*, 2007. **127**(11).
3. Ishitsuka, Y., et al., *Amphiphilic Poly(phenyleneethynylene)s Can Mimic Antimicrobial Peptide Membrane Disordering Effect by Membrane Insertion*. *Journal of the American Chemical Society*, 2006. **128**(40): p. 13123-13129.

4. Santore, M.M., et al., *Effect of Surfactant on Unilamellar Polymeric Vesicles: Altered Membrane Properties and Stability in the Limit of Weak Surfactant Partitioning*. Langmuir, 2002. **18**(20): p. 7299-7308.
5. Olbrich, K., et al., *Water Permeability and Mechanical Strength of Polyunsaturated Lipid Bilayers*. Biophysical Journal, 2000. **79**(1): p. 321-327.
6. Cheung, J.C., et al., *A novel method for monitoring the cytosolic delivery of peptide cargo*. Journal of Controlled Release, 2009. **137**(1): p. 2-7.
7. Kim, Y., S. Binauld, and M.H. Stenzel, *Zwitterionic Guanidine-Based Oligomers Mimicking Cell-Penetrating Peptides as a Nontoxic Alternative to Cationic Polymers to Enhance the Cellular Uptake of Micelles*. Biomacromolecules, 2012. **13**(10): p. 3418-3426.

## BIBLIOGRAPHY

1. Al-Badri, Z.M., et al., *Investigating the Effect of Increasing Charge Density on the Hemolytic Activity of Synthetic Antimicrobial Polymers*. *Biomacromolecules*, 2008. **9**(10): p. 2805-2810.
2. Almeida, P.F. and A. Pokorny, *Mechanisms of Antimicrobial, Cytolytic, and Cell-Penetrating Peptides: From Kinetics to Thermodynamics*. *Biochemistry*, 2009. **48**(34): p. 8083-8093.
3. Al-Taei, S., et al., *Intracellular Traffic and Fate of Protein Transduction Domains HIV-1 TAT Peptide and Octaarginine. Implications for Their Utilization as Drug Delivery Vectors*. *Bioconjugate Chemistry*, 2006. **17**(1): p. 90-100.
4. Alves, I.D., et al., *Relationships between Membrane Binding, Affinity and Cell Internalization Efficacy of a Cell-Penetrating Peptide: Penetratin as a Case Study*. *PLoS ONE*, 2011. **6**(9).
5. Alves, I.D., et al., *Cell biology meets biophysics to unveil the different mechanisms of penetratin internalization in cells*. *Biochimica et Biophysica Acta (BBA) - Biomembranes*, 2010. **1798**(12): p. 2231-2239.
6. Arav, A., et al., *Phase Transition Temperature and Chilling Sensitivity of Bovine Oocytes*. *Cryobiology*, 1996. **33**(6): p. 589-599.
7. Beseničar, M., et al., *Surface plasmon resonance in protein–membrane interactions*. *Chemistry and Physics of Lipids*, 2006. **141**(1–2): p. 169-178.
8. Braun, A.R., et al.,  *$\alpha$ -Synuclein induces both positive mean curvature and negative Gaussian curvature in membranes*. *Journal of the American Chemical Society*, 2012. **134**(5): p. 2613-2620.
9. Cevc, G. and D. Marsh, *Phospholipid bilayers: physical principles and models* 1987: Wiley. 472.
10. Chapman, D., *Phase transitions and fluidity characteristics of lipids and cell membranes*. *Quarterly Reviews of Biophysics*, 1975. **8**(2): p. 185-235.
11. Chemburu, S., et al., *Light-Induced Biocidal Action of Conjugated Polyelectrolytes Supported on Colloids*. *Langmuir*, 2008. **24**(19): p. 11053-11062.
12. Cheung, J.C., et al., *A novel method for monitoring the cytosolic delivery of peptide cargo*. *Journal of Controlled Release*, 2009. **137**(1): p. 2-7.
13. Colak, S., et al., *Hydrophilic Modifications of an Amphiphilic Polynorbornene and the Effects on its Hemolytic and Antibacterial Activity*. *Biomacromolecules*, 2009. **10**(2): p. 353-359.
14. Conner, S.D. and S.L. Schmid, *Regulated portals of entry into the cell*. *Nature*, 2003. **422**(6927): p. 37-44.
15. Cooley, C.B., et al., *Oligocarbonate Molecular Transporters: Oligomerization-Based Syntheses and Cell-Penetrating Studies*. *Journal of the American Chemical Society*, 2009. **131**(45): p. 16401-16403.
16. Corbitt, T.S., et al., *Light and dark biocidal activity of cationic poly(arylene ethynylene) conjugated polyelectrolytes*. *Photochemical & Photobiological Sciences*, 2009. **8**(7).
17. Corbitt, T.S., et al., *Conjugated Polyelectrolyte Capsules: Light-Activated Antimicrobial Micro "Roach Motels"*. *ACS Applied Materials & Interfaces*, 2009. **1**(1): p. 48-52.
18. Dautry-Varsat, A., A. Ciechanover, and H.F. Lodish, *pH and the recycling of transferrin during receptor-mediated endocytosis*. *Proceedings of the National Academy of Sciences of the United States of America*, 1983. **80**(8): p. 2258-2262.

19. Davies, A., M. Bentley, and B.S. Field, *Comparison of the Action of Vantocil, Cetrimide and Chlorhexidine on Escherichia coli and its Spheroplasts and the Protoplasts of Gram Positive Bacteria*. Journal of Applied Microbiology, 1968. **31**(4): p. 448-461.
20. Davies, A. and B.S. Field, *Action of Biguanides, Phenols and Detergents on Escherichia coli and its Spheroplasts*. Journal of Applied Microbiology, 1969. **32**(2): p. 233-243.
21. Davies, G.E., et al., *1:6-di-4'-chlorophenyldiguanidohexane ("hibitane")*. Laboratory investigation of a new antibacterial agent of high potency. British Journal of Pharmacology and Chemotherapy, 1954. **9**(2): p. 192-196.
22. Deshayes, S., et al., *Delivery of proteins and nucleic acids using a non-covalent peptide-based strategy*. Advanced Drug Delivery Reviews, 2008. **60**(4-5): p. 537-547.
23. Ding, L., et al., *Insight into the Mechanism of Antimicrobial Poly(phenylene ethynylene) Polyelectrolytes: Interactions with Phosphatidylglycerol Lipid Membranes* Langmuir 25th Year: Molecular and macromolecular self-assemblies. Langmuir, 2009. **25**(24): p. 13742-13751.
24. Ding, L., et al., *Insight into the Mechanism of Antimicrobial Conjugated Polyelectrolytes: Lipid Headgroup Charge and Membrane Fluidity Effects*. Langmuir, 2010. **26**(8): p. 5544-5550.
25. Drin, G., et al., *Studies on the Internalization Mechanism of Cationic Cell-penetrating Peptides*. Journal of Biological Chemistry, 2003. **278**(33): p. 31192-31201.
26. Drin, G., et al., *Translocation of the pAntp Peptide and Its Amphipathic Analogue AP-2AL<sup>T</sup>*. Biochemistry, 2001. **40**(6): p. 1824-1834.
27. El-Sayed, A., S. Futaki, and H. Harashima, *Delivery of Macromolecules Using Arginine-Rich Cell-Penetrating Peptides: Ways to Overcome Endosomal Entrapment*. The AAPS Journal, 2009. **11**(1): p. 13-22.
28. Elson-Schwab, L., et al., *Guanidinylated Neomycin Delivers Large, Bioactive Cargo into Cells through a Heparan Sulfate-dependent Pathway*. Journal of Biological Chemistry, 2007. **282**(18): p. 13585-13591.
29. Epanand, R.F., et al., *Dual Mechanism of Bacterial Lethality for a Cationic Sequence-Random Copolymer that Mimics Host-Defense Antimicrobial Peptides*. Journal of Molecular Biology, 2008. **379**(1): p. 38-50.
30. Eren, T., et al., *Antibacterial and Hemolytic Activities of Quaternary Pyridinium Functionalized Polynorbornenes*. Macromolecular Chemistry and Physics, 2008. **209**(5): p. 516-524.
31. Fawell, S., et al., *Tat-mediated delivery of heterologous proteins into cells*. Proceedings of the National Academy of Sciences, 1994. **91**(2): p. 664-668.
32. Fischer, D., et al., *In vitro cytotoxicity testing of polycations: influence of polymer structure on cell viability and hemolysis*. Biomaterials, 2003. **24**(7): p. 1121-1131.
33. Frankel, A.D. and C.O. Pabo, *Cellular uptake of the tat protein from human immunodeficiency virus*. Cell, 1988. **55**(6): p. 1189-1193.
34. Fretz, M., et al., *Effects of Na<sup>+</sup>/H<sup>+</sup> exchanger inhibitors on subcellular localisation of endocytic organelles and intracellular dynamics of protein transduction domains HIV-TAT peptide and octaarginine*. Journal of Controlled Release, 2006. **116**(2): p. 247-254.
35. Fretz, Marjan M., et al., *Temperature-, concentration- and cholesterol-dependent translocation of L- and D-octa-arginine across the plasma and nuclear membrane of CD34<sup>+</sup> leukaemia cells*. Biochemical Journal, 2007. **403**(2).
36. Frey, S.L. and K.Y.C. Lee, *Temperature Dependence of Poloxamer Insertion Into and Squeeze-Out from Lipid Monolayers*. Langmuir, 2007. **23**(5): p. 2631-2637.

37. Frey, S.L., et al., *Effects of block copolymer's architecture on its association with lipid membranes: Experiments and simulations*. The Journal of Chemical Physics, 2007. **127**(11).
38. Futaki, S., *Membrane-permeable arginine-rich peptides and the translocation mechanisms*. Advanced Drug Delivery Reviews, 2005. **57**(4): p. 547-558.
39. Futaki, S., et al., *Arginine-rich Peptides AN ABUNDANT SOURCE OF MEMBRANE-PERMEABLE PEPTIDES HAVING POTENTIAL AS CARRIERS FOR INTRACELLULAR PROTEIN DELIVERY*. Journal of Biological Chemistry, 2001. **276**(8): p. 5836-5840.
40. Gabriel, G.J., et al., *Synthetic Mimic of Antimicrobial Peptide with Nonmembrane-Disrupting Antibacterial Properties*. Biomacromolecules, 2008. **9**(11): p. 2980-2983.
41. Gabriel, G.J., et al., *Synthetic Mimic of Antimicrobial Peptide with Nonmembrane-Disrupting Antibacterial Properties*. Biomacromolecules, 2008. **9**(11): p. 2980-2983.
42. Gabriel, G.J., et al., *Comparison of Facially Amphiphilic versus Segregated Monomers in the Design of Antibacterial Copolymers*. Chemistry - A European Journal, 2009. **15**(2): p. 433-439.
43. Gabriel, G.J., et al., *Interactions between Antimicrobial Polynorbornenes and Phospholipid Vesicles Monitored by Light Scattering and Microcalorimetry*. Langmuir, 2008. **24**(21): p. 12489-12495.
44. Gabriel, G.J., et al., *Infectious disease: Connecting innate immunity to biocidal polymers*. Materials Science and Engineering: R: Reports, 2007. **57**(1-6): p. 28-64.
45. Gabriel, G.J. and G.N. Tew, *Conformationally rigid proteomimetics: a case study in designing antimicrobial aryl oligomers*. Organic & Biomolecular Chemistry, 2008. **6**(3): p. 417-423.
46. Gait, M.J., *Peptide-mediated cellular delivery of antisense oligonucleotides and their analogues*. Cellular and molecular life sciences: CMLS, 2003. **60**(5): p. 844-853.
47. Ganz, T., *Defensins: antimicrobial peptides of innate immunity*. Nature Reviews Immunology, 2003. **3**(9): p. 710-720.
48. Green, M. and P.M. Loewenstein, *Autonomous functional domains of chemically synthesized human immunodeficiency virus tat trans-activator protein*. Cell, 1988. **55**(6): p. 1179-1188.
49. Gump, J.M. and S.F. Dowdy, *TAT transduction: the molecular mechanism and therapeutic prospects*. Trends in Molecular Medicine, 2007. **13**(10): p. 443-448.
50. Gunstone, F., *The Lipid handbook*. 2nd ed. ed1994, London ;;New York: Chapman and Hall.
51. Guterstam, P., et al., *Elucidating cell-penetrating peptide mechanisms of action for membrane interaction, cellular uptake, and translocation utilizing the hydrophobic counter-anion pyrenebutyrate*. Biochimica et Biophysica Acta (BBA) - Biomembranes, 2009. **1788**(12): p. 2509-2517.
52. Hammersley, A. *THE FIT2D HOME PAGE*. 2014/04/20/13:41:53; Available from: <http://www.esrf.eu/computing/scientific/FIT2D/>.
53. Harper, P.E. and S.M. Gruner, *Electron density modeling and reconstruction of infinite periodic minimal surfaces (IPMS) based phases in lipid-water systems. I. Modeling IPMS-based phases*. The European Physical Journal E, 2000. **2**(3): p. 217-228.
54. Heitz, F., M.C. Morris, and G. Divita, *Twenty years of cell-penetrating peptides: from molecular mechanisms to therapeutics*. British Journal of Pharmacology, 2009. **157**(2): p. 195-206.



55. Hennig, A., et al., *Stimuli-Responsive Polyguanidino-Oxanorbornene Membrane Transporters as Multicomponent Sensors in Complex Matrices*. Journal of the American Chemical Society, 2008. **130**(31): p. 10338-10344.
56. Herce, H.D. and A.E. Garcia, *Molecular dynamics simulations suggest a mechanism for translocation of the HIV-1 TAT peptide across lipid membranes*. Proceedings of the National Academy of Sciences, 2007. **104**(52): p. 20805-20810.
57. Hierrezuelo, J., et al., *Electrostatic Stabilization of Charged Colloidal Particles with Adsorbed Polyelectrolytes of Opposite Charge*. Langmuir, 2010. **26**(19): p. 15109-15111.
58. Huang, C. and J.T. Mason, *Structure and properties of mixed-chain phospholipid assemblies*. Biochimica et Biophysica Acta, 1986. **864**(3-4): p. 423-470.
59. Ikeda, T., et al., *Interaction of a polymeric biguanide biocide with phospholipid membranes*. Biochimica et Biophysica Acta (BBA) - Biomembranes, 1984. **769**(1): p. 57-66.
60. Ikeda, T., et al., *Time-resolved fluorescence anisotropy studies on the interaction of biologically active polycations with phospholipid membranes*. Biochimica et Biophysica Acta (BBA) - Biomembranes, 1990. **1021**(1): p. 56-62.
61. Ikeda, T., S. Tazuke, and M. Watanabe, *Interaction of biologically active molecules with phospholipid membranes: I. Fluorescence depolarization studies on the effect of polymeric biocide bearing biguanide groups in the main chain*. Biochimica et Biophysica Acta (BBA) - Biomembranes, 1983. **735**(3): p. 380-386.
62. Ikeda, T., H. Yamaguchi, and S. Tazuke, *New polymeric biocides: synthesis and antibacterial activities of polycations with pendant biguanide groups*. Antimicrobial Agents and Chemotherapy, 1984. **26**(2): p. 139-144.
63. Ikeda, T., H. Yamaguchi, and S. Tazuke, *Phase separation in phospholipid bilayers induced by biologically active polycations*. Biochimica et Biophysica Acta (BBA) - Biomembranes, 1990. **1026**(1): p. 105-112.
64. Ilavsky, J., *Nika*: software for two-dimensional data reduction. Journal of Applied Crystallography, 2012. **45**(2): p. 324-328.
65. Ilker, M.F., et al., *Tuning the Hemolytic and Antibacterial Activities of Amphiphilic Polynorbornene Derivatives*. Journal of the American Chemical Society, 2004. **126**(48): p. 15870-15875.
66. Ilker, M.F., H. Schule, and E.B. Coughlin, *Modular Norbornene Derivatives for the Preparation of Well-Defined Amphiphilic Polymers: Study of the Lipid Membrane Disruption Activities*. Macromolecules, 2004. **37**(3): p. 694-700.
67. Ishitsuka, Y., et al., *Amphiphilic Poly(phenyleneethynylene)s Can Mimic Antimicrobial Peptide Membrane Disordering Effect by Membrane Insertion*. Journal of the American Chemical Society, 2006. **128**(40): p. 13123-13129.
68. Israelachvili, J., *Intermolecular and surface forces*. 3rd ed. ed2011, Burlington MA: Academic Press.
69. Ivanov, I., et al., *Characterization of Nonbiological Antimicrobial Polymers in Aqueous Solution and at Water-Lipid Interfaces from All-Atom Molecular Dynamics*. Journal of the American Chemical Society, 2006. **128**(6): p. 1778-1779.
70. Iwasa, A., et al., *Cellular uptake and subsequent intracellular trafficking of R8-liposomes introduced at low temperature*. Biochimica et Biophysica Acta (BBA) - Biomembranes, 2006. **1758**(6): p. 713-720.
71. Jacobson, K. and D. Papahadjopoulos, *Phase transitions and phase separations in phospholipid membranes induced by changes in temperature, pH, and concentration of bivalent cations*. Biochemistry, 1975. **14**(1): p. 152-161.

72. Jiao, C.-Y., et al., *Translocation and Endocytosis for Cell-penetrating Peptide Internalization*. Journal of Biological Chemistry, 2009. **284**(49): p. 33957-33965.
73. Kanazawa, A., T. Ikeda, and T. Endo, *Polymeric phosphonium salts as a novel class of cationic biocides. IV. Synthesis and antibacterial activity of polymers with phosphonium salts in the main chain*. Journal of Polymer Science Part A: Polymer Chemistry, 1993. **31**(12): p. 3031-3038.
74. Kaplan, I.M., J.S. Wadia, and S.F. Dowdy, *Cationic TAT peptide transduction domain enters cells by macropinocytosis*. Journal of Controlled Release, 2005. **102**(1): p. 247-253.
75. Killian, J.A. and G. von Heijne, *How proteins adapt to a membrane–water interface*. Trends in Biochemical Sciences, 2000. **25**(9): p. 429-434.
76. Kim, Y., S. Binauld, and M.H. Stenzel, *Zwitterionic Guanidine-Based Oligomers Mimicking Cell-Penetrating Peptides as a Nontoxic Alternative to Cationic Polymers to Enhance the Cellular Uptake of Micelles*. Biomacromolecules, 2012. **13**(10): p. 3418-3426.
77. Klausner, R.D., et al., *Receptor-mediated endocytosis of transferrin in K562 cells*. Journal of Biological Chemistry, 1983. **258**(8): p. 4715-4724.
78. Kleimann, J., et al., *Super-Stoichiometric Charge Neutralization in Particle–Polyelectrolyte Systems*. Langmuir, 2005. **21**(8): p. 3688-3698.
79. Kolonko, E.M. and L.L. Kiessling, *A Polymeric Domain That Promotes Cellular Internalization*. Journal of the American Chemical Society, 2008. **130**(17): p. 5626-5627.
80. Kolonko, E.M., et al., *General Synthetic Route to Cell-Permeable Block Copolymers via ROMP*. Journal of the American Chemical Society, 2009. **131**(21): p. 7327-7333.
81. Kosuge, M., et al., *Cellular Internalization and Distribution of Arginine-Rich Peptides as a Function of Extracellular Peptide Concentration, Serum, and Plasma Membrane Associated Proteoglycans*. Bioconjugate Chemistry, 2008. **19**(3): p. 656-664.
82. Koynova, R. and M. Caffrey, *Phases and phase transitions of the phosphatidylcholines*. Biochimica et Biophysica Acta (BBA) - Reviews on Biomembranes, 1998. **1376**(1): p. 91-145.
83. Kretschmann, E., *Die Bestimmung optischer Konstanten von Metallen durch Anregung von Oberflächenplasmaschwingungen*. Zeitschrift für Physik, 1971. **241**(4): p. 313-324.
84. Kuroda, K., G.A. Caputo, and W.F. DeGrado, *The Role of Hydrophobicity in the Antimicrobial and Hemolytic Activities of Polymethacrylate Derivatives*. Chemistry – A European Journal, 2009. **15**(5): p. 1123-1133.
85. Kuroda, K. and W.F. DeGrado, *Amphiphilic Polymethacrylate Derivatives as Antimicrobial Agents*. Journal of the American Chemical Society, 2005. **127**(12): p. 4128-4129.
86. Ladbrooke, B.D., R.M. Williams, and D. Chapman, *Studies on lecithin-cholesterol-water interactions by differential scanning calorimetry and X-ray diffraction*. Biochimica et Biophysica Acta (BBA) - Biomembranes, 1968. **150**(3): p. 333-340.
87. Lehrer, R.I., *Primate defensins*. Nature Reviews Microbiology, 2004. **2**(9): p. 727-738.
88. Lepock, J.R., et al., *Thermotropic lipid and protein transitions in chinese hamster lung cell membranes: relationship to hyperthermic cell killing*. Canadian journal of biochemistry and cell biology = Revue canadienne de biochimie et biologie cellulaire, 1983. **61**(6): p. 421-427.
89. Lewin, M., et al., *Tat peptide-derivatized magnetic nanoparticles allow in vivo tracking and recovery of progenitor cells*. Nature Biotechnology, 2000. **18**(4): p. 410-414.
90. Lienkamp, K., et al., *"Doubly Selective" Antimicrobial Polymers: How Do They Differentiate between Bacteria?* Chemistry - A European Journal, 2009. **15**(43): p. 11710-11714.

91. Lienkamp, K., et al., *Antimicrobial Polymers Prepared by Ring-Opening Metathesis Polymerization: Manipulating Antimicrobial Properties by Organic Counterion and Charge Density Variation*. Chemistry - A European Journal, 2009. **15**(43): p. 11715-11722.
92. Lienkamp, K., et al., *Antimicrobial Polymers Prepared by ROMP with Unprecedented Selectivity: A Molecular Construction Kit Approach*. Journal of the American Chemical Society, 2008. **130**(30): p. 9836-9843.
93. Liu, D., et al., *Nontoxic Membrane-Active Antimicrobial Arylamide Oligomers*. Angewandte Chemie International Edition, 2004. **43**(9): p. 1158-1162.
94. Love, J.A., et al., *A practical and highly active ruthenium-based catalyst that effects the cross metathesis of acrylonitrile*. Angew Chem Int Ed, 2002. **41**(21): p. 4035-7.
95. Mäe, M. and Ü. Langel, *Cell-penetrating peptides as vectors for peptide, protein and oligonucleotide delivery*. Current Opinion in Pharmacology, 2006. **6**(5): p. 509-514.
96. Maiolo, J.R., M. Ferrer, and E.A. Ottinger, *Effects of cargo molecules on the cellular uptake of arginine-rich cell-penetrating peptides*. Biochimica et Biophysica Acta (BBA) - Biomembranes, 2005. **1712**(2): p. 161-172.
97. Matsuzaki, K., et al., *Relationship of Membrane Curvature to the Formation of Pores by Magainin 2<sup>†</sup>*. Biochemistry, 1998. **37**(34): p. 11856-11863.
98. McMahon, H.T. and J.L. Gallop, *Membrane curvature and mechanisms of dynamic cell membrane remodelling*. Nature, 2005. **438**(7068): p. 590-596.
99. Mishra, A., et al., *HIV TAT Forms Pores in Membranes by Inducing Saddle-Splay Curvature: Potential Role of Bidentate Hydrogen Bonding*. Angewandte Chemie International Edition, 2008. **47**(16): p. 2986-2989.
100. Mishra, A., et al., *Translocation of HIV TAT peptide and analogues induced by multiplexed membrane and cytoskeletal interactions*. Proceedings of the National Academy of Sciences of the United States of America, 2011. **108**(41): p. 16883-16888.
101. Mitchell, D.j., et al., *Polyarginine enters cells more efficiently than other polycationic homopolymers*. The Journal of Peptide Research, 2000. **56**(5): p. 318-325.
102. Morgan, D.M., V.L. Larvin, and J.D. Pearson, *Biochemical characterisation of polycation-induced cytotoxicity to human vascular endothelial cells*. Journal of Cell Science, 1989. **94 ( Pt 3)**: p. 553-559.
103. Morton, T.A., D.G. Myszka, and I.M. Chaiken, *Interpreting complex binding kinetics from optical biosensors: a comparison of analysis by linearization, the integrated rate equation, and numerical integration*. Analytical Biochemistry, 1995. **227**(1): p. 176-185.
104. Moulton, H.M. and J.D. Moulton, *Arginine-rich cell-penetrating peptides with uncharged antisense oligomers*. Drug Discovery Today, 2004. **9**(20).
105. Mowery, B.P., et al., *Mimicry of Antimicrobial Host-Defense Peptides by Random Copolymers*. Journal of the American Chemical Society, 2007. **129**(50): p. 15474-15476.
106. Mozsolits, H. and M.-I. Aguilar, *Surface plasmon resonance spectroscopy: An emerging tool for the study of peptide-membrane interactions*. Peptide Science, 2002. **66**(1): p. 3-18.
107. Nagahara, H., et al., *Transduction of full-length TAT fusion proteins into mammalian cells: TAT-p27Kip1 induces cell migration*. Nature medicine, 1998. **4**(12): p. 1449-1452.
108. Nakase, I., et al., *Cellular Uptake of Arginine-Rich Peptides: Roles for Macropinocytosis and Actin Rearrangement*. Molecular Therapy, 2004. **10**(6): p. 1011-1022.
109. Nakase, I., et al., *Interaction of Arginine-Rich Peptides with Membrane-Associated Proteoglycans Is Crucial for Induction of Actin Organization and Macropinocytosis<sup>†</sup>*. Biochemistry, 2007. **46**(2): p. 492-501.

110. Needham, D. and E. Evans, *Structure and mechanical properties of giant lipid (DMPC) vesicle bilayers from 20.degree.C below to 10.degree.C above the liquid crystal-crystalline phase transition at 24.degree.C*. *Biochemistry*, 1988. **27**(21): p. 8261-8269.
111. Nelson, D.L. and M.M. Cox, *Lehninger Principles of Biochemistry, Fourth Edition*. 4th edition ed2004, New York: W. H. Freeman. 1100.
112. Nishihara, M., et al., *Arginine magic with new counterions up the sleeve*. *Organic & Biomolecular Chemistry*, 2005. **3**(9): p. 1659-1669.
113. Olbrich, K., et al., *Water Permeability and Mechanical Strength of Polyunsaturated Lipid Bilayers*. *Biophysical Journal*, 2000. **79**(1): p. 321-327.
114. Palermo, E.F. and K. Kuroda, *Chemical Structure of Cationic Groups in Amphiphilic Polymethacrylates Modulates the Antimicrobial and Hemolytic Activities*. *Biomacromolecules*, 2009. **10**(6): p. 1416-1428.
115. Palermo, E.F., I. Sovadinova, and K. Kuroda, *Structural Determinants of Antimicrobial Activity and Biocompatibility in Membrane-Disrupting Methacrylamide Random Copolymers*. *Biomacromolecules*, 2009. **10**(11): p. 3098-3107.
116. Papoian, G.A., et al., *Water in protein structure prediction*. *Proceedings of the National Academy of Sciences of the United States of America*, 2004. **101**(10): p. 3352-3357.
117. Parhamifar, L., et al., *Polycation cytotoxicity: a delicate matter for nucleic acid therapy—focus on polyethylenimine*. *Soft Matter*, 2010. **6**(17): p. 4001-4009.
118. Pednekar, D., A. Tendulkar, and S. Durani, *Electrostatics-defying interaction between arginine termini as a thermodynamic driving force in protein–protein interaction*. *Proteins: Structure, Function, and Bioinformatics*, 2009. **74**(1): p. 155-163.
119. Persson, D., et al., *Application of a Novel Analysis To Measure the Binding of the Membrane-Translocating Peptide Penetratin to Negatively Charged Liposomes†*. *Biochemistry*, 2003. **42**(2): p. 421-429.
120. Räägel, H., P. Säälük, and M. Pooga, *Peptide-mediated protein delivery--Which pathways are penetrable?* *Biochimica et Biophysica Acta (BBA) - Biomembranes*, 2010. **1798**(12): p. 2240-2248.
121. Reynwar, B.J., et al., *Aggregation and vesiculation of membrane proteins by curvature-mediated interactions*. *Nature*, 2007. **447**(7143): p. 461-464.
122. Richard, J.P., et al., *Cellular Uptake of Unconjugated TAT Peptide Involves Clathrin-dependent Endocytosis and Heparan Sulfate Receptors*. *Journal of Biological Chemistry*, 2005. **280**(15): p. 15300-15306.
123. Richard, J.P., et al., *Cell-penetrating Peptides*. *Journal of Biological Chemistry*, 2003. **278**(1): p. 585-590.
124. Richard, J.P., et al., *Cell-penetrating Peptides A REEVALUATION OF THE MECHANISM OF CELLULAR UPTAKE*. *Journal of Biological Chemistry*, 2003. **278**(1): p. 585-590.
125. Rose, F.L. and G. Swain, *850. Bisdiguanydes having antibacterial activity*. *Journal of the Chemical Society (Resumed)*, 1956.
126. Rothbard, J.B., et al., *Role of membrane potential and hydrogen bonding in the mechanism of translocation of guanidinium-rich peptides into cells*. *Journal of the American Chemical Society*, 2004. **126**(31): p. 9506-9507.
127. Rothbard, J.B., T.C. Jessop, and P.A. Wender, *Adaptive translocation: the role of hydrogen bonding and membrane potential in the uptake of guanidinium-rich transporters into cells*. *Advanced Drug Delivery Reviews*, 2005. **57**(4): p. 495-504.
128. Rothbard, J.B., et al., *Arginine-Rich Molecular Transporters for Drug Delivery: Role of Backbone Spacing in Cellular Uptake*. *Journal of Medicinal Chemistry*, 2002. **45**(17): p. 3612-3618.

129. Sakai, N. and S. Matile, *Anion-Mediated Transfer of Polyarginine across Liquid and Bilayer Membranes*. Journal of the American Chemical Society, 2003. **125**(47): p. 14348-14356.
130. Santore, M.M., et al., *Effect of Surfactant on Unilamellar Polymeric Vesicles: Altered Membrane Properties and Stability in the Limit of Weak Surfactant Partitioning*. Langmuir, 2002. **18**(20): p. 7299-7308.
131. Schmid, S.L. and L.L. Carter, *ATP is required for receptor-mediated endocytosis in intact cells*. Journal of Cell Biology, 1990. **111**(6 Pt 1): p. 2307-2318.
132. Schmidt, N., et al., *Arginine-rich cell-penetrating peptides*. FEBS Letters, 2010. **584**(9): p. 1806-1813.
133. Schmidt, N.W., et al., *Molecular Basis for Nanoscopic Membrane Curvature Generation from Quantum Mechanical Models and Synthetic Transporter Sequences*. Journal of the American Chemical Society, 2012. **134**(46): p. 19207-19216.
134. Schmidt, N.W., et al., *Criterion for amino acid composition of defensins and antimicrobial peptides based on geometry of membrane destabilization*. Journal of the American Chemical Society, 2011. **133**(17): p. 6720-6727.
135. Schmidt, N.W., et al., *Arginine in  $\alpha$ -defensins: differential effects on bactericidal activity correspond to geometry of membrane curvature generation and peptide-lipid phase behavior*. The Journal of biological chemistry, 2012. **287**(26): p. 21866-21872.
136. Schug, K.A. and W. Lindner, *Noncovalent Binding between Guanidinium and Anionic Groups: Focus on Biological- and Synthetic-Based Arginine/Guanidinium Interactions with Phosph[on]ate and Sulf[on]ate Residues*. Chemical Reviews, 2005. **105**(1): p. 67-114.
137. Schwarze, S.R., K.A. Hruska, and S.F. Dowdy, *Protein transduction: unrestricted delivery into all cells?* Trends in Cell Biology, 2000. **10**(7): p. 290-295.
138. Selsted, M.E. and A.J. Ouellette, *Mammalian defensins in the antimicrobial immune response*. Nature Immunology, 2005. **6**(6): p. 551-557.
139. Sgolastra, F., et al., *The Importance of Sequence Specific Hydrophobicity in Synthetic Protein Transduction Domain Mimics*. Biomacromolecules, 2014. **15**(3): p. 812-820.
140. Sgolastra, F., et al., *Sequence Segregation Improves Non-covalent Protein Delivery*, 2014, University of Massachusetts--Amherst: Amherst, MA.
141. Silverstein, S.C., R.M. Steinman, and Z.A. Cohn, *Endocytosis*. Annual Review of Biochemistry, 1977. **46**(1): p. 669-722.
142. Simon, S.A. and T.J. McIntosh, *Peptide-Lipid Interactions* 2002: Academic Press. 606.
143. Snyder, E.L. and S.F. Dowdy, *Cell Penetrating Peptides in Drug Delivery*. Pharmaceutical Research, 2004. **21**(3): p. 389-393.
144. Som, A., A. Reuter, and G.N. Tew, *Protein Transduction Domain Mimics: The Role of Aromatic Functionality*. Angewandte Chemie International Edition, 2012. **51**(4): p. 980-983.
145. Som, A., et al., *Self-Activation in De Novo Designed Mimics of Cell-Penetrating Peptides*. Angewandte Chemie International Edition, 2011. **50**(27): p. 6147-6150.
146. Som, A., et al., *Self-Activation in De Novo Designed Mimics of Cell-Penetrating Peptides*. Angewandte Chemie International Edition, 2011. **50**(27): p. 6147-6150.
147. Som, A., et al., *Divalent Metal Ion Triggered Activity of a Synthetic Antimicrobial in Cardiolipin Membranes*. Journal of the American Chemical Society, 2009. **131**(42): p. 15102-15103.

148. Stanzl, E.G., et al., *Fifteen Years of Cell-Penetrating, Guanidinium-Rich Molecular Transporters: Basic Science, Research Tools, and Clinical Applications*. Accounts of Chemical Research, 2013.
149. Takeuchi, T., et al., *Direct and Rapid Cytosolic Delivery Using Cell-Penetrating Peptides Mediated by Pyrenebutyrate*. ACS Chemical Biology, 2006. **1**(5): p. 299-303.
150. Ter-Avetisyan, G., et al., *Cell Entry of Arginine-rich Peptides Is Independent of Endocytosis*. Journal of Biological Chemistry, 2009. **284**(6): p. 3370-3378.
151. Tew, G.N., et al., *De novo design of biomimetic antimicrobial polymers*. Proceedings of the National Academy of Sciences of the United States of America, 2002. **99**(8): p. 5110-5114.
152. Tew, G.N., et al., *De Novo Design of Antimicrobial Polymers, Foldamers, and Small Molecules: From Discovery to Practical Applications*. Accounts of Chemical Research, 2010. **43**(1): p. 30-39.
153. Tezgel, A.O., *Protein Transduction Domain Mimics by ROMP and Their Bioactive Cargo Delivery*, in *Polymer Science and Engineering 2013*, University of Massachusetts--Amherst: Amherst, MA. p. 156.
154. Tezgel, A.Ö., et al., *Novel Protein Transduction Domain Mimics as Nonviral Delivery Vectors for siRNA Targeting NOTCH1 in Primary Human T cells*. Molecular Therapy, 2013. **21**(1): p. 201-209.
155. Tezgel, A.O., J.C. Telfer, and G.N. Tew, *De Novo Designed Protein Transduction Domain Mimics from Simple Synthetic Polymers*. Biomacromolecules, 2011. **12**(8): p. 3078-3083.
156. Tezgel, A.O.z.l., J.C. Telfer, and G.N. Tew, *De Novo Designed Protein Transduction Domain Mimics from Simple Synthetic Polymers*. Biomacromolecules, 2011. **12**(8): p. 3078-3083.
157. Thorén, P.E.G., et al., *Membrane destabilizing properties of cell-penetrating peptides*. Biophysical Chemistry, 2005. **114**(2-3): p. 169-179.
158. Torchilin, V.P., et al., *TAT peptide on the surface of liposomes affords their efficient intracellular delivery even at low temperature and in the presence of metabolic inhibitors*. Proceedings of the National Academy of Sciences, 2001. **98**(15): p. 8786-8791.
159. Tossi, A., L. Sandri, and A. Giangaspero, *Amphipathic,  $\alpha$ -helical antimicrobial peptides*. Peptide Science, 2000. **55**(1): p. 4-30.
160. Vivès, E., P. Brodin, and B. Lebleu, *A Truncated HIV-1 Tat Protein Basic Domain Rapidly Translocates through the Plasma Membrane and Accumulates in the Cell Nucleus*. Journal of Biological Chemistry, 1997. **272**(25): p. 16010-16017.
161. Wadia, J.S., R.V. Stan, and S.F. Dowdy, *Transducible TAT-HA fusogenic peptide enhances escape of TAT-fusion proteins after lipid raft macropinocytosis*. Nature Medicine, 2004. **10**(3): p. 310-315.
162. Walrant, A., et al., *Different membrane behaviour and cellular uptake of three basic arginine-rich peptides*. Biochimica et Biophysica Acta (BBA) - Biomembranes, 2011. **1808**(1): p. 382-393.
163. Wang, Y., et al., *Membrane Perturbation Activity of Cationic Phenylene Ethynylene Oligomers and Polymers: Selectivity against Model Bacterial and Mammalian Membranes*. Langmuir, 2010. **26**(15): p. 12509-12514.
164. Watkins, C.L., et al., *Low concentration thresholds of plasma membranes for rapid energy-independent translocation of a cell-penetrating peptide*. Biochemical Journal, 2009. **420**(2): p. 179-189.
165. Wender, P.A., et al., *The design of guanidinium-rich transporters and their internalization mechanisms*. Advanced Drug Delivery Reviews, 2008. **60**(4-5): p. 452-472.

166. Wender, P.A., et al., *Dendrimeric Molecular Transporters: Synthesis and Evaluation of Tunable Polyguanidino Dendrimers That Facilitate Cellular Uptake*. *Organic Letters*, 2005. **7**(22): p. 4815-4818.
167. Wender, P.A., et al., *The design, synthesis, and evaluation of molecules that enable or enhance cellular uptake: Peptoid molecular transporters*. *Proceedings of the National Academy of Sciences of the United States of America*, 2000. **97**(24): p. 13003-13008.
168. Wender, P.A., et al., *Oligocarbamate Molecular Transporters: Design, Synthesis, and Biological Evaluation of a New Class of Transporters for Drug Delivery*. *Journal of the American Chemical Society*, 2002. **124**(45): p. 13382-13383.
169. Wenk, M.R. and J. Seelig, *Magainin 2 Amide Interaction with Lipid Membranes: Calorimetric Detection of Peptide Binding and Pore Formation†*. *Biochemistry*, 1998. **37**(11): p. 3909-3916.
170. White, S.H. and W.C. Wimley, *MEMBRANE PROTEIN FOLDING AND STABILITY: Physical Principles*. *Annual Review of Biophysics and Biomolecular Structure*, 1999. **28**(1): p. 319-365.
171. Wieprecht, T., M. Beyermann, and J. Seelig, *Binding of Antibacterial Magainin Peptides to Electrically Neutral Membranes: Thermodynamics and Structure†*. *Biochemistry*, 1999. **38**(32): p. 10377-10387.
172. Wimley, W.C. and S.H. White, *Experimentally determined hydrophobicity scale for proteins at membrane interfaces*. *Nature Structural & Molecular Biology*, 1996. **3**(10): p. 842-848.
173. Wu, G., et al., *Effects of bilayer phases on phospholipid-ploxamer interactions*. *Soft Matter*, 2009. **5**(7): p. 1496-1503.
174. Yandek, L.E., et al., *Mechanism of the Cell-Penetrating Peptide Transporter 10 Permeation of Lipid Bilayers*. *Biophysical Journal*, 2007. **92**(7): p. 2434-2444.
175. Yang, L., et al., *Synthetic Antimicrobial Oligomers Induce a Composition-Dependent Topological Transition in Membranes*. *Journal of the American Chemical Society*, 2007. **129**(40): p. 12141-12147.
176. Yang, L., et al., *Mechanism of a prototypical synthetic membrane-active antimicrobial: Efficient hole-punching via interaction with negative intrinsic curvature lipids*. *Proceedings of the National Academy of Sciences*, 2008. **105**(52): p. 20595-20600.
177. Yau, W.-M., et al., *The Preference of Tryptophan for Membrane Interfaces†*. *Biochemistry*, 1998. **37**(42): p. 14713-14718.
178. Yeaman, M.R. and N.Y. Yount, *Mechanisms of Antimicrobial Peptide Action and Resistance*. *Pharmacological Reviews*, 2003. **55**(1): p. 27-55.
179. Yuzlenko, O. and T. Lazaridis, *Interactions between Ionizable Amino Acid Side Chains at a Lipid Bilayer–Water Interface*. *The Journal of Physical Chemistry B*, 2011. **115**(46): p. 13674-13684.
180. Zasloff, M., *Magainins, a class of antimicrobial peptides from *Xenopus* skin: isolation, characterization of two active forms, and partial cDNA sequence of a precursor*. *Proceedings of the National Academy of Sciences of the United States of America*, 1987. **84**(15): p. 5449-5453.
181. Zatsepin, T., et al., *Conjugates of Oligonucleotides and Analogues with Cell Penetrating Peptides as Gene Silencing Agents*. *Current Pharmaceutical Design*, 2005. **11**(28): p. 3639-3654.
182. Ziegler, A., *Thermodynamic studies and binding mechanisms of cell-penetrating peptides with lipids and glycosaminoglycans*. *Advanced Drug Delivery Reviews*, 2008. **60**(4–5): p. 580-597.

183. Zimmerberg, J. and M.M. Kozlov, *How proteins produce cellular membrane curvature*. Nature Reviews Molecular Cell Biology, 2006. **7**(1): p. 9-19.